EDELWEISS-LT

Direct low-mass WIMP searches with HPGe Semiconductor Bolometers

JINR group

V. Brudanin, Z. Kalaninova, A. Lubashevskiy, D. Filosofov, N. Mirzaev, L. Perevoshchikov, D. Ponomarev, A. Rakhimov, I. Rozova, S. Rozov, K. Shakhov and E. Yakushev

Dubna, 2017

Form No. 24

Direct low-mass WIMP searches with HPGe Semiconductor Bolometers

EDELWEISS-LT

CODE OF THEME 03-2-1100-2010/2018

V. Brudanin, Z. Kalaninova, A. Lubashevskiy, D. Filosofov, N. Mirzaev, L. Perevoshchikov, D. Ponomarev, A. Rakhimov, I. Rozova, S. Rozov, K. Shakhov and E. Yakushev

Laboratory of Nuclear Problems, JINR

NAMES OF PROJECT LEADERS: E. Yakushev

NAME OF PROJECT DEPUTY LEADERS: S. Rozov

DATE OF SUBMISSION OF PROPOSAL OF PROJECT TO SOD _____

DATE OF THE LABORATORY STC _____ DOCUMENT NUMBER _____

STARTING DATE OF PROJECT __January 2019_____(FOR EXTENSION OF PROJECT — DATE OF ITS FIRST APPROVAL) _December 2004_____

Form No. 25

PROJECT ENDORSEMENT LIST

Direct low-mass WIMP searches with HPGe Semiconductor Bolometers

EDELWEISS-LT

CODE OF THEME 03-2-1100-2010/2018

NAME OF PROJECT LEADER: Evgeny Yakushev

APPROVED BY JINR DIRECTOR		
	SIGNATURE	DATE
ENDORSED BY		
JINR VICE-DIRECTOR		
CHIEF SCIENTIFIC SECRETARY		
CHIEF ENGINEER		
HEAD OF SCIENCE ORGANIZATION DEPARTMENT		
LABORATORY DIRECTOR		
LABORATORY CHIEF ENGINEER		
PROJECT LEADER		
PROJECT DEPUTY LEADERS		
ENDORSED		
RESPECTIVE PAC		

Form No. 26

Schedule proposal and resources required for the implementation of the Project

EDELWEISS-LT

List of parts and devices; Resources; Financial sources			Cost of parts (K US$), resources needs	Allocation of resources and money		
				1st year	2nd year	3rd year
Main parts and equipment	1. Materials required for tests of low threshold detectors (shielding, veto system, etc). Materials and equipments for the clean room.		30	10	10	10
	2. Spectroscopic electronics for point contact detectors at LSM.		15	5	5	5
	3. Low background neutron spectrometers with iodine containing detectors.		15	5	5	5
	4. Materials and equipment for maintenance of JINR EDELWEISS detectors (three neutron detectors, two radon detectors, alpha spectrometer, HPGe spectrometer).		21	7	7	7
	5. Materials and equipment for calibration purposes. It includes making of new radioactive source. Radiochemistry equipment.		15	5	5	5
	6. Materials and equipments for R&D at JINR (electronics, clean room materials, laboratory equipments)		9	3	3	3
	Total		**105**	**35**	**35**	**35**
Resources	Norm-hours	JINR workshop	3300	1100	1100	1100
		DLNP workshop	1500	500	500	500
Financial sources	JINR budget	Budget spending	**105**	**35**	**35**	**35**
	Off-budget sources	Grants; Other sources (these funds are not currently guaranteed)	*30*	*10*	*10*	*10*

PROJECT LEADER E. Yakushev

Form No. 29

Estimated expenditures for the Project EDELWEISS-LT, Direct low-mass WIMP searches with HPGe Semiconductor Bolometers

#	Designation for outlays	Total cost	1 year	2 year	3 year
	Direct expenses for the project				
1.	Networking	3.0K US$	1.0	1.0	1.0
2.	DLNP workshop	1500 norm-hours	500	500	500
3.	JINR workshop	3300 norm-hours.	1100	1100	1100
4.	Materials	36.0K US$	12.0	12.0	12.0
5.	Equipment	69.0K US$	23.0	23.0	23.0
6.	Collaboration fee	60.0K US$	20.0	20.0	20.0
7.	Travel expenses	60.0K US$	20.0	20.0	20.0
	Total	**228.0K US$**	**76.0K US$**	**76.0K US$**	**76.0K US$**

PROJECT LEADER

LABORATORY DIRECTOR

LABORATORY CHIEF ENGINEER-ECONOMIST

Форма № 24

Прямой поиск легких WIMP с HPGe полупроводниковыми болометрами

Проект EDELWEISS-LT

ШИФР ТЕМЫ 03-2-1100-2010/2018

АВТОРЫ ОТ ОИЯИ:
В.Б. Бруданин, З. Каланинова, А.В. Лубашевский, Н.А. Мирзаев, Л.Л. Перевощиков, Д.В. Пономарев, А.В. Рахимов, И.Е. Розова, С.В. Розов, Д.В. Философов, К.В. Шахов и Е.А. Якушев

Объединенный институт ядерных исследований, ЛЯП (Дубна)

РУКОВОДИТЕЛЬ ПРОЕКТА: Якушев Е.А.

ЗАМЕСТИТЕЛЕЙ РУКОВОДИТЕЛЯ ПРОЕКТА: Розов С.В.

ДАТА ПРЕДСТАВЛЕНИЯ ПРОЕКТА В НОО _____

ДАТА НТС ЛАБОРАТОРИИ _____ НОМЕР ДОКУМЕНТА _____

ДАТА НАЧАЛА ПРОЕКТА EDELWEISS-LT: ___январь 2019_____
(ДАТА ПЕРВОГО УТВЕРЖДЕНИЯ ПРОЕКТА (EDELWEISS-II) на НТС ЛЯП): 4 декабря 2004

Форма № 25

ЛИСТ СОГЛАСОВАНИЙ ПРОЕКТА

ПОЛНОЕ НАЗВАНИЕ ПРОЕКТА: Прямой поиск легких WIMP с HPGe полупроводниковыми болометрами

УСЛОВНОЕ ОБОЗНАЧЕНИЕ ПРОЕКТА ИЛИ КОЛЛАБОРАЦИИ: EDELWEISS-LT

ШИФР ТЕМЫ 03-2-1100-2010/2018

ФИО РУКОВОДИТЕЛЯ ПРОЕКТА: Якушев Евгений Александрович

УТВЕРЖДЕН ДИРЕКТОРОМ ОИЯИ		
	ПОДПИСЬ	ДАТА
СОГЛАСОВАНО		
ВИЦЕ-ДИРЕКТОР ОИЯИ		
ГЛАВНЫЙ УЧЕНЫЙ СЕКРЕТАРЬ		
ГЛАВНЫЙ ИНЖЕНЕР		
НАЧАЛЬНИК НОО		
ДИРЕКТОР ЛАБОРАТОРИИ		
ГЛАВНЫЙ ИНЖЕНЕР ЛАБОРАТОРИИ		
РУКОВОДИТЕЛЬ ПРОЕКТА		
ЗАМ. РУКОВОДИТЕЛЯ ПРОЕКТА		
ОДОБРЕН		
ПКК ПО НАПРАВЛЕНИЮ		

Форма № 26

Предлагаемый план-график и необходимые ресурсы для осуществления проекта EDELWEISS-LT

Наименование узлов и систем установки, ресурсов, источников финансирования			Стоимость узлов (тыс.$) установки. Потребности в ресурсах	Предложения Лабораторий по распределению финансирования и ресурсов		
				1 год	2 год	3 год
Основные узлы и оборудование	1. Материалы для тестирования низкопороговых детекторов (защита, вето система и т.д.). Материалы и оборудование чистой комнаты.		30	10	10	10
	2. Спектроскопическая электроника для детектор с точечным контактом в LSM.		15	5	5	5
	3. Низкофоновые нейтронные спектрометры на основе йодсодержащих детекторов.		15	5	5	5
	4. Материалы и оборудование для поддержания работоспособности детекторов, находящихся под нашем управлением в EDELWEISS (3 нейтронных детектора, 2 радоновых детектора, альфа-спектрометр, HPGe спектрометр).		21	7	7	7
	5. Материалы и оборудование для проведения калибровок, включая создание калибровочных источников. Радиохимическое оборудование.		15	5	5	5
	6. Материалы и оборудование для проведения R&D в ЛЯП (электроника, материалы для чистой комнаты, оборудование лабораторий).		9	3	3	3
	Итого		**105**	**35**	**35**	**35**
Необходимые ресурсы	Нормо-часы	ОП ОИЯИ	3300	1100	1100	1100
		ООЭП ЛЯП	1500	500	500	500
Источники финансирования	Бюджет	Затраты из бюджета	**105**	**35**	**35**	**35**
	Внебюджетные средства	*Средства по грантам. Другие источники финансирования (получение данных средства в настоящее время не гарантировано)*	*30*	*10*	*10*	*10*

РУКОВОДИТЕЛЬ ПРОЕКТА Е.А. Якушев

Форма № 29

Смета затрат по проекту EDELWEISS-LT, Прямой поиск легких WIMP с HPGe полупроводниковыми болометрами

№№ пп	Наименование статей затрат	Полная стоимость	1 год	2 год	3 год
	Прямые затраты на Проект				
1.	Компьютерная связь	3.0K US$	1.0	1.0	1.0
2.	ООЭП ЛЯП	1500 норм ч.	500	500	500
3.	ОП ОИЯИ	3300 норма ч.	1100	1100	1100
4.	Материалы	36.0K US$	12.0	12.0	12.0
5.	Оборудование	69.0K US$	23.0	23.0	23.0
6.	Взнос в коллаборацию	60.0K US$	20.0	20.0	20.0
7.	Командировочные расходы	60.0K US$	20.0	20.0	20.0
	Итого по прямым расходам	**228.0K US$**	**76.0K US$**	**76.0K US$**	**76.0K US$**

РУКОВОДИТЕЛЬ ПРОЕКТА

ДИРЕКТОР ЛАБОРАТОРИИ

ВЕДУЩИЙ ИНЖЕНЕР-ЭКОНОМИСТ ЛАБОРАТОРИИ

1. Abstract 3

2. Introduction 3

3. Main results for the previous implementation period 4

4. State-of-the-art of the science case proposed 7

5. Description of the proposed research 9

6. Estimation of human resources 14

7. SWOT (Strengths, Weaknesses, Opportunities, Threat) analysis 15

8. Contribution of JINR group 17

9. References 20

10. Appendix 1, EDELWEISS experiment, technical paper (printed as a separate document) 23

11. Appendix 2 24

1. Abstract

The project is continuation of the EDELWEISS scientific program conducting by JINR in the international collaboration. The EDELWEISS experiment searches for evidence of direct WIMPs from Milky Way galaxy scattering of Ge nuclei within cryogenic Ge crystals. The main objective of the experiment is now shifted to the low-mass WIMPs region (10 GeV/c^2 and below) which could investigated in the experiment thanks to advantage of 100 eV energy resolution reachable with HPGe bolometers via the Neganov-Luke effect of internal amplification of the heat signal. Search of "light WIMPs" become especially motivated due to controversial results of some other experiments. Some theoretical models are also favorable to the "light WIMP" scenario. Since there are no Dark Matter particles in the Standard Model, their search in a wide mass region (from 1 GeV/c^2) is simultaneously an important test for new physics. During the project measurements with several low threshold bolometers will be performed. That will target light WIMP - nucleon cross section on the level of better of 10^{-41} cm^2 competitive with best results of other experiments. In the same time the experiment R&D program will be continued in direction of even lower energy threshold and background.

JINR team of the project is expected to contribute to: 1) Development of new low threshold Ge detectors; Assembly and commissioning; 2) Development of methods for underground site low background measurements; 3) Data taking (this includes daily routine procedures, as well as regular and special calibration runs); 4) Low background study and development of methods of neutron and radon detection; 5) Detector simulations and data analysis; Publication of results.

Participation in the project provides for JINR an important access to low background infrastructure needed for R&D of JINR neutrino experiments at the Kalinin NPP.

2. Introduction

Understanding the content of the Universe has been a one of the main problems of cosmology for a long time. There are strong evidences of the existence of non-baryonic dark matter (DM) at almost every cosmic scale [1,2]. Theories and simulations regarding hierarchical structure formation indicate that this non-luminous component may manifest itself in the form of a gas of Weakly Interacting Massive Particles (WIMPs) [3] (see also Appendix 2 for further discussion about WIMPs). There is no viable candidate in the Standard Model for the composition of this cold DM. It is very intriguing that the most favored solution to the problem of hierarchy in particle physics, SUSY, predicts that the Universe is filled with WIMPs. Natural candidates, like the neutralino, have a predicted mass in the range of a few GeV/c^2 to TeV/c^2 and an elastic scattering cross section on nucleons at the weak scale [4]. Furthermore, they are characterized by a dominant interaction with atomic nuclei, inducing low-energy nuclear recoils in the target material, and could be thus detected in the so-called direct detection experiments [5]. There is an intense experimental activity on the direct detection since many years, for which the most promising results have been obtained with liquid noble and cryogenic detectors (see e.g. [6–13] and references therein). Direct search for WIMPs is the fundamental scientific problem addressed by the EDELWEISS. It searches for WIMPs using an array of cryogenic germanium bolometers able to identify events consisting of WIMP-induced nuclear recoils. In the present time there is an increasing gain of interest for the search of low-mass WIMPs arising

on the one hand from non evidence yet for SUSY at the LHC and on the other hand from new theoretical approaches favouring lighter candidates [17-19]. As an example, asymmetric DM models linking the relic density to the baryon asymmetry predict DM particles of a few GeV/c^2 [20-21]. A wide region of the parameter space (σ_{SI} m_W) giving spin-independent WIMP-nucleon cross-sections as a function of WIMP mass is thus yet to be explored at such low WIMP masses. With fact that liquid xenon experiments stand now as a leader in high-mass WIMP searches (10 GeV/c^2 to 1 TeV/c^2) [14-16], a division of work is taking shape in the hunt for DM particles: an exploration of the high-mass region led by experiments with liquid scintillators, and light WIMP models to be tested by cryogenic detector experiments. In this new context, the EDELWEISS experiment originally designed for the search of WIMPs of *O*(100 GeV/c^2) (see Appendix 1 for details) has undergone a redirection of its strategy to optimization detectors for low-mass (light) WIMP searches (EDELWEISS-LT).

The EDELWEISS experiment is installed in the deep underground laboratory, the Laboratoire Souterrain de Modane (LSM). It houses the largest operating mass of HPGe detectors devoted to the search for DM with twenty-four 820-890 g high purity Ge cylindrical crystals, called FID (Fully Inter-Digitized) detectors. These are cooled down to cryogenic temperatures (18 mK) in order to perform a double measurement of ionization and heat signals, which is used to discriminate nuclear recoils induced by WIMP elastic scattering on Ge nuclei from electronic recoils induced by γ- and β- rays. Charge collection is carried out by concentric electrodes interleaved on all the absorber surfaces. The readout of the four types of electrodes allows fiducial selection of events and results in an crucial background rejection for surface α- and β-events. FID detectors are also equipped with two NTD (Neutron Transmutation Doped) Ge sensors glued on their two planar surfaces, allowing to measure temperature elevations of a few μK. The main improvement in EDELWEISS-LT stage allowing investigation of low mass WIMPs will be due to amplification of the phonon signal through Neganov-Luke effect (in addition to inducing the ionization signal, the drift of the electrons and holes created following a particle interaction amplifies the heat signal).

3. Main results for the previous implementation period

The detailed description of EDELWEISS setup and detectors is given in the Appendix 1 (copy of the technical review of the experiment published in Journal of Instrumentation, 12, 08, P08010, 2017). During the current stage of the project number of improvements to the setup including detectors, shield, data acquisition were implemented and described in the above paper. It corresponds to general philosophy of the experiment: continuous improvement of the energy resolution and energy threshold, increasing of detector mass, with simultaneous reduction of the background. Thanks to this approach during each of previous stages of the EDELWEISS experimental program world leading results of DM search have been obtained.

Already at the current stage of the experiment the most important from results is connected with investigation of low-mass WIMPs region from 4 to 30 GeV/c^2 (Fig. 1). For the extreme case for WIMPs with m_χ = 4 GeV/c^2 the 90 % C.L. exclusion limit set currently by EDELWEISS is 1.6×10^{-39} cm^2. Therefore, positive results reported by some others experiments were directly verified. It is important that the achieved by EDELWEISS-III sensitivity completely covered region of positive CoGeNT results received on the same nuclear (Ge).

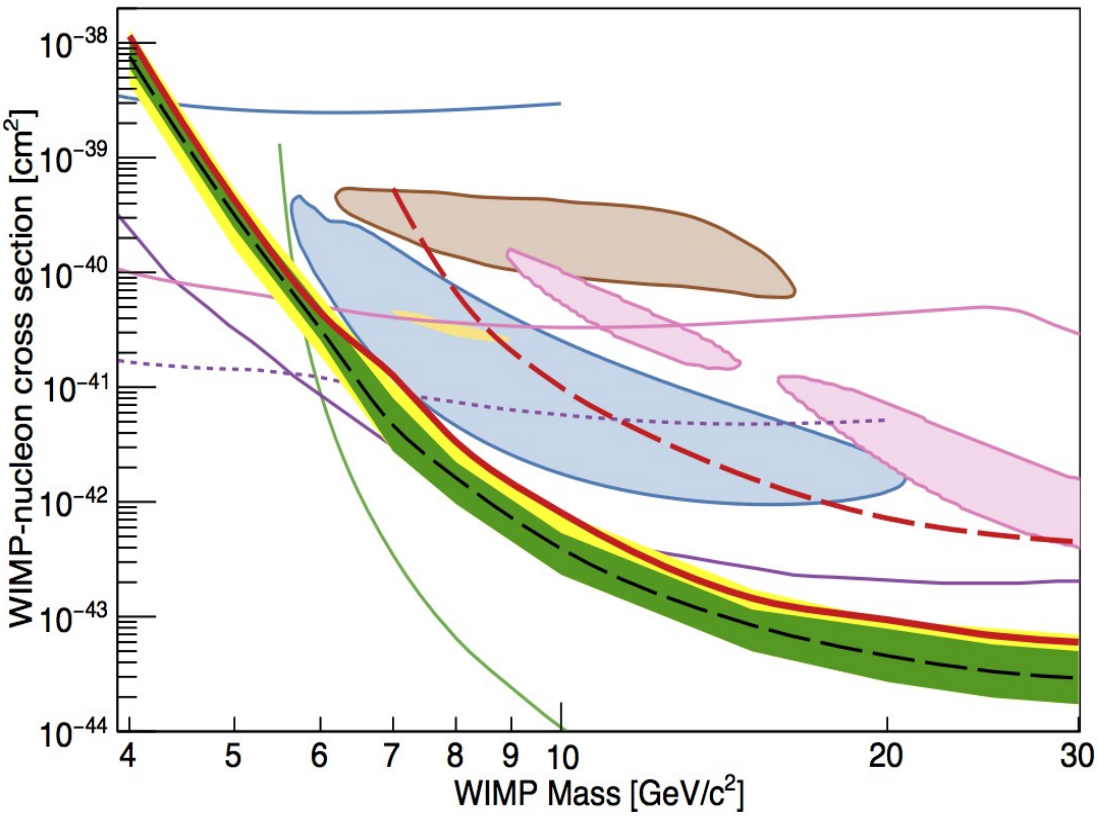

Fig. 1: Red curve: 90% CL limit on the spin-independent WIMP-nucleon cross-section obtained by EDELWEISS. The green (resp. yellow) band represents the expected 1σ (resp. 2σ) sensitivity region in the absence of a signal. The yellow, blue, pink and brown contours are respectively from CoGeNT [23], CDMS-Si [25], CRESST-II [24] and DAMA [26]. We also represent other limits by EDELWEISS-II [27] (dashed red), LUX [29] (green), DAMIC [30] (blue), CRESST [31] (pink), CDMSLite [32] (dashed violet) and SuperCDMS [33] (violet).

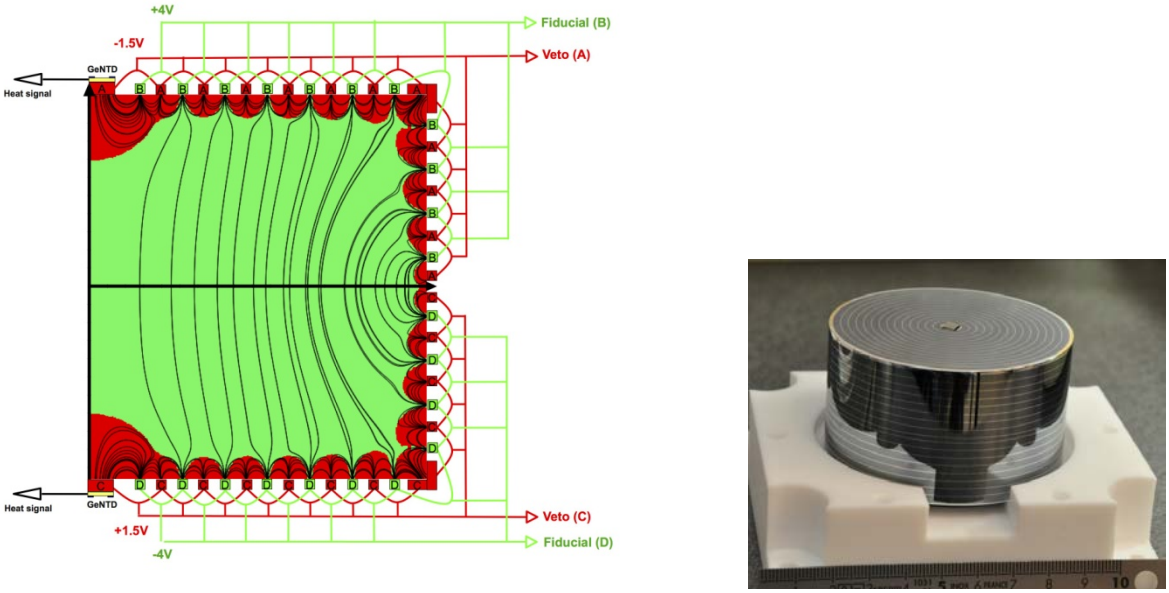

Fig. 2: Left: Cross-sectional view of an 800-g FID detector. The fiducial and veto electrodes are represented with their corresponding wirings. Electric field lines are shown inside the detector, as derived from a numerical calculation. The associated fiducial volume is represented in green, while charge depositions taking place inside the red regions are tagged by signals on a veto electrode. Right: photo of one of FID800 detectors.

During the current stage of the EDELWEISS experiment WIMP search run in low-background conditions is carried out with an array of twenty-four innovative FID detectors. Results of R&D of these detectors is by itself a breakthrough in development of HPGe detectors with highly-efficient surface background rejection capability. The detectors used in this search consist of 820 to 890 g cylindric high-purity Ge monocrystals with an appropriate surface treatment. Fig. 2 illustrates the operation principle of these detectors. Interleaved ring electrodes were evaporated over both their planar and side surfaces. Under nominal operation, these electrodes are polarised alternatively at +4 and -1.5 V on the top side, and opposite-sign voltages on the bottom. All electrodes at a given voltage are wired together, so that there are four charge readout channels per detector. The resulting electric field inside the crystal causes charges created far from the surface to generate a time-integrated signal only on the so-called fiducial electrodes polarized at ±4 V. This defines the so-called fiducial volume, whose mass is on average 625 g. The fiducial volume results from the electric field geometry and charge propagation effects, and does not depend on the mechanism generating the initial charge deposition. Charges created close to the surface will generate signals both on the fiducial and the veto electrodes. For each detector, two neutron transmutation doped (NTD) thermistors are glued on the top and bottom surfaces. When operated at low temperature, they provide a measurement of the total energy deposited in the detector after thermalisation. These detectors diffeer from the ID bolometers used in the previous phase of the experiment by their large mass, and by being fully covered with interleaved electrodes, hence the name "FID". However, their working principle is similar. For each recorded interaction, the measurement of charge topology enables the rejection of surface interactions such as those generated by ^{210}Pb subsequent decays and by ^{14}C at the detector surface and immediate surroundings. The corresponding rejection factor for 800-g FID detectors is better than 4×10^{-5} (90% CL) above 15 keV recoil energies, as derived from the exposure of two detectors to ^{210}Pb sources. After fiducial selection, the combined heat and fiducial ionisation measurements provide a way to distinguish electron recoils (ER) and nuclear recoils (NR), since they have different ionisation yields. EDELWEISS demonstrated with using ^{133}Ba sources that the fraction of electron recoils present in a region with 90% acceptance for nuclear recoils is less than 6×10^{-6} (90% CL). No sign of a degradation of this rejection performance as a function of energy is observed, except for the case when the signal amplitudes are similar to their baseline fluctuations.

The main result achieved during the current stage is connected with number intermediate "small" results that are not subject for this report. Details can be found in the EDELWEISS publications for last 5 years listed below in the chronological order:

Q Arnaud, et al (EDELWEISS collaboration) Optimizing EDELWEISS detectors for low-mass WIMP searches, 2017, arXiv preprint arXiv:1707.04308, submitted to Phys. Rev. D

E Armengaud, et al (EDELWEISS collaboration), Measurement of the cosmogenic activation of germanium detectors in EDELWEISS-III, Astroparticle Physics, 91, 2017, 51-64

E Armengaud, et al (EDELWEISS collaboration) Performance of the EDELWEISS-III experiment for direct dark matter searches, Journal of Instrumentation, 12, 08, P08010, 2017, arXiv preprint arXiv:1706.01070

L Hehn, et al (EDELWEISS collaboration) Improved EDELWEISS-III sensitivity for low-mass WIMPs using a profile likelihood approach, 2016, The European Physical Journal C 76 (10), 548

E Armengaud, et al (EDELWEISS collaboration) Constraints on low-mass WIMPs from the EDELWEISS-III dark matter search, 2016, Journal of Cosmology and Astroparticle Physics 2016 (05), 019
AV Rakhimov, et al, Neutron activation analysis of polyethylene from neutron shield of EDELWEISS experiment, Radiochimica Acta 103 (9), 673-678, 2015
G Angloher et al, EURECA conceptual design report, Physics of the Dark Universe, 3, 41-74, 2014
B Schmidt et al. Muon-induced background in the EDELWEISS dark matter search. 2013, Astroparticle Physics 44, 28-39.
E. Armengaud et al. (EDELWEISS collaboration) Axion searches with the EDELWEISS-II experiment. In: JCAP 1311 (2013), p. 067. arXiv: 1307.1488 [astro-ph.CO];
E Armengaud, et al (EDELWEISS collaboration) Background studies for the EDELWEISS dark matter experiment, Astroparticle Physics 47, 1-9, 2012
E Armengaud, et al (EDELWEISS collaboration) Search for low-mass WIMPs with EDELWEISS-II heat-and-ionization detectors, Physical Review D 86 (5), 051701, 2012

During participation of JINR in the EDELWEISS program the most cited (more than 300 times) article is: E Armengaud et al. “Final results of the EDELWEISS-II WIMP search using a 4-kg array of cryogenic germanium detectors with interleaved electrodes”. Phys.Lett. B702 (2011), pp. 329–335. arXiv: 1103.4070 [astro-ph.CO]

4. State-of-the-art of the science case proposed (need for EDELWEISS-LT)

Identification of a WIMP interaction in a detector is a challenging task, owing to the rate of WIMP interactions being very small compared with the event rates expected from background radioactivity of present detectors with highest purity and from cosmic radiation. In addition, the recoil energies produced by elastic WIMP-nucleus scattering are very small, in the range of a hundreds of eV to a few tens of keV.

In the early 1980s, a number of groups began researching cryogenic detectors, operating in the millikelvin temperature range, for applications in neutrino physics and DM searches. After over two decades of development, the technique has matured and there are numerous science results that have been obtained with cryogenic detectors. These results cover a wide range of topics: contributions to x-ray astronomy, the spectrometry of heavy biomolecules, the detection of extremely rare events (*e.g.*, neutrino-less double beta decay), and several DM results. The main reason for beginning an intense technology development program more than twenty years ago was the clearly identified need for lower energy threshold and better energy resolution in massive detectors for rare event searches. Cryogenic detectors were, and are, considered to be a most promising technique, requiring only milli-eV for producing a countable information carrier, compared with ~3 eV for semiconductor detectors and in the region of ~100 eV for scintillators. Consequently, at an energy of 5.89 keV (^{55}Fe source), the energy resolutions obtained are 3.2 eV (Si-thermistors) and 3.9 eV (Ti/Au TES) for small cryodetectors. This can be compared to resolutions of ~2000 eV for NaI-Tl scintillators. Although good energy resolution seems not to be a top priority for measuring the largely featureless energy spectra of

WIMP induced nuclear recoil, it is rather important for: 1) identifying backgrounds; 2) low mass WIMP search.

The EDELWEISS experiment is searching for WIMP DM using natural HPGe detectors. The EDELWEISS detectors are cryogenic (work temperature is about 20 mK) Ge bolometers with simultaneous measurement of phonon and ionization signals. The comparison of the two signals provides a highly efficient event-by-event discrimination between nuclear recoils (induced by WIMP and also by neutron scattering) and electrons. The experiment is located in the LSM laboratory to reject background caused by cosmic radiation. EDELWEISS successfully demonstrated it reliability from early stages, when it was the first experiment to reach a sensitivity below $2x10^{-42}$ cm^2 [34]. However first 2 years of running of second phase of the experiment demonstrated that classical germanium detectors-bolometers suffer from the inability to reject events occurring close to the surface of the detectors, for which a deficient charge collection can mimic the ionization yield of nuclear recoils [35, 36]. Despite successes in reducing the surface contamination in EDELWEISS (mostly due to ^{210}Pb daughters), sensitivity levels were still limited to $5x10^{-43}$ cm^2. Therefore, within EDELWEISS were developed detectors with an innovative interleaved electrodes design, able to discriminate against events occurring within 1 mm from the detector surface. With this technique in hands, EDELWEISS is able to explore the 10^{-44} cm^2 range and beyond for WIMP masses from 10 to 100 GeV/c^2 [37]. Now third phase (EDELWEISS-III) of the experiment competitive with world leading dark matter search experiments is ongoing. The EDELWEISS-III project consists in an upgrade of both the EDELWEISS-II setup and detectors. The derived by EDELWEISS constraint for WIMP-nucleon cross section in the so-called low mass region is in tension with hints of WIMP signals from some recent experiments [23-26], thus confirming results obtained with different detection techniques. Nevertheless, in the present time there is an increasing gain of interest for the search of low-mass WIMPs (with mass below 10 GeV/c^2) arising on the one hand from non evidence yet for SUSY at the LHC and on the other hand from new theoretical approaches favoring lighter candidates [17-19]. Thermal relics in this mass range are somewhat disfavored both from constraints set by Fermi-LAT searches for annihilation signals in dwarf galaxies [38], and from the impact that WIMP annihilation would leave on the cosmic microwave background anisotropies [39]. However, many scenarios have been proposed where the evolution of the "dark" and "visible" sectors in the early Universe are such that the relic DM number density is naturally close to the baryon density [40-42]. The current measurements of the corresponding mass densities, Ω_c and Ω_b, then imply that $M_X \sim 5$ GeV/c^2, which is thus definitely become the desired subject of experimental search. EDELWEISS cryogenic bolometers with excellent energy resolutions are then a natural choice for investigation of low mass WIMP region.

Reducing thresholds is a common objective shared by all DM experiments as the theoretical recoil energy spectrum falls typically with an exponential behavior. It is compulsory for low-mass WIMP searches as the spectrum is increasingly softer as the WIMP mass gets lower. The Neganov-Luke boost will be used by EDELWEISS-LT to lower thresholds by amplifying the signal through the application of high voltage biases on collecting electrodes. For Ge detectors, the amplification gain provided by the increase of the collection-bias between two electric potentials V_1 and V_2 is $(1 + Q(E_r)\ V_2 / \epsilon_\gamma)/(1 + Q(E_r)\ V_1 / \epsilon_\gamma)$. Performed by EDELWEISS R&D [43] Fig. A, demonstrated that ~100 eV energy resolution can be reachable with existing EDELWEISS detectors. The next step to improve exclusion limits on the spin independent WIMP-nucleon cross-section is to reach and eventually enter the solar neutrino coherent scattering floor will be a large exposure of 50 000 kgd in a dedicated environment with

high radiopurity level, considering that the R&D upgrade has been achieved on heat baseline resolution, with σ_{Eheat} = 100 eV.

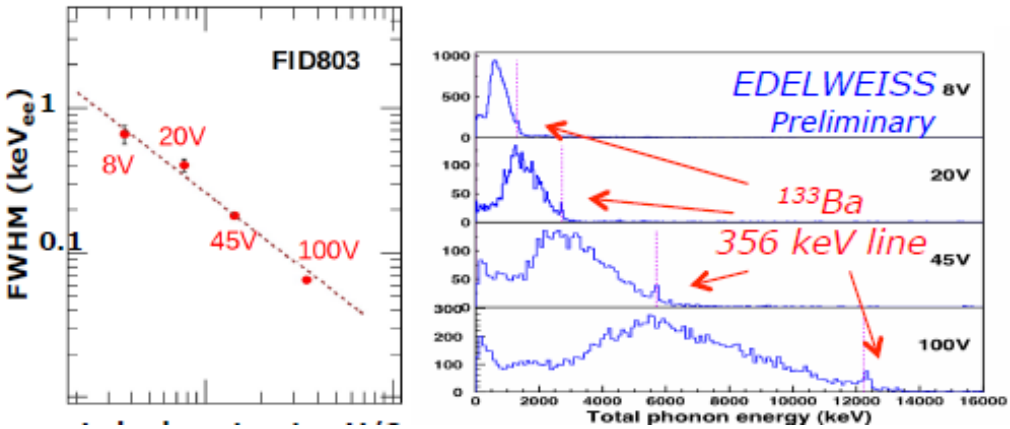

Fig. A: Experimental demonstration from EDELWEISS R&D data of internal amplification of heat signal due to Neganov-Luke effect. Left: energy resolution near threshold versus high voltage biases. Right: ^{133}Ba calibration spectra obtained with HV biases at 8, 20, 45 and 100 V. Observed shift of 356 keV γ- line clearly revealed amplification of the signal.

5. Description of the proposed research

5.1 Base for the experiment

The EDELWEISS experiment is dedicated to the search for non-baryonic cold DM in the form of WIMPs. The direct detection principle consists in the measurement of the energy released by nuclear recoils produced in an ordinary matter target by elastic collisions of WIMPs from the galactic halo. The EDELWEISS detectors are cryogenic HPGe bolometers with simultaneous measurement of phonon and ionization signals. The comparison of the two signals provides an excellent event-by-event discrimination between nuclear recoils (induced by WIMP or neutron scattering) and electronic recoils (induced by β– or γ– radioactivity).

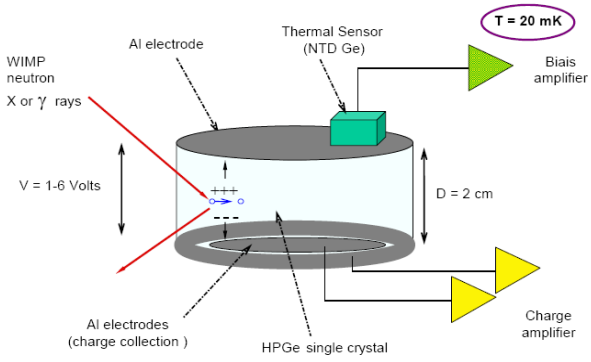

Fig. 3: Scheme of detection principle of a heat and ionization detector

The EDELWEISS-LT will be based on the same experimental infrastructure (shield, dilution cryosystem and low background cryostat, acquisition system) that is currently available in the LSM underground laboratory. It detailed description is given in Appendix 1.

In EDELWEISS bolometers after an interaction in addition to inducing the ionization signal, the drift of the created N_p electrons and holes amplifies the heat signal through Neganov-Luke effect. The full conversion into phonons of the work done on the charge carriers during the drift produces an additional heat contribution E_{NL} equal to:

$$E_{NL} = Q(E_r)\frac{E_r}{\epsilon_\gamma}eV,$$

where V is the collection bias and $Q(E_r)$ is the ionization yield associated to the recoil energy E_r. The quantity $\epsilon_\gamma = 3\ eV$ per electron charge is the average energy required to create an electron-hole pair for electronic recoils in germanium. This quantity is approximately four time less than the energy required by a nuclear recoil to produce a pair, a factor that is taken into account by the normalized ionization yield factor $Q(E_r)$. The total energy of the heat signal is thus:

$$E_{heat} = E_r + E_{NL} = E_r \times \left(1 + \frac{Q(E_r)V}{3}\right).$$

In the limit of biases up to 100 V, E_{NL} dominates and both phonon and ionization signals become proportional to N_p, effectively losing the discrimination power offered by the double measurement. To prevent this, the detectors are commonly operated at biases of a few volts. However, in the context of low-mass WIMP searches, the optimal bias needs to be re-evaluated in view of the constraints imposed by the experimental backgrounds and the required thresholds. To answer this question, a modeling of both EDELWEISS backgrounds and signal, as well as the detector response, has been carried out as described in next subsections.

5.2 Background model

Our background model is data driven by the current physics run of the EDELWEISS-III experiment. Each background component is characterized by a spectral shape, an event rate and an ionization yield $Q(E_r)$. The associated recoil energy spectra are shown in solid lines in Fig. 4 for each individual background described below.

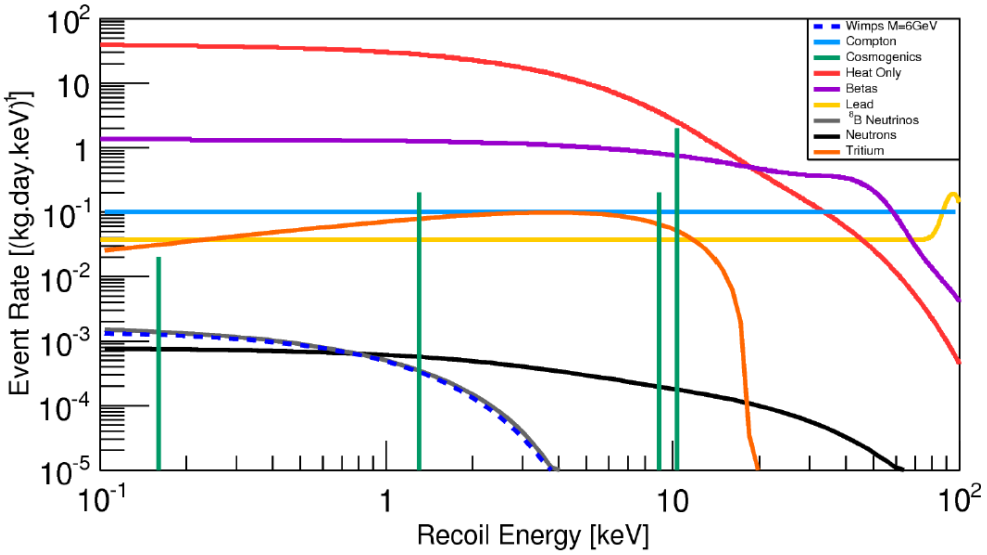

Fig. 4: Event rate for a total exposure of 1 kgd as a function of the recoil energy. Solid lines correspond to the recoil energy spectra of the different background components as indicated by the color code. The blue dashed-line shows the theoretical spectrum of a 6 GeV/c^2 WIMP with σ_{SI} = 4.4 x 10^{-45} cm^2, which is extremely similar to the one of solar ^{8}B neutrinos represented in gray solid-line.

The three backgrounds considered first have been studied by EDELWEISS extensively: 1) Compton induced electronic recoils, which are well described by a flat spectrum in the region of interest. 2) Tritium β-decays, inducing electronic recoils. 3) Cosmogenic activation induced X-ray peaks following the electron capture from atomic shells. Background associated with surface events has been studied during low-mass WIMP analyses of the EDELWEISS-III data using the eight detectors having the best performance: associated energy spectra have been directly measured for top and bottom sides of each detector independently, according to their ionization topologies, and then extrapolated down to lower energy.

Three other backgrounds have been modeled, namely heat-only events and nuclear recoils arising from either neutrons or ^{8}B solar neutrinos: 1) The dominant background in the EDELWEISS-III low energy data is due to heat-only events characterized by no ionization

signal. Investigations are still ongoing to clearly identify the origin of these events and eliminate them. It has been found that the shape of the heat-only background does not vary with bias voltage therefore allowing us to properly model them at 8 V, where we can separate them from other background components and extrapolate them at higher voltages. 2) Radiogenic neutrons can produce single scatter nuclear recoils with the same ionization yield as WIMPs and thus mimic their signal. The neutron spectral shape is obtained from a fit on the EDELWEISS-III GEANT4 simulations. 3) Background from coherent neutrino-nucleus scattering induced by solar ^{8}B neutrinos, whose spectral shape is given in [44], can produce single scatter nuclear recoils with the same ionization yield as neutrons or WIMPs. Also their spectral shape is extremely similar to the one of a 6 GeV/c^2 WIMP with $\sigma_{SI} = 4.4\text{x}10^{-45}$ cm^2.

5.3 Signal model

To compare our projected sensitivities to previous experimental limits, we assume the Standard Halo Model described by a truncated Maxwell-Boltzmann WIMP velocity distribution. For the sake of comparison with running experiments, we will consider the standard values of the different astrophysical parameters: ρ_0 = 0.3 GeV/c^2/cm^3, v_0 = 220 km/s, V_{lab} = 232 km/s and V_{esc} = 544 km/s.

5.4 Thresholds and Neganov-Luke boost

The Neganov-Luke boost will be used by EDELWEISS-LT to lower thresholds by amplifying the signal through the application of high voltage biases on collecting electrodes. For Ge detectors, the amplification gain provided by the increase of the collection-bias between two electric potentials V_1 and V_2 is $(1 + Q(E_r)\ V_2 / \epsilon_\gamma)/(1 + Q(E_r)\ V_1/ \epsilon_\gamma)$. However, since the Neganov-Luke effect linearly depends on the number of charge carriers, its enhancement tends to transform the heat measurement into a pale copy of the ionization measurement and thus gradually disables the discrimination between nuclear and electronic recoils.

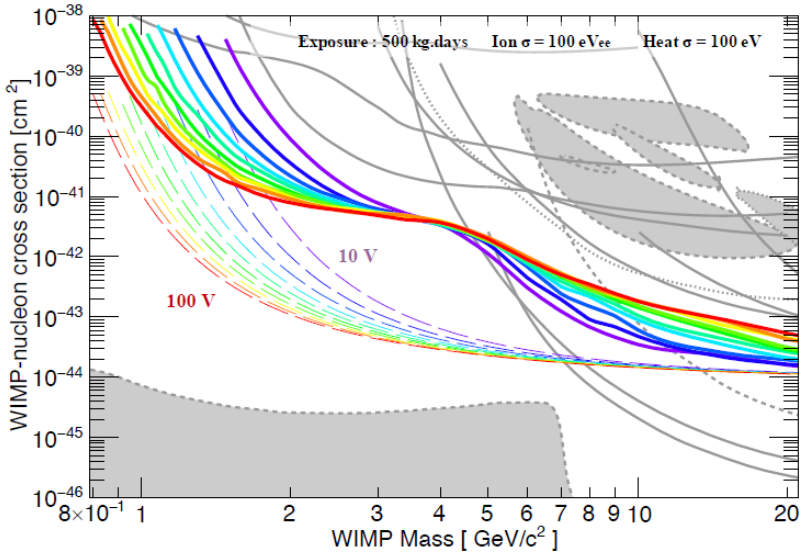

Fig. 5: Influence of the bias voltage on the sensitivity at fixed ionization and heat resolutions (E_{heat} = 100 eV, E_{fid} = 100 eVee). The color code indicates the bias condition rising with a 10 V step from 10 V in purple to 100 V in red. Solid and dashed lines refer to the exclusion limits and to the background-free sensitivities for an exposure of 500 kg d.

Achievable sensitivities will be affected by these two opposite effects. In Fig. 5, we show how the projected sensitivities vary by increasing the bias voltage from 10 V to 100 V while keeping

all other detector characteristics the same: the whole set of EDELWEISS-III backgrounds with a fixed exposure of 500 kg d. We observe that the WIMP mass range is clearly splitted in two regions, below and above 4 GeV/c^2, which are the so-called low-mass and intermediate-mass regions, respectively: - above 4 GeV/c2, we observe a loss of the sensitivity with increasing bias attributable to a decreasing discrimination power. The latter is particularly marked for WIMP masses around 10 GeV/c^2 with a sensitivity reduction by almost one order of magnitude when varying V_{fid} from 10 V to 100 V. - below 4 GeV/c^2, the signal amplification provides sensitivity to lower WIMP masses since both the trigger and analysis thresholds depend on the heat resolution. Furthermore, for a given WIMP mass, high biases lead to much more stringent limits. A similar improvement of both the background-free sensitivities and the exclusion limits in presence of backgrounds is observed, which could indicate that below 4 GeV/c^2, the discrimination power is not affected anymore by the use of high biases.

5.5 EDELWEISS-LT first target

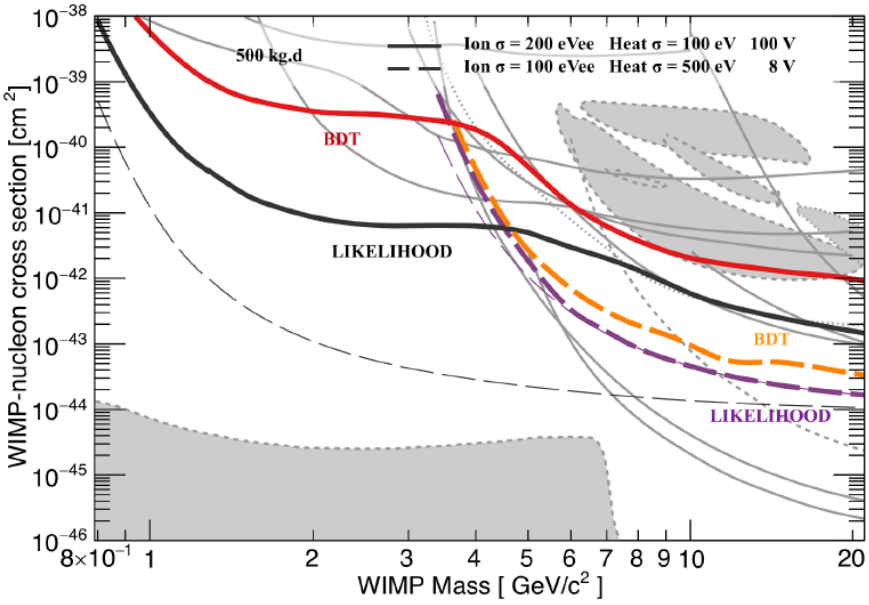

Fig. 6: EDELWEISS-LT projected sensitivities considering that expected R&D upgrades will be achieved either for ionization or heat resolutions, with current LSM setup and background budget. Exclusion limits are derived from both boosted decision tree (BDT) and profile likelihood ratio approaches and for the two extreme bias voltage conditions (8V and 100V). For both values a likelihood analysis gives better limits than a BDT one. Below WIMP masses of 4-5 GeV/c^2, the best sensitivity will be obtained by lowering the thresholds, with the Luke-Neganov boost corresponding to a bias voltage of 100 V, keeping current ionization resolution at 200 eVee and improving heat resolution to 100 eV. Official EDELWEISS-LT low-mass projected sensitivity is thus given by the black solid line exclusion limit. The background-free sensitivity is shown in thin dashed lines.

Fig. 6 presents the two major scenarios for near future low-mass WIMP search with EDELWEISS-LT, considering efforts have been put on the R&D, aiming at improving at least one of the energy resolutions, either for heat or for ionization signals. Sensitivities have been computed with both BDT and likelihood methods for a total exposure of 500 kg d with our current background levels and setup at the LSM. Improving ionization resolution could be done through the implementation of High Electron Mobility Transistors (HEMT) to replace Junction Field Effect Transistors (JFET) used for charge measurements on the Al electrodes collecting

electron-hole pairs. As been shown experimentally a calibrated baseline energy resolution of 91 eV_{ee} has been already achieved with a HEMT-based charge amplifier. Thus, the next R&D step could be the coupling of this charge amplifier to an EDELWEISS detector with the goal of obtaining the ionization resolution at 100 eV_{ee}. Concerning heat resolution improvement, dedicated R&D is also in progress on baseline performance with the achievable objective of reaching σ_{Eheat} = 100 eV: a coherent thermal model has been constructed by EDELWEISS and is used to extract relevant parameters of the heat signal in order to build new thermal sensors which would provide the expected heat energy resolution improvement. It could lead to nuclear recoil energy thresholds ranging from 400 to 100 eV_{nr}, depending on the applied bias voltage across the crystal.

5.6 EDELWEISS-LT 50000 kgd-scale

Further ahead the requirements to the EDELWEISS-LT will to approach the neutrino floor, which corresponds to the coherent scattering of neutrinos from several astrophysical sources as solar ^{8}B neutrinos. Fig. 7 shows sensitivity projections derived from the likelihood analysis for a large exposure of 50000 kg d and resolutions of both heat and ionization channels at 100 eV. Limits are computed for both 8 V and 100 V bias voltages and plotted in purple and black, respectively. Solid lines of Fig. 7 correspond to the expected limits achievable considering the current EDELWEISS background budget, with the exception of heat-only events, which are supposed to be completely suppressed. Thick dashed lines (dot dashed lines) are obtained assuming not only no more heat-only events (a reduction of heat-only events by a factor 100), but also no more neutrons and a reduction of the Compton background by a factor 10. The background-free sensitivity is shown in thin dashed lines.

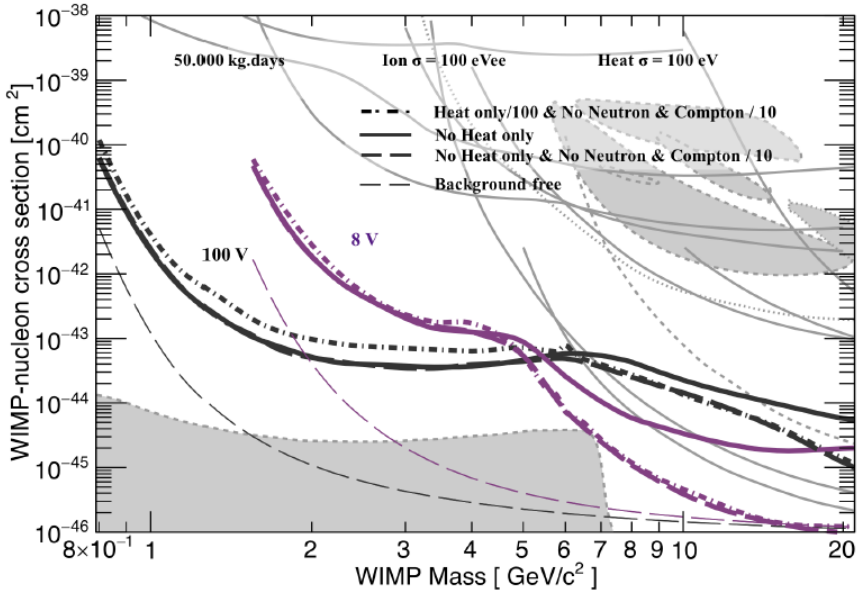

Fig. 7: Projected sensitivities for a large exposure of 50 000 kg d with strongly improved background levels and R&D upgrade performance achieved, with baseline resolutions of heat and ionization channels at 100 eV. Limits are computed using a likelihood analysis at 8 V (purple) and 100 V (black) assuming a suppression of the heat-only background (solid line), and no more neutron background associated with a reduction of the Compton background by a factor 10 (thick dashed line). The background-free sensitivity is shown in thin dashed lines

5.7 Milestones EDELWEISS-LT

Time	**Task**
2017-2018	Search for source of heat only events (Building and testing of HPGe crystals with different termistors, holders, crystal treatments, delivery of the detectors to LSM, measurements)
2018-2019	Delivery (production) of EDELWEISS-LT detectors
2019	Delivery of the upgrades (cryogenics, wiring, electronics, internal shield)
2019	500 kgd EDELWEISS-LT result
2019	Decision about ultimate EDELWEISS-LT detectors design
2019-2020	Accumulation of WIMP data, improving of background, preparation to 50000 kgd phase (production of detector, tests, calibrations).
2020-2021	Upgrade of EDELWEISS shield, cryogenic, start of 50000 kgd phase of EDELWEISS-LT

6. Estimation of human resources

EDELWEISS is a small international collaboration that includes about 50 scientists from France, Germany, UK and JINR.

Institutes forming the collaboration are:

1) Centre de Spectroscopie Nucleaire et de Spectroscopie de Masse, IN2P3-CNRS, Universite Paris XI, Orsay, France
2) Institut de Physique Nucleaire de Lyon-UCBL, IN2P3-CNRS, France
3) Institut Neel, CNRS/UJF, Grenoble, France
4) IRAMIS, CEA, Universite Paris-Saclay, Gif-sur-Yvette, France
5) IRFU, CEA, Universite Paris-Saclay, Gif-sur-Yvette, France
6) Karlsruhe Institute of Technology, Institut fur Kernphysik, Karlsruhe, Germany
7) Karlsruhe Institute of Technology, Institut fur Experimentelle Kernphysik, Karlsruhe, Germany
8) Karlsruhe Institute of Technology, Institut fur Prozessdatenverarbeitung und Elektronik, Karlsruhe, Germany
9) Laboratory of Nuclear Problems, JINR, Dubna, Russia
10) University of Oxford, Department of Physics, Oxford, UK.
11) University of Sheffield, Department of Physics and Astronomy, Sheffield, UK

By performing of previous stages of EDELWEISS the collaboration demonstrated that has experts required to build and produce new innovative HPGe detectors, building of mK cryostat and it running, performing of low background measurements in underground environment.

JINR group human resources are

Name	Category	Responsibilities	Time that each participant will give to the work under the Project in relation to its Full Time Equivalent(FTE)
V. Brudanin	Head of department	Administrative work	0.1
Z. Kalaninova	Researcher	MC, data analysis	1.0
A. Lubashevskiy	Senior Researcher	MC, running of JINR low threshold detectors, radon measurement, data analysis	0.2
D. Filosofov	Head of sector	Radiochemistry, low background technique	0.3
N. Mirzaev	Junior researcher	Radiochemistry, low background technique	0.3
L. Perevoshchikov	Researcher	Nuclear spectroscopy	0.2
D. Ponomarev	Engineer	Neutron background measurements, detectors building, testing. Experiment running.	0.5
A. Rakhimov	Junior researcher	Radiochemistry, neutron activation analysis, nuclear spectroscopy	0.3
I. Rozova	Engineer	Data analysis	0.5
S. Rozov	Engineer	Background study and improvement, detector building, testing, calibration, running.	0.7
K. Shakhov	Engineer	Radon gas, radon emanation detection / development and measurements	1.0
E. Yakushev	Head of sector	Administrative work, radon and neutron measurements, detectors building, commissioning, running	0.7
Total FTE (Engineers): 2.7, Total FTE (Scientific staff): 3.1, Total FTE: 5.8			

7. SWOT (Strengths, Weaknesses, Opportunities, Threat) analysis

First let point out major risk for EDELWEISS-LT stage.

The schedule of the project can be significantly affected due to factors connected with stability of running of all components of the experiment including cryosystem with dilution cryostat and it stability, electronics, acquisition system, subsystems (muon veto, anti-radon factory, shield suspension, etc). Though failure of different components of the setup is difficult to predict, the collaboration already accumulated more than 12 years of running of the setup, with accumulated experience in fixing of arising problems including problems with the cryosystem in short time.

One of critical part of any low background experiment is avoiding of it contamination from outside. The trace activities on unacceptable level can be accumulated due to calibrations with not properly tested (on radioactive leak and integrity) radioactive sources, due to radon and

other radioactive gases in atmosphere, due to dust and dirt. To avoid these problems set of special procedure is in place during all stages of experiment starting from detector production to calibration measurements. Only EDELWEISS certified materials can be entered into the clean room surrounding the setup. All works performed in the clean room are under continuous control of dust and radon level. Only double encapsulated and properly tested radioactive sources are used for calibrations. Minimal quantity of such sources is allowed.

Now, let consider the scientific challenges: The main challenge for EDELWEISS-LT rare-event search experiment is to distinguish a potential WIMP signal from recoils induced by natural radioactivity, cosmic rays and other sources. In other words, the most important problem in any Dark Matter search experiment is the background. Thus the key to the success of the experiment is the possibility to identify with high efficiency the background events which can mimic WIMP signal. The EDELWEISS experiment together with traditional methods of background reduction uses several special methods for discrimination of WIMP induced events (heat/ionization measurements, FID detectors for discrimination of surface events, PSD for reduction of the noise). In beginning of the current stage of EDELWEISS-LT main task will be to find the source of so-called heat-only events appearing as the main background component. This work will be done in parallel with accumulation of 500 kg d with Neganov-Luke amplification of the heat signal. On this stage final result will be not significantly affected by heat-only background and the desired sensitivity level at 10^{-41} cm^2 for low mass WIMPs will be obtained. In the same time the collaboration has about two years to find and eliminate the source of heat only events. To move to 50000 kg d phase EDELWEISS-LT will have to improve also total background index including neutrons and gammas. The work in this direction is ongoing and includes searching for low background materials, a comprehensive experimental study of the existing shield with the aim of it further improvement, MC of the detector and shields.

Finally, let consider the existing competitions from other experiments. As already was discussed in the Introduction section liquid xenon experiments stand now as a leader in high-mass WIMP searches (10 GeV/c^2 to 1 TeV/c^2), thus a division of work is taking shape in the hunt for DM particles: an exploration of the high-mass region led by experiments with liquid scintillators, and light WIMP models to be tested by cryogenic detector experiments. There is only one experiment targeting similar aims with HPGe detectors-bolometers: the CDMS experiment at SNO laboratory. At the first stage of EDELWEISS-LT (500 kg d) our experiment considering existing schedules will receive results before of CDMS. For 50000 kg d there is a chance of targeting of this aim together with CDMS at SNO laboratory with keeping of current EDELWEISS setup for R&D. However this will be strongly depends from the background level demonstrated by CDMS in first runs in the SNO laboratory. As an alternative significant upgrade of current EDELWEISS shields is also possible. There are some other experiments targeting of low mass WIMP region with different nuclei. All these experiment are complimentary to each other since allowing to make "true" discovery of WIMPs. Such conclusion is also valid for results of accelerator and not-direct search experiments.

8. Contribution of JINR group

Dubna team of the EDELWEISS project is formed on the base of Department of Nuclear Spectroscopy, DLNP. This department has huge almost 50-year experience in high-precision nuclear spectroscopy using semiconductor and scintillator detectors in general and 30-years experience of rare process study in underground environment.

Dubna team participates and makes commitment to follow parts of EDELWEISS project:

1) Assembly and commissioning of experimental setup;
2) Data taking (include daily routine procedures, as well as regular and special calibration runs);
3) Low background study and development of methods of neutron and radon detection; screening of materials on their radioactive contamination;
5) Development of new detectors;
6) Detector simulations, data acquisition (digital filtering) and data analysis.

Below some of above topics described in details:

8.1 Assembly and commissioning of EDELWEISS setup, data taking

From start of the second phase of EDELWEISS experiment in 2005 Dubna team did a sufficient commitment in setup assembly. Our responsibilities include commissioning of EDELWEISS environment (clean room operation and procedures, developing procedures of operation with radioactive sources on the site, etc); participation in cryostat assembly and detector installation and wiring; sources on site certifications before its using for EDELWEISS. We participate in commissioning and debugging of electronics and data taking. The data taking process includes need for everyday procedures as detectors regenerations, calibrations, etc. That requires participation in shift duties shared between experts on data taking in few EDELWEISS institutions. Significant part of this work is done from Dubna.

8.2 Low background study and development of methods of neutron and radon detection

For unbiased interpretation of results of DM search experiments it is critically important to have a wide knowledge and understanding of all background sources. But not only value of background but also changes of it with time are important. Main activities of Dubna team are connected with experimental and MC studies of backgrounds. Experimental studies include:

a) participation in material selection process (measurements on designated for these measurements and located at LSM HPGe low background spectrometers);
b) continuous monitoring of fast neutrons with build at JINR detection system;
c) measurement of fast neutrons produced by muons in coincidence with EDELWEISS muon veto system;
d) measurement of thermal neutrons with build in JINR low background neutron detection system;

e) monitoring of radon level at proximity to EDELWEISS cryostat and at output of anti-radon factory as well at detector storage with build in JINR high sensitive (1 mBq/m^3) and low background radon detection systems.

Main results of above studies are:

1) We measured fast and thermal neutron levels and its changes with time at LSM underground laboratory. Continuous measurements of neutron flux are already continued for about 10 years.

2) We achieved level of ^{222}Rn at EDELWEISS cryostat proximity below of 20 mBq/m^3. With continuous control of the radon level at time of WIMPs data taking, gamma background at EDELWEISS has been reduced by several times.

Some of detectors owning by JINR group are shown on figures 9-11.

Fig. 9: Detectors developed at JINR for study of neutron background at EDELWEISS environment. Left picture is detector of fast neutrons; right one is detector of thermal neutrons (on the wall).

Fig. 10: Photo of the ^{3}He filled proportional counter installed at close proximity to the EDELWEISS cryostat.

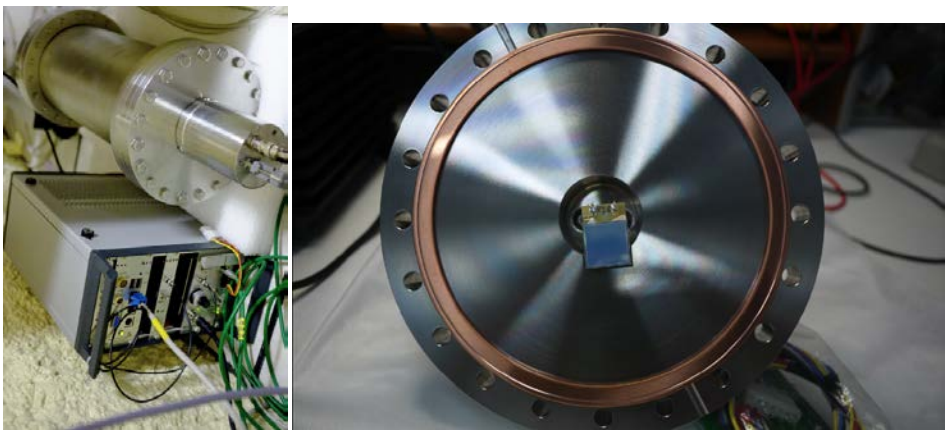

Fig. 11: Mobile high sensitive radon detection system.

8.3 MC simulations of background at EDELWEISS

Performed in our group MC studies were mainly dedicated to interpretation of background caused by ^{210}Pb trace contamination of detectors' surfaces. To study this background, source of ^{210}Pb has been prepared and installed into EDELWEISS in front of one of the detector. As first step we created detailed particle generator, which simulates particles from ^{210}Pb → ^{210}Bi → ^{210}Po → ^{206}Pb decay chain, including low energy atomic process. Low energy physic packages of Geant4 and Penelope toolkits have been used for particle's transport. Using experimental information about number of detected α from ^{210}Po decay we were able to explain nature of background events in low-energy region including nuclear recoil band. This provided key information on interpretation of detected background at WIMPs runs. From comparison of experimental and MC data we were also able to obtain function of the efficiency of charge collection on the detector's surface. This parameter is important for applying of physics based cuts on fiducial volume.

As result of our MC work 2 main aims were achieved:

1) We clearly demonstrated that surface background events are connected with lead contamination (we were able to reproduce experimental spectrum in low energy region based only on known intensity of alpha particles with high energy).
2) Parameters for fiducial volume cuts for ID/FID detectors were estimated.

8.4 Low radioactivity, study in LSM

In LSM our group is (partly) responsible for selection of materials with low radioactive level. Two HPGe detectors available for screening of material radioactivities in LSM. Additionally for detailed and deep study of background conditions at LSM and at EDELWEISS at particular we build and delivered to EDELWEISS site alpha spectrometer with an alpha detector of high area.

Fig. 14: Photo of the vacuum chamber of the alpha spectrometer containing electronic module (preamplifier, shaping amplifier, power supply, vacuum control module).

8.5 Low threshold detectors for EDELWEISS

In 2010 EDELWEISS collaboration decided to extend it research to low mass WIMPs with using low threshold point contact HPGe detectors. This work is extremely important for JINR since provides base and infrastructure for development and test of low radioactive low energy threshold setups for neutrino experiments at Kalinin NPP. The EDELWEISS-I shield is provided for the point contact detector tests. In the same time other facilities as clean room, radon-free air, etc are also available and used. In 2018 JINR group will start of tests of unique point contact detectors with masses from 1 to 1.5 kg and with energy thresholds at about 200 eV.

9. References

[1] L. Bergstrom, Non-Baryonic Dark Matter - Observational Evidence and Detection Methods, Rep.Prog. Phys. **63** (2000) 793 [hep-ph/0002126]

[2] G. Bertone, D. Hooper and J. Silk, Particle Dark Matter: Evidence, Candidates and Constraints, Phys. Rep. **405** (2005) 279 [hep-ph/0404175]

[3] J.L. Feng, Dark Matter Candidates from Particle Physics and Methods of Detection, Ann. Rev. Astron.Astrophys. **48** (2010), 495 [arXiv:1003.0904]

[4] J.L. Feng, Supersymmetry and Cosmology, Ann. Phys. **315** (2005) 2–51 [hep-ph/0405215]

[5] D.G. Cerdeno and A.M. Green, Direct detection of WIMPs, Chapter 17 of "Particle Dark Matter: Observations, Models and Searches" ed. G. Bertone, (2010) Cambridge University Press [arXiv:1002.1912]

[6] XENON10 collaboration, E. Aprile et al., Design and Performance of the XENON10 Dark Matter Experiment, Astropart. Phys. **34** (2011) 679-698 [arXiv:1001.2834]

[7] XENON100 collaboration, E. Aprile et al., First Dark Matter Results from the XENON100 Experiment Phys. Rev. Lett. **105** (2010) 131302 [arXiv:1005.0380v3]

[8] LUX collaboration, D.S. Akerib et al., The Large Underground Xenon (LUX) Experiment, Nucl. Instrum. Meth. in Phys. Res. A **577** (2013) 111–126 [arXiv:1211.3788]

[9] PandaX collaboration, X.G. Cao et al., PandaX: A Liquid Xenon Dark Matter Experiment at CJPL, Sci. China Phys. Mech. Astron. **57** (2014) 1476–1494 [arXiv:1405.2882]
[10] DarkSide-50 collaboration, P. Agnes et al., First Results from the DarkSide-50 Dark Matter Experiment at Laboratori Nazionali del Gran Sasso, Phys. Lett. B **743** (2015) 456–466 [arXiv:1410.0653]
[11] CRESST-II Collaboration, G. Angloher et al., Commissioning Run of the CRESST-II Dark Matter Search, Astropart. Phys. **31** (2009) 270-276 [arXiv:0809.1829]
[12] SuperCDMS collaboration, R. Agnese et al., Improved WIMP-search reach of the CDMS II
germanium data, Phys. Rev. D **92** (2015) [arXiv:1504.05871]
[13] DAMA collaboration, R. Bernabei et al., Performances of the new high quantum efficiency PMTs in DAMA/LIBRA, JINST **7** (2012) P03009
[14] E. Aprile et al. [XENON], XENON100 Dark Matter Results from a Combination of 477 Live Day, Phys. Rev. D 94, (2016) 122001, arXiv:1609.06154.
[15] D.S. Akerib et al. [LUX], Results from a search for dark matter in the complete LUX exposure, Phys. Rev. Lett. 118 (2017) 021303, arXiv:1608.07648.
[16] A. Tan et al. [PandaX-II], Dark Matter Results from First 98.7-day Data of PandaX-II Experiment, Phys. Rev. Lett. 117 (2016) 121303, arXiv:1607.07400.
[17] R. Essig, J. Kaplan, P. Schuster and N. Toro, On the Origin of Light Dark Matter Species (2010), arXiv:1004.0691
[18] C. Cheung, J.T. Ruderman, L.-T. Wang and I. Yavin, Kinetic Mixing as the Origin of Light Dark Scales, Phys. Rev. D 80 (2009) 035008, arXiv:0902.3246.
[19] D. Hooper and W. Xue, Possibility of Testing the Light Dark Matter Hypothesis with the Alpha Magnetic Spectrometer, Phys. Rev. Lett. 110 (2013) 041302.
[20] A. Falkowski, J.T. Ruderman and T. Volansky, Asymmetric Dark Matter from Leptogenesis, JHEP 1105 (2011) 106, arXiv:1101.4936.
[21] K. Petraki and R.R. Volkas, Review of asymmetric dark matter, Int. J. Mod. Phys. A 28 (2013) 1330028, arXiv:1305.4939
[22] K. M. Zurek, Asymmetric Dark Matter: Theories, Signatures, and Constraints, Phys. Rep. 537 (2014) 91, arXiv:1308.0338
23] CoGeNT Collaboration, C. Aalseth et al, Results from a Search for Light-Mass Dark Matter with a p-Type Point Contact Germanium Detector, Phys. Rev. Lett. 106 (2011) 131301 [arXiv:1002.4703].
[24] CRESST Collaboration, G. Angloher et al., Results from 730 kg days of the CRESST-II Dark Matter Search, Eur. Phys. J. C72 (2012) 1971 [arXiv:1109.0702].
[25] CDMS Collaboration, R. Agnese et al., Silicon Detector Dark Matter Results from the Final Exposure of CDMS II, Phys. Rev. Lett. 111 (2013) 25, 251301 [arXiv:1304.4279].
[26] DAMA Collaboration, R. Bernabei et al., Final model independent result of DAMA/LIBRA-phase1, Eur. Phys. J. C 73 (2013) 2648 [arXiv:1308.5109].
[27] EDELWEISS Collaboration, E. Armengaud et al., Search for low-mass WIMPs with EDELWEISS-II heat-and-ionization detectors, Phys. Rev. D86 (2012) 051701(R) [arXiv:1207.1815].
[29] LUX Collaboration, D. Akerib et al., First Results from the LUX Dark Matter Experiment at the Sanford Underground Research Facility, Phys. Rev. Lett. 112 (2014) 091303 [arXiv:1310.8214].
[30] J. Barreto et al., Direct search for low mass dark matter particles with CCDs, Phys. Lett. B

711 (2012) 264?269 [arXiv:1105.5191].
[31] CRESST Collaboration, G. Angloher et al., Results on light dark matter particles with a low-threshold CRESST-II detector, Eur. Phys. J. C 76 (2016) 25 [arXiv:1509.01515].
[32] SuperCDMS Collaboration, R. Agnese et al., New Results from the Search for Low-Mass Weakly Interacting Massive Particles with the CDMS Low Ionization Threshold Experiment, Phys. Rev. Lett. 116 (2016) 071301 [arXiv:1509.02448].
[33] SuperCDMS Collaboration, R. Agnese et al., Search for Low-Mass Weakly Interacting Massive Particles with SuperCDMS, Phys. Rev. Lett. 112 (2014) 24, 241302 [arXiv:1402.7137].
[34] A. Benoit, et al, 2002. Phys. Lett. B545, 43
[35] D. Sanglard et al., Phys. Rev. D 71 (2005) 122002.
[36] S. Fiorucci et al. (EDELWEISS Coll.), Astropart. Phys. 28 143 (2007).
[37] E Armengaud et al. “Final results of the EDELWEISS-II WIMP search using a 4-kg array of cryogenic germanium detectors with interleaved electrodes”. Phys.Lett. B702 (2011), pp. 329–335. arXiv: 1103.4070 [astro-ph.CO]
[38] Fermi-LAT Collaboration, M. Ackermann et al., Searching for Dark Matter Annihilation from Milky Way Dwarf Spheroidal Galaxies with Six Years of Fermi Large Area Telescope Data, Phys. Rev. Lett. 115 (2015) 23, 231301 [arxiv:1503.02641].
[39] Planck Collaboration, P.A.R. Ade et al., Planck 2015 results. XIII. Cosmological parameters [arxiv:1502.01589].
[40] D. Kaplan, M. Luty and K. Zurek, Asymmetric dark matter, Phys. Rev. D 79 (2009) 115016 [arxiv:0901.4117].
[41] A. Falkowski, J. Ruderman and T. Volanski, Asymmetric Dark Matter from Leptogenesis, J. High Energy Phys. 1105 (2011) 106 [arXiv:1101.4936].
[42]K. Petraki and R. Volkas, Review of asymmetric dark matter, Int. J. Mod. Phys. A28 (2013) 1330028 [arXiv:1305.4939].
[43] Q Arnaud, et al (EDELWEISS collaboration) Optimizing EDELWEISS detectors for low-mass WIMP searches, 2017, arXiv preprint arXiv:1707.04308, submitted to Phys. Rev. D
[44]F. Ruppin et al., Complementarity of dark matter detectors in light of the neutrino background, Phys. Rev. D 90 (2014) 083510.

Appendix 1, EDELWEISS experiment, technical paper

E Armengaud, et al (EDELWEISS collaboration) Performance of the EDELWEISS-III experiment for direct dark matter searches, Journal of Instrumentation, 12, 08, P08010, 2017, arXiv preprint arXiv:1706.01070
Printed as a separate document

Appendix 2, WIMPs

Main subject of the EDELWEISS experiment are WIMPs, so here is short explanation about their nature. Particles that were in the thermal equilibrium in the early stages of the Universe and that decoupled from the primordial plasma when they were non-relativistic, could potentially be cold Dark Matter. These particles would have to be massive to account for (a part of) the Dark Matter. They would also have to be weakly interactive, which would explain why they have not been observed yet and would allow their relic density today to be cosmologically relevant. Namely such particles are covered with a generic name Weakly Interactive Massive Particles (WIMPs). To turn the argument around, it can be shown that the relic density of these particles today is inversely proportional to their annihilation cross-section. If their density today is to be of the order of the critical density, the annihilation cross-section must be of the weak-interaction scale. Note, however, that this does not imply weak interactions themselves! By the crossing argument, the elastic scattering off of nucleons should be of the weak scale as well. WIMPs are particularly attractive because a natural WIMP candidate is offered by SUSY. Of importance for cosmology is the fact that SUSY requires the existence of a new particle for each particle in the Standard Model. These SUSY partners differ by half a unit of spin, and come under the names of sleptons (partners of the eptons), squarks (partners of the quarks), gauginos (partners of the gauge bosons) and higgsinos (partners of the Higgs bosons). Sleptons and squarks have spin 0, and gauginos and higgsinos have spin 1/2. If SUSY would be an explicit symmetry of nature, superpartners would have the same mass as their corresponding Standard Model particle. However, no Standard Model particle has a superpartner of the same mass. It is therefore assumed that SUSY, much as the weak symmetry, is broken. Superpartners can then be much heavier than their normal counterparts, explaining why they have not been detected so far. However, the mechanism of SUSY breaking is not completely understood, and in practice it is implemented in the model by a set of supersymmetry-breaking parameters that govern the values of the superpartners masses (the superpartners couplings are fixed by supersymmetry). Namely, the lightest supersymmetric particle in the Minimal Supersymmetric Standard Model (MSSM) is expected to be stable, massive and interact with ordinary matter on the weak scale - exactly the properties of a WIMP. Moreover, SUSY very elegantly solves some of the remaining problems with the Standard Model of Particles, such as the mass hierarchy problem, and is, therefore, one of the most favored extensions of the Standard Model. Thus, WIMP as Dark Matter is certainly “fashionable”.

Published by IOP Publishing for Sissa Medialab

Received: *June 23, 2017*
Accepted: *July 23, 2017*
Published: *August 16, 2017*

Performance of the EDELWEISS-III experiment for direct dark matter searches

The Edelweiss collaboration

E. Armengaud,[a] **Q. Arnaud,**[b,1] **C. Augier,**[b,*] **A. Benoît,**[c] **L. Bergé,**[d] **T. Bergmann,**[e] **J. Billard,**[b] **T. de Boissière,**[a] **G. Bres,**[c] **A. Broniatowski,**[d,f] **V. Brudanin,**[g] **P. Camus,**[c] **A. Cazes,**[b] **M. Chapellier,**[d] **F. Charlieux,**[b] **M. De Jésus,**[b] **L. Dumoulin,**[d] **K. Eitel,**[h] **D. Filosofov,**[g] **N. Foerster,**[f] **N. Fourches,**[a] **G. Garde,**[c] **J. Gascon,**[b] **A. Giuliani,**[d] **M. Grollier,**[c] **M. Gros,**[a] **L. Hehn,**[h,2] **S. Hervé,**[a] **G. Heuermann,**[f] **V. Humbert,**[d] **Y. Jin,**[i] **A. Juillard,**[b] **C. Kéfélian,**[b,f,3] **M. Kleifges,**[e] **V. Kozlov,**[f] **H. Kraus,**[j] **V. A. Kudryavtsev,**[k] **H. Le-Sueur,**[d] **J. Lin,**[j,4] **R. Maisonobe,**[b] **M. Mancuso,**[d] **S. Marnieros,**[d] **A. Menshikov,**[e] **X.-F. Navick,**[a] **C. Nones,**[a,*] **E. Olivieri,**[d] **P. Pari,**[l] **B. Paul,**[a] **D. Poda,**[d] **E. Queguiner,**[b] **M. Robinson,**[k] **H. Rodenas,**[c] **S. Rozov,**[g] **V. Sanglard,**[b] **B. Schmidt,**[f,2] **S. Scorza,**[f,5] **B. Siebenborn,**[h] **D. Tcherniakhovski,**[e] **L. Vagneron,**[b] **M. Weber,**[e] **E. Yakushev,**[g] **X. Zhang**[j,1] **and A. Zolotarova**[a]

[a] *IRFU, CEA, Université Paris-Saclay, F-91191 Gif-sur-Yvette, France*
[b] *Univ Lyon, Université Lyon 1, CNRS/IN2P3, IPN-Lyon, F-69622, Villeurbanne, France*
[c] *Institut Néel, CNRS/UJF, 25 rue des Martyrs, BP 166, 38042 Grenoble, France*
[d] *CSNSM, Univ. Paris Sud, CNRS/IN2P3, Université Paris-Saclay, 91405 Orsay, France*
[e] *Karlsruher Institut für Technologie, Institut für Prozessdatenverarbeitung und Elektronik, Postfach 3640, 76021 Karlsruhe, Germany*
[f] *Karlsruher Institut für Technologie, Institut für Experimentelle Kernphysik, Gaedestr. 1, 76128 Karlsruhe, Germany*
[g] *JINR, Laboratory of Nuclear Problems, Joliot-Curie 6, 141980 Dubna, Moscow Region, Russian Federation*
[h] *Karlsruher Institut für Technologie, Institut für Kernphysik, Postfach 3640, 76021 Karlsruhe, Germany*
[i] *Laboratoire de Photonique et de Nanostructures, CNRS, Route de Nozay, 91460 Marcoussis, France*

*Corresponding author.
[1] Now at Physics Department, Queen's University, Kingston, ON, Canada.
[2] Now at Nuclear Science Division, Lawrence Berkeley National Laboratory, Berkeley, CA, US.
[3] Now at Physics Department, University of California, Berkeley, CA, U.S.A.
[4] Now at SNOLAB, Lively, ON, Canada.

https://doi.org/10.1088/1748-0221/12/08/P08010

2017 JINST 12 P08010

[j] University of Oxford, Department of Physics, Keble Road, Oxford OX1 3RH, U.K.
[k] University of Sheffield, Department of Physics and Astronomy, Sheffield, S3 7RH, U.K.
[l] DSM/IRAMIS, CEA, Université Paris-Saclay, F-91191 Gif-sur-Yvette, France

E-mail: claudia.nones@cea.fr

Abstract: We present the results of measurements demonstrating the efficiency of the EDELWEISS-III array of cryogenic germanium detectors for direct dark matter searches. The experimental setup and the FID (Fully Inter-Digitized) detector array is described, as well as the efficiency of the double measurement of heat and ionization signals in background rejection. For the whole set of 24 FID detectors used for coincidence studies, the baseline resolutions for the fiducial ionization energy are mainly below 0.7 keV$_{ee}$ (FHWM) whereas the baseline resolutions for heat energies are mainly below 1.5 keV$_{ee}$ (FWHM). The response to nuclear recoils as well as the very good discrimination capability of the FID design has been measured with an AmBe source. The surface β- and α-decay rejection power of $R_{\rm surf} < 4 \times 10^{-5}$ per α at 90% C.L. has been determined with a ^{210}Pb source, the rejection of bulk γ-ray events has been demonstrated using γ-calibrations with ^{133}Ba sources leading to a value of $R_{\gamma-{\rm mis}-{\rm fid}} < 2.5 \times 10^{-6}$ at 90% C.L.. The current levels of natural radioactivity measured in the detector array are shown as the rate of single γ background. The fiducial volume fraction of the FID detectors has been measured to a weighted average value of (74.6 ± 0.4)% using the cosmogenic activation of the ^{65}Zn and ^{68,71}Ge isotopes. The stability and uniformity of the detector response is also discussed. The achieved resolutions, thresholds and background levels of the upgraded EDELWEISS-III detectors in their setup are thus well suited to the direct search of WIMP dark matter over a large mass range.

Keywords: Bolometers for dark matter research; Cryogenic detectors; Dark Matter detectors (WIMPs, axions, etc.); Large detector-systems performance

ArXiv ePrint: 1706.01070

2017 JINST 12 P08010

Contents

1 Introduction **2**

2 EDELWEISS FID detectors **4**

3 Cryogenic system **6**

4 Active and passive shielding **9**
4.1 Shielding against cosmogenic background 9
4.2 Shielding against radiogenic background 10

5 Readout of signal channels **11**
5.1 Heat channel readout 12
5.2 Ionization channel readout 12
5.3 Time resolved ionization readout 13
5.4 Upgrade for the Neganov-Luke amplification 14

6 Data acquisition system **15**
6.1 The DAQ crate 15
6.2 SAMBA 17
6.3 ORCA 18

7 Detector performance **19**
7.1 Energy calibration and detector regeneration procedures 19
7.1.1 Radioactive sources 20
7.1.2 Energy calibration procedure 20
7.1.3 Definition of energy variables 22
7.2 800-g FID detector baseline resolutions 23
7.3 Fiducial volume of the 800-g FID detectors 24
7.3.1 Definition of fiducial cuts 24
7.3.2 Determination of the fiducial volume 27
7.4 γ-ray rejection factor 31
7.5 Surface rejection factor 32

8 Performance of the EDELWEISS-III detector array **34**
8.1 Shielding performance against μ-induced neutron backgrounds 36
8.2 Shielding performance against radiogenic neutrons and γ-rays 36

9 Summary and prospects **39**

2017 JINST 12 P08010

1 Introduction

There is strong evidence in favour of the existence of non-baryonic dark matter at almost every cosmic scale [1, 2]. Theories and simulations regarding hierarchical structure formation indicate that this non-luminous component may manifest itself in the form of a gas of Weakly Interacting Massive Particles (WIMPs) [3]. There is no viable candidate in the Standard Model of particle physics for the composition of this cold dark matter gas. There are however theories beyond the Standard Model, specifically developed to solve problems inherent to elementary particle physics, that lead to very attractive dark-matter candidates in the form of WIMPs. Natural and popular candidates, like the supersymmetric neutralino, have a predicted mass in the range of a few GeV/c^2 to TeV/c^2 and an elastic scattering cross section on nucleons at or below the weak scale [4]. Furthermore, they are characterized by a dominant interaction with atomic nuclei, inducing therefore low-energy nuclear recoils in the target material, and could be thus detected in the so-called direct detection experiments [5]. There is an intense experimental activity on dark matter direct detection since many years, for which the most promising results have been obtained with liquid noble or cryogenic detectors: see e.g. [6–13] and references therein for information on their technical designs and performance.

The goal of the EDELWEISS experiment is to perform a direct search for WIMPs from the galactic halo using an array of cryogenic germanium detectors able to identify events consisting of WIMP-induced nuclear recoils with a kinetic energy in the keV to tens of keV range. The main challenge for this rare-event search experiment is to distinguish a potential WIMP signal from recoils induced by natural radioactivity and cosmic rays.

The EDELWEISS detectors, working at 18 mK, are hosted inside a cryostat and operated in a radiopure underground environment located in the Modane Underground Laboratory (Laboratoire Souterrain de Modane, LSM) in France. As shown in figure 1, shields of polyethylene (PE) and lead, as well as an active muon veto, surround the detector setup allowing both passive and active background rejection. The remaining dominant background, due to β and γ natural radioactivity, is suppressed by using the capability of the germanium detectors of clearly separating the electron recoils induced by β and γ radiation from nuclear recoils, which are potential signals, using a double-readout event-by-event discrimination: a calorimetric measurement of the total deposited energy and the ionization yield. At the operating temperature of 18 mK the nuclear recoils induce a temperature increase of roughly 0.1 µK per 1 keV that is measured with heat sensors. The ionization signal is collected on electrodes covering all the surfaces.

In 2009 and 2010, the EDELWEISS collaboration conducted a WIMP search using an array of ten 400 g Inter-Digitized (ID) detectors [14]. It was found that the remaining events after rejection were compatible with the ionization yield of electron recoils and revealed the limitations of the ID design. The results of the background studies performed in the context of EDELWEISS-II have highlighted a need of improving the shielding. It was also shown that the primary source of γ background in EDELWEISS-II originated from a range of copper elements in the vicinity of the detectors, whereas neutron background was mainly dominated by the (α, n) reactions in electronic components inside the lead shielding [15].

The initial goal of EDELWEISS-III was to probe WIMP-nucleon cross sections down to 10^{-9} pb for a WIMP mass of ≈ 50 GeV with 12 000 kg · d exposure. Many technical upgrades were made

2017 JINST 12 P08010

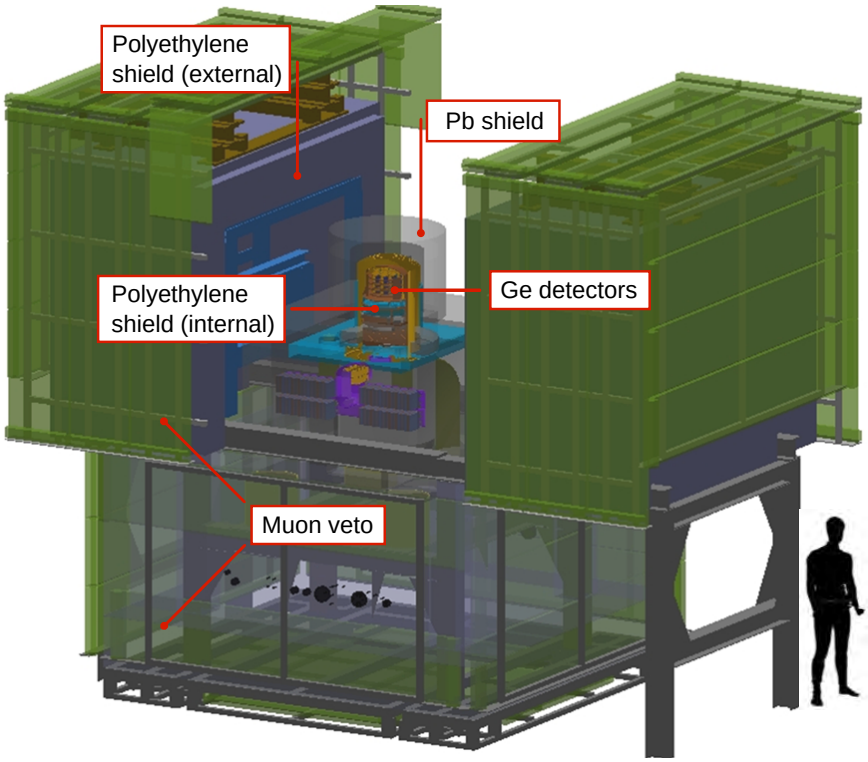

Figure 1. Schematic view of the EDELWEISS-III setup showing in the center the cryostat hosting the germanium bolometers, surrounded by passive lead (Pb) and polyethylene shields and an active muon veto in order to protect the detectors from various backgrounds.

to reduce the residual background to less than one event for one year of data taking. With the aim of increasing the detection efficiency for low-mass WIMPs at [$\approx$5,20] GeV, both the electronics (readout and DAQ) and the cryogenic systems have been modified to improve the energy resolutions and subsequently lower the energy threshold. These changes have been coupled to a new germanium bolometer design, called FID (Fully Inter-Digitized) detector, that allows to reach very good active background rejection as described in this paper.

The detector characterization being the focus of this paper is based on data obtained during a period of 10 months. For this run (Run 308) 36 FID detectors were installed in the EDELWEISS cryostat in a tower array configuration. This long run, for which only 24 detectors were read out, was focused on WIMP search, with frequent calibrations and several tests in between. The studies presented here were performed on a data set which was not blinded for the WIMP search analysis, notably multiple hit events, events outside the fiducial volume and fiducial events with an ionization yield larger than 0.5. Shorter dedicated data taking periods have been used to demonstrate the rejection power efficiency or the high-voltage capabilities of the FID design.

The present paper is organized as follows: sections 2 to 4 focus on the general description of the detectors, cryogenics and shielding, then sections 5 and 6 describe the read out and acquisition parts. It is followed by an overview of the detector performance in terms of resolution and active background rejection (section 7), while the efficiencies of the shielding and muon-veto are given in section 8. Concluding remarks and prospects can be found in section 9.

2017 JINST 12 P08010

2 EDELWEISS FID detectors

Detectors used in the EDELWEISS-III experiment, called FID, are made of ultrapure germanium cylindrical crystals with a height of 4 cm, a diameter of 7 cm and a mass of 820–890 g.[1] These detectors are instrumented to perform a double heat-and-ionization measurement of signals arising from particle interactions. The double read-out is used to discriminate background-induced electron recoils (ER) from potential WIMP-induced nuclear recoils (NR) on an event-by-event basis.

Heat signals are measured with two Neutron Transmutation Doped (NTD) Ge sensors [16] glued on the center of the top and bottom surfaces of the crystal thanks to a veil of Araldit glue. Their working principle and characteristics are given in section 5.1. NTD of two different productions are used with geometries of $4 \times 4 \times 0.45$ mm^3 and $3 \times 5 \times 1$ mm^3 respectively. Charge signals are measured with a set of evaporated electrodes.

The dual heat-ionisation measurement allows to discriminate ER vs NR events when charge collection is complete, as described in section 7. In addition, to reject interactions taking place close to the crystal surfaces, a special concentric-electrode scheme, based on the co-planar grid technique for event localization [17], has been first developed and tested in the EDELWEISS-II experiment with an array of ten 400-g ID detectors [14, 18]. These are heat-and-ionization cryogenic detectors equipped with interleaved electrodes on flat surfaces for the rejection of near-surface events. The same concentric-electrode scheme has been improved for FID detectors, as shown in figure 2: 200 nm thick Al electrodes are evaporated on the whole Ge crystal, both flat and side surfaces, in the form of annular concentric rings 150 μm wide with a 2 mm pitch. A surface passivation treatment, with a 60 to 80 nm amorphous layer of hydrogenated Ge is deposited only under the electrodes, the surface between electrodes being left unprocessed. To reduce possible residual leakage current, a preventive post-processing XeF_2 pulsed dry etching of the detector is applied [19].

Figure 2. Images of an 800-g FID detector with concentric ring electrodes covering the entire crystal surface and one of the two NTD sensors glued onto the top surface. On the right photo, the bolometer is surrounded by its copper casing and held by Teflon clamps.

[1]Crystals are from CANBERRA Industries, see http://www.canberra.com/products/, or Baltic Scientific Instruments (BSI), see http://bsi.lv/en/. No specific cleaning has to be carried out on the crystals produced by these two companies.

2017 JINST 12 P08010

Each detector is fully surrounded by a low-radioactivity copper casing to protect it from infrared radiation and is held by Teflon clamps (see figure 2, right). The thermal connection to the bath needed to return the detectors to equilibrium is formed through a gold pad directly evaporated onto the crystal with typically 20 Au wires of 25 µm diameter each.

To reduce possible surface contamination, all copper and PTFE pieces are cleaned before the detector installation with the following procedure: cleaning with ethanol, etching with a solution prepared using nitric acid and ultrapure water, rinsing with deionized ultrapure water, drying using industrial dryer. Concerning PTFE pieces, only the cleaning step with ethanol is carried out.

The concentric electrodes are connected electrically such that all odd-numbered rings are connected to each other as well as all even-numbered rings. With two sets of rings on the top half and the other two on the bottom half, biasing requires four voltages to measure the charge. This full coverage of the ultra-pure Ge crystals with interleaved electrodes, connected by ultrasonic wedge bonding with Al wires, is a key feature of the EDELWEISS FID detectors. In contrast to a planar scheme, when voltages are set, interleaved electrodes induce much higher electric fields along both flat and cylindrical surfaces allowing an efficient discrimination between bulk and surface events.

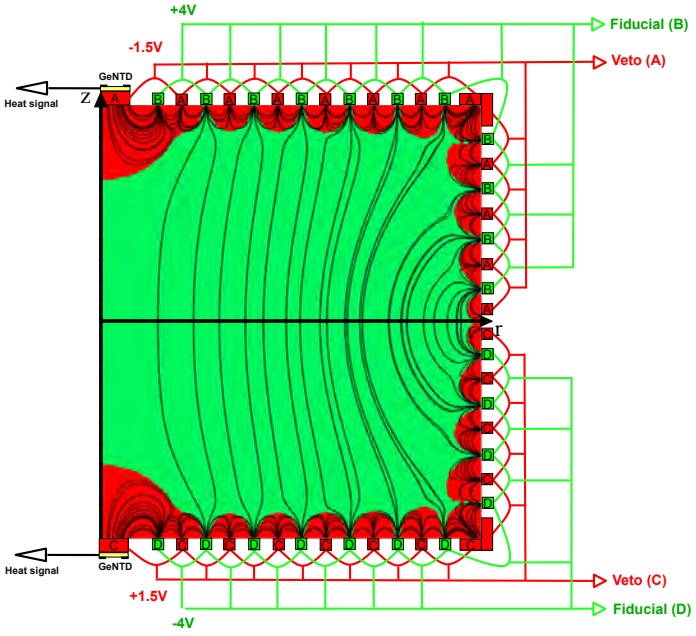

Figure 3. Cross-section of the FID detector design showing the interleaved electrode scheme. In a standard configuration, B and D collecting electrodes are biased at $V_B = +4$ V and $V_D = -4$ V and define the fiducial volume (green region). A and C veto electrodes are biased at $V_A = -1.5$ V and $V_C = +1.5$ V and define the surface volume (red region). In the bulk of the detector, the field lines are nearly vertical. Near the surfaces they are parallel to the surfaces.

As explained in sections 7.1.2 and 7.3.1, by applying appropriate selection cuts on both veto and fiducial channels, interactions which take place in the regions of detectors highlighted in red in figure 3 can be identified. Events occurring near the border between the surface and bulk region exhibit charge sharing between more than two measurement channels and are also tagged and eventually rejected by these selection rules.

2017 JINST 12 P08010

Typical voltage settings for FID detectors are ±4 V and ∓1.5 V. This corresponds to a range high enough to provide sufficient electric field inside the crystal for charge drift [20], but low enough in order not to spoil the ER rejection due to the Neganov-Luke effect [21, 22] (see section 7.1.2). The limit imposed by leakage current on the highest applicable voltage varies from detector to detector. Two of the detectors (see table 2) are limited to ±3.2 V while some others could be operated at ±50 V in Neganov-Luke-boost mode (see section 5.4). A specific surface treatment has been developed [19] in order to ensure that all but two detectors have smaller than 1 fA current at the standard voltage ±4 V and that the typical voltage limit across any pair of adjacent electrodes is greater than 15 V.

3 Cryogenic system

The EDELWEISS-III cryostat is an upgrade of the EDELWEISS-II one which ran at the LSM from January 2006 to February 2013. It is a reversed dilution custom-made cryostat built with selected low-radioactivity materials.[2] It is a ^{3}He/^{4}He dilution refrigerator with an effective volume of 50 liters for the detector setup. The cryostat has been designed with the experimental volume on top of a helium dewar. In figure 4 the dewar can be seen as the blue chamber in the center, the experimental volume with the thermal screens is above. Compressors and pumps are installed on the cavern wall outside the shields and connected by a cryoline with mechanical decoupling elements. The part containing the experimental chamber is mounted on a pneumatic damper system acting as a low-pass filter (> 1 Hz).[3] This system is equipped with remote-controlled level adjustment capability, which is useful for optimizing resilience against mechanical interference or vibration.

A picture of the open cryostat with mounted electronic components can be seen in figure 5. The detector chamber in the top of the cryostat is made of four copper plates to hold bolometers, which are arranged in 12 towers. This experimental volume is covered by five consecutive thermal copper screens like a matryoshka doll. The temperature decreases from the outermost screen at room temperature over four temperature stages from roughly 80–100 K, 45–55 K, 1–4.2 K towards 10–20 mK denominated the 100K, 50K, 1K and 10mK stages respectively. The cooling power of the cryostat is 200 μW at 100 mK. The cooling power at the first, second and third temperature stage is 100 W, 20 W and 1.5 W, respectively.

The EDELWEISS-II cryostat has been modified significantly to reduce the microphonics level, to decrease the temperature of the first and second stages, to improve the ionization baseline resolutions and to decrease the helium consumption. As explained in section 4, an additional shield of 14 cm Roman lead is installed inside the cryostat at the third stage (see figure 5). Its main purpose is to shield the detectors from radioactive background of the bolometer box, the cold electronics (FET boxes at the 100K stage) and the connectors and cables at the 1K stage (see section 5). For EDELWEISS-III the detector volume was slightly decreased to allow additional space for the installation of a PE shield. This shield is mounted between the 1K lead shield and the detectors, and has a temperature of ∼ 1 K. Each bolometer installed inside the experimental volume is thermally connected to the 10 mK screen, which serves as a thermal bath.

[2]The cryostat has been designed and built by Institut Néel, Grenoble.

[3]EFFBE company, now Gamma-SA company, see http://www.gamma-sa.fr.

2017 JINST 12 P08010

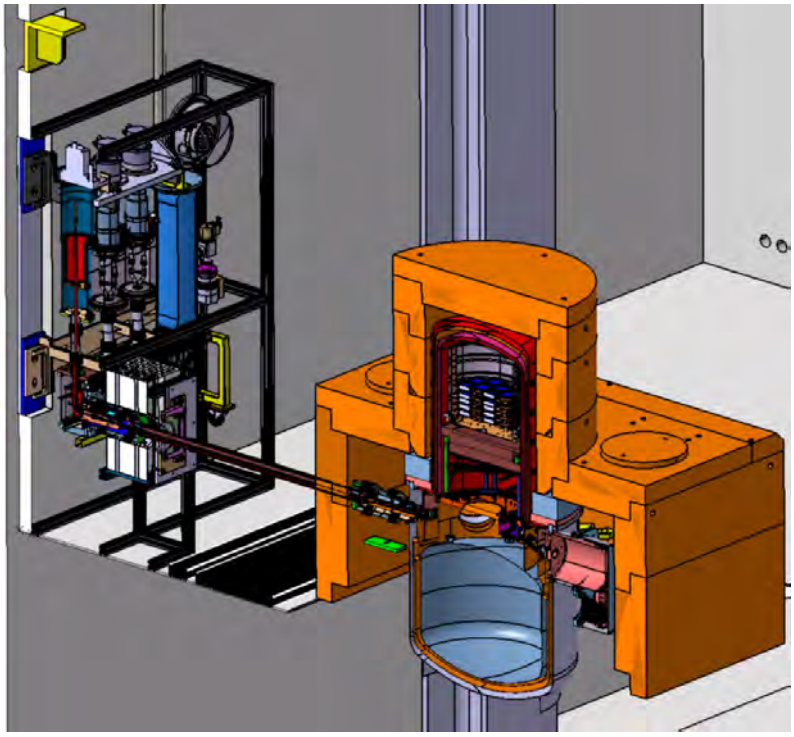

Figure 4. Cross-section of the EDELWEISS-III reversed cryostat connected by a cryoline to the three thermal machines mounted on the cavern wall to reduce vibrations and radioactive background inside the shields. Only a part of the lead shield is shown (orange) and the He dewar is the blue structure at the bottom.

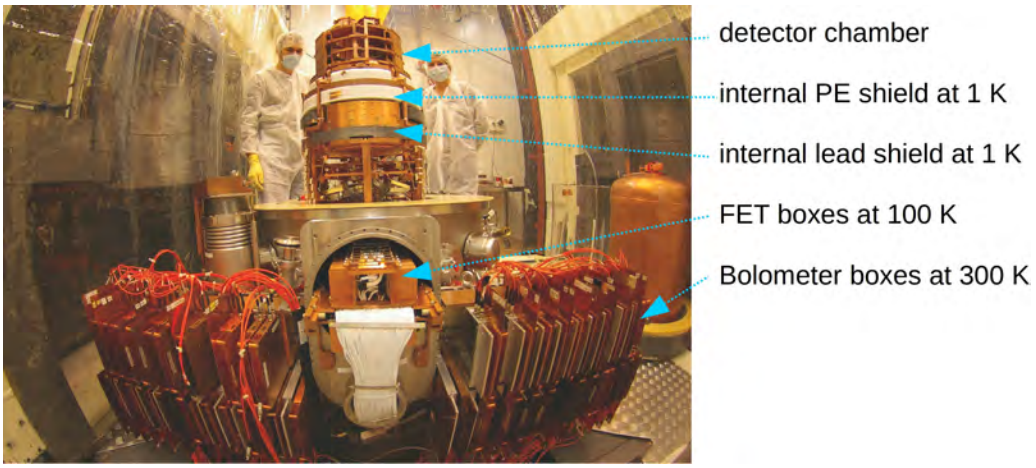

Figure 5. Picture of the open cryostat with installed bolometer boxes and cold FET boxes. The internal lead and PE shields are visible below the detector chamber.

Control of the cryostat during cool-down and data taking periods is carried out using three National Instruments FieldPoint (FP) controllers [23]. Labview-based user-interface software has been developed to access, control and monitor all relevant parameters of the cryogenics [23]. A TRMC2 controller manages the cryostat temperatures and bolometer heater, and communicates the

2017 JINST 12 P08010

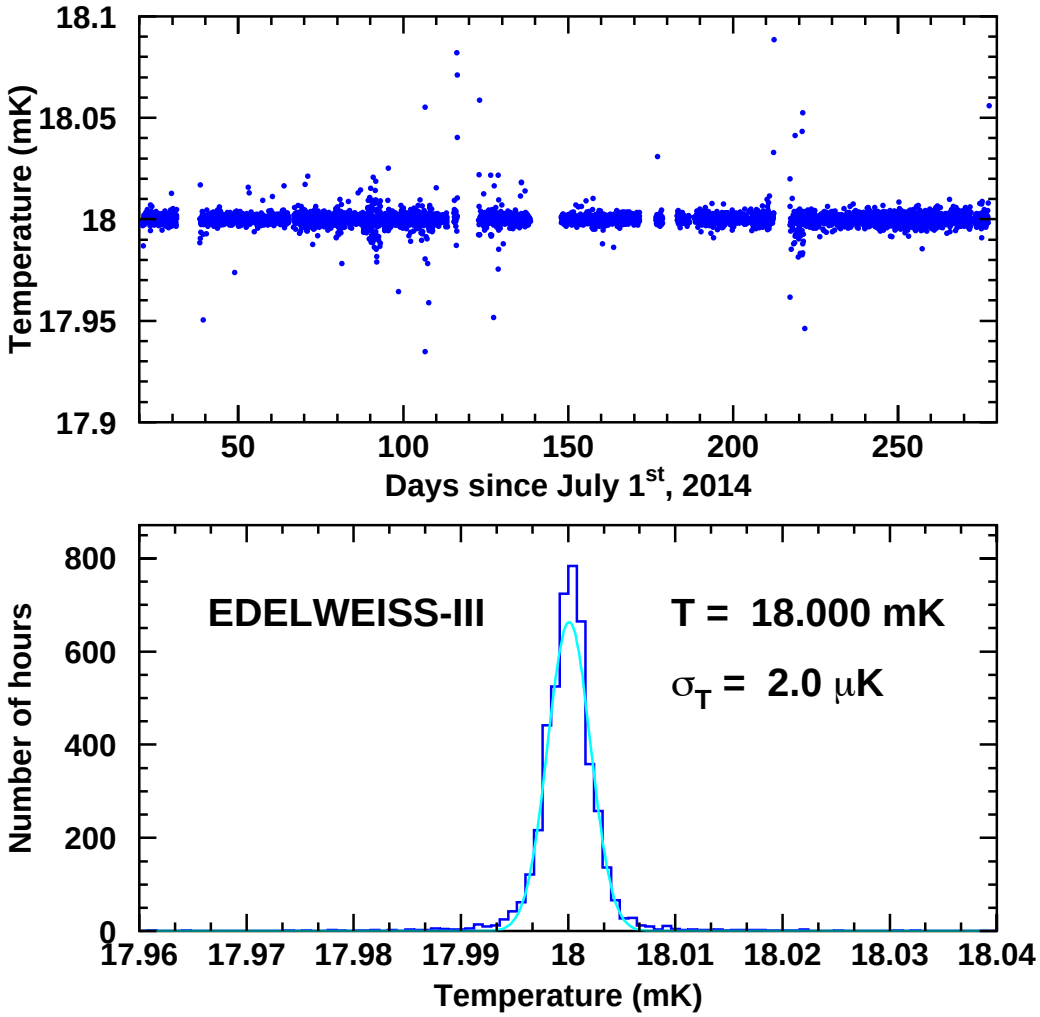

Figure 6. Example of regulated bolometer temperature as a function of days since the start of the EDELWEISS Run 308 demonstrating the stability at 18 mK.

data to the FieldPoint automats by TCP/IP protocol.[4] The 100K- and 50K-screens are cooled in series by the cold ^{4}He gas cryoline at 2 bars, which is itself cooled by two Gifford Mac-Mahon single-stage thermal machines. The cryoline allows a full mechanical decoupling of the cold heads from the cryostat. The temperature of the ^{4}He gas at 2 bars is about 40 K at the entrance of the 50K-stage and 80 K at the output of the 100K-stage. ^{4}He pressure and mass flow can be controlled to stabilize the 50K- and 100K-stages, with running temperatures at about 50–55 K and 85–90 K, respectively.

The consumption of liquid ^{4}He is minimized by the use of a cold vapor reliquefaction system, based on a third Gifford Mac-Mahon machine. The whole 1K-stage is isolated from the main cryostat vacuum and is cooled by a 1K-pot controlled by a cold valve connected to the ^{4}He bath. The approximate cooldown time from room temperature to 20 mK is about one week. During

[4]For more details see http://www.neel.cnrs.fr/spip.php?article149&lang=en.

2017 JINST 12 P08010

standard operation, the regulated temperature is fixed at 18 mK, which takes 2–3 days more to reach. As shown in figure 6, this temperature has been maintained without any major interruption during Run 308 (almost 10 months for the example shown in the top of the figure 6). It is clear from inspecting the data shown in figure 6 that the weekly cryogenic fluid refill does not affect this temperature. The stability of the working temperature is better demonstrated in figure 6 (bottom), which shows that the bolometer temperature is gaussian distributed around 18.000 mK with a variance of $\sigma_T = 2$ μK. With this temperature the helium consumption is roughly 10 liters per day which implies a helium refill once per week.

4 Active and passive shielding

The EDELWEISS experiment is located in the LSM [24] in the Frejus highway tunnel connecting France and Italy in the Alps. The mean rock thickness of 1 700 m (about 4 800 m water equivalent) reduces the muon flux down to about 5 muons/m^2/d [25], which is more than 10^6 times smaller than at the surface. The natural radioactivity from laboratory walls is reduced by passive shielding, and all materials used to build the experiment as well as the detectors were selected rigorously based on their high radiopurity level. A systematic campaign of radiopurity measurements of materials was undertaken with the Gentiane HPGe detector, in operation at the LSM since 1997 and dedicated to the EDELWEISS experiment. It is an n-type HPGe diode of about 210 cm^3 mounted in a closed-ended coaxial configuration. Its sensitivity allows activity measurements down to the mBq level for U/Th chains, as shown in table 5 of section 8.

4.1 Shielding against cosmogenic background

Despite the significantly reduced muon flux at LSM, cosmogenic neutrons produced by remaining muons and associated showers can still represent problematic background, if an efficient muon detection is not available (see e.g. [25] and section 8.1 of this article). An active muon veto therefore surrounds the whole experiment for an effective muon tagging [25]. Fourty-six individual plastic scintillator modules (Bicron BC-412) of 65 cm width, 5 cm thickness and lengths of 2 m, 3.15 m, 3.75 m and 4 m add up to a total surface of 100 m^2. Each module is viewed by two groups of 2-inch PMTs, where each PMT group is provided with its individual high voltage (HV) setting and readout. In order to optimize the geometrical coverage, the muon veto has two distinct parts: the upper one attached to the external polyethylene shielding around the cryostat, and the one below the cryostat covering the pumping section of the cryostat. The upper part is positioned on rails of two movable PE blocks which allows opening of the shields right in the middle and gaining access to the cryostat during maintenance periods (figure 1). The exact positions of the two mobile veto parts are monitored via regular position measurements using laser interferometry. The upper part almost completely covers the cryostat, while the lower part has a number of gaps due to cryogenic supply lines and the pillars of the experimental structure. The geometrical coverage for through-going muons is about 98% [25]. Out of a total of 46 modules, four last modules were installed in July 2010 within the upgrade program towards EDELWEISS-III. These 4 modules cover a small gap right above the cryostat appearing between the two movable parts of the muon veto. In spite of only a few cm width, this gap would lead to a significant loss in identification of coincidences between the muon veto and bolometers. The gap appeared as a result of the cryogenic upgrade, in particular,

2017 JINST 12 P08010

of the installation of thermal machines outside of the shielding and the corresponding cryogenic line with a diameter larger than in EDELWEISS-II (see section 3).

The muon veto DAQ is based on VME electronics and in-house developed cards. It is separate from the bolometer readout but both systems are synchronized with a 10 µs clock. The synchronous clock was upgraded for EDELWEISS-III to ensure the delivery of a reliable and precise time information (see section 6). An event recording in the veto system is triggered once the two PMT groups of a module each pass a trigger threshold within a coincidence window of 100 ns. Within an event, all hits above threshold in the modules are recorded within a fixed interval. For each signal channel, the individual time of a hit and the integrated scintillation light are recorded. A complete description of the electronics, readout and data acquisition of the muon-veto can be found in [25].

During running periods, the status of the overall muon veto system and each of the 46 individual modules is checked online using web-based monitoring tools. They were significantly improved for EDELWEISS-III to guarantee continuous running of the system and taking data of good quality, including e.g. the data rate of the whole system and individual modules, ADC, TDC spectra, and their variation with time for each module.

4.2 Shielding against radiogenic background

Radiogenic gamma and neutron backgrounds arise from natural radioactivity present in the cavern rock and concrete and in the materials of the experiment.

The residual neutron background is estimated by Monte-Carlo simulations of spontaneous fissions and (α, n) reactions. Neutron flux in LSM below 10 MeV is mainly due to spontaneous fission of ^{238}U and its daughters present in the cavern and (α, n) reactions in light materials. The averaged 4π thermal neutron flux in the vicinity of the EDELWEISS experiment, outside the shields, has been measured to be $(3.57 \pm 0.05(stat) \pm 0.27(syst)) \times 10^{-6}$ neutrons/cm^2/s [15, 26]. The fast neutron flux above 1 MeV outside the shields was evaluated to be $(1.1 \pm 0.1(stat)) \times 10^{-6}$ neutrons/cm^2/s [27]. These fast neutrons can affect the sensitivity for dark matter search since they produce nuclear recoils of similar energy (few keV to few tens of keV) to those expected from WIMPs. Radiogenic neutrons are moderated and some of them are captured in the PE shielding of at least 50 cm thickness which follows the muon-veto (see figure 1). The 35 tons of this PE castle reduce the fast neutron background component in the experimental volume by 5–6 orders of magnitude [15].

The inner part closest to the cryogenic detectors is shielded using 20 cm thick lead covering the dilution refrigeration unit and the cryostat structures. The 40 tons of the Pb shielding are used against gamma backgrounds. Lead itself contains the long-lived radioactive isotope ^{210}Pb with a half-life of 22.3 years. Therefore, the innermost 2 cm of the lead shielding are made of Roman lead from a sunken galley [25] with an activity in ^{210}Pb of less than 120 mBq/kg, more than two orders of magnitude lower than the other 18 cm of low radioactivity lead (<30 Bq/kg of ^{210}Pb). Note that the shielding efficiency of the 2 cm Roman Pb is equivalent to 10 cm of copper.

Another significant source of background arises from the radon isotope ^{222}Rn. This radioactive gas with a 3.8 days half-life is a decay product of ^{238}U present in the rock and construction materials. The radon level is controlled in the whole laboratory where its measured activity is ~10–15 Bq/m^3 [24], thanks to the ventilation system supplying air from outside of the mountain at a circulation rate of two laboratory volumes per hour. In addition the experiment is located in a

2017 JINST 12 P08010

clean room (class 10000) to avoid contamination from dust. It is mounted on the mild steel structure with rails, which allows the opening of the shields in two parts to access the cryostat. The radon level is also controlled in the EDELWEISS clean room and the empty space between the lead shield and the outermost thermal screen of the cryostat is flushed with radon depleted air with a residual activity of about 30 mBq/m^3 [28].

Simulations performed for the EDELWEISS-II experiment showed that some specific materials presenting a high contribution to neutron background had to be replaced [15]. The EDELWEISS-III setup was notably improved with respect to the previous phase of the experiment. As shown in figure 5, a new internal PE shield was added between the detection volume and the 1K-plate and another PE shield was added outside the cryostat above warm electronics. Furthermore, the copper used for the cryostat thermal screens, detector housings and for the 10 mK area was replaced by much purer copper (NOSV Electronic Tough Pitch copper produced by Aurubis formerly Norddeutsche Affinerie) [29, 30].

5 Readout of signal channels

The EDELWEISS-III electronics has been designed to obtain a FWHM baseline resolution below one keV on both heat and ionization signals to provide a 10^5 discrimination factor for nuclear recoil deposits against electron recoils above 10 keV. The corresponding electrical signals to be read out simultaneously are voltage variations over few MΩ NTD thermistors (heat) and charge measurements on the four Al electrodes collecting electron-hole pairs (ionization). The use of Si-JFET based cold electronics is well adapted to these high-impedance signals.[5] Low temperature stages are available to cool parts of the electronic components, helping to reduce the current noise of the JFETs as well as thermal noise from resistances. Long integration times are possible thanks to the low event rate of only a fraction of Hz. The main challenges concern the long distance between detectors and the first elements of the cold electronics, the power dissipation allowed by the cooling power of the dilution unit and the cryostat, and finally the radiopurity requirements.

Connections from the detectors to the bottom of the detector chamber are made with in-house developed Kapton cables [31]. Beyond this point, EDELWEISS-III is using special cryogenic coaxial cables designed in collaboration with the Axon Cable group.[6] It is needed to keep the cross-talk between adjacent channels below few percents and to minimize the stray capacitances (40 pF/m), the sensitivity to microphonics, the electromagnetic noise and the power dissipation. The cold JFETs are mounted on extractable boxes screwed on the 100K screen of the cryostat (see figure 9).

The electronics for the JFET biasing, DACs to bias the detectors, post-amplification, anti-aliasing filtering and digitization are all integrated in a single room-temperature module (so-called bolometer box), which is directly bolted onto the cryostat (see figure 9). All input/output functions of this module are carried out via optical fibers. The data of all channels are digitized continuously at a rate of 100 kHz with 16-bit resolution and sent to computers via dispatching units. Filtering, triggering and data flow control are done online in the trigger computers (see section 6). A common

[5] JFET is used for junction gate field-effect transistor.

[6] For more details see http://www.axon-cable.com/en/.

2017 JINST 12 P08010

control, sampling frequency and clock allows easy identification and subtraction of common noise patterns due to electronic interference.

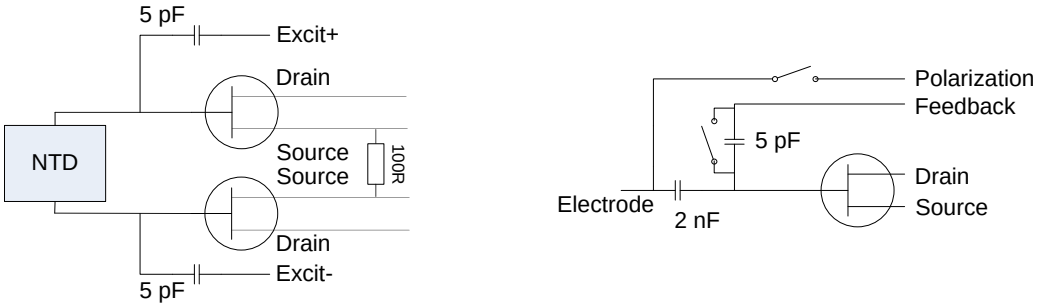

Figure 7. EDELWEISS-III signal readout: heat (left) and ionization (right) channels.

5.1 Heat channel readout

The experimental optimal heat energy resolution is obtained with impedances of the NTD thermistors of a few MΩ and a current bias of a few nA at 18 mK. These values are a compromise between the sensitivity to microphonics at such high impedance and non-linearity of the $V_{NTD}(I)$ responses (NTD voltage versus bias current). These non-linearities appear due to thermal decoupling of the detectors from the bath via the heat sink, thermal decoupling of the NTD from the germanium crystal via the glue in between them and electron-phonon decoupling within the NTD [32].

The typical heat capacity for a fully equipped FID detector is about 2 nJ/K at 18 mK, so the expected temperature elevation for an energy deposition of 1 keV is roughly 0.1 μK. With a typical heat response of 0.5 V/K, an energy sensitivity of 50 nV/keV is obtained. Typical time constants at 18 mK are 10 ms for the rise time and 10 and 100 ms for the two main decay times respectively (see [32] for details).

EDELWEISS-III heat pre-amplification electronics is based on IFN860 bi-JFETs with a noise plateau at about 1–2 nV/$\sqrt{Hz}$ rms. The white noise contribution of the NTD Johnson noise is in the same range. Considering only these two sources of white noise and a decay time constant of 100 ms lead to an electronic baseline resolution of about 300 eV FWHM. Heat current excitation is modulated in the 500 Hz range: at both ends of the NTD two opposite current squares are created by differentiating a triangular voltage pulse on a 5 pF capacitance (figure 7, left). This square modulation technique has been originally developed for the Archeops balloon and Planck satellite [33]. The demodulation is done after the digitization at 100 kHz either online or offline by means of software. All noise that has not been modulated is rejected and the noise level is the one at the modulation frequency. The electronics 1/f noise is thus efficiently rejected by the modulation and the common-mode noise is rejected by the differential measurement. A reference square could be subtracted before the second stage of amplification to enhance the dynamic range.

5.2 Ionization channel readout

The mean energy to generate an electron-hole pair is 3 eV in germanium [34]. Therefore a 1 keV ionization energy baseline resolution corresponds to a charge of 330 electrons equivalent at the input. If an electric field is applied through the detector, the electron-hole pairs drift through the detector

2017 JINST 12 P08010

before being collected on electrodes. During this charge drift of a fraction of a µs, charges are induced on the collection electrodes; these charges could be integrated on the feedback capacitance of a charge amplifier or on the total input capacitance in the case of a voltage amplifier. It can be noted that the signal-to-noise ratio is not affected by the presence of a feedback capacitance and is the same for both schemes. EDELWEISS-III ionization electronics is based on IF1320 JFETs. The main difference with respect to the previous electronics scheme of EDELWEISS-II is the use of a voltage amplifier to measure the ionization. The first stage of amplification consists of a follower, and no detector bias and feedback resistors are used to avoid their thermal noise contribution (figure 7, right). Based on the ADC output sampled at 100 kHz, the gate voltage is periodically adjusted on the timescale of minutes through a capacitance by firmware in an FPGA. The detector is biased through mechanical relays. The low FET and detector leakage currents (< 1 fA) allow biasing of a detector once every few hours, otherwise the relays are open and the detector is floating. As a consequence, the response of the system to a charge deposit is a step function. The FID800 detector capacitance is about 150 pF, the cabling stray capacitance is about 100 pF and the FET gate to source capacitance is about 50 pF. The detector response at the input is thus 180 nV/keV. The integration time for the charge signal is only limited by pile-up. With the adopted integration time of 1 s, we obtain a baseline resolution FHWM at the 500 eV level, a factor two better on average than those achieved in EDELWEISS-II [14]. The ionization resolution is limited by the current noise of the FET, introducing a 1/f noise below 1 kHz [35].

As an illustration of both ionization and heat channel readout features, figure 8 presents noise amplitudes in the frequency domain for one FID detector. The bottom part shows the noise amplitude for one of the two heat channels whereas the top part shows it for one of the four ionization channels, after application of the amplitude correction described in [20]. This amplitude correction allows to reduce the peak structures due to the correlated microphonic noise between the four electrodes, but it also minimizes the smooth envelope mostly due to uncorrelated noise, without affecting the amplitude even in case of charge trapping. The associated power spectra expected for a 1 keV electron equivalent signal are also shown in both figures. Associated expected resolutions FWHM from an optimal filtering are 0.68 keV_{ee} for the ionization channel and 0.21 keV_{ee} for the heat channel shown in figure 8.

5.3 Time resolved ionization readout

It was shown in [17] that a rise time analysis of an ionization signal can help to discriminate surface and fiducial events. As part of the EDELWEISS-III R&D program, a prototype readout card allowing sampling at a rate of 40 MHz with 16 bit resolution was implemented in one of the bolometer boxes. The card receives two analog channels from one detector, hosts FPGA and 8 MB total memory, whereas 2 MB is assigned per channel and further divided into two memory pages for deadtime-free readout of up to two consecutive events. Signal splitting into the standard 100 kHz and the 40 MHz branches is done between the analog pre-amplification and anti-aliasing filters inside a bolometer box such that it does not affect the EDELWEISS standard acquisition. The digital data rate of the prototype card is 1.28 Gbit/s and exceeds the available bandwidth of 3.2 Mbit/s of the optical fiber communication between bolometer boxes and DAQ crate. Therefore, an event based readout for this type of channel [36] is implemented through the DAQ crate and

2017 JINST 12 P08010

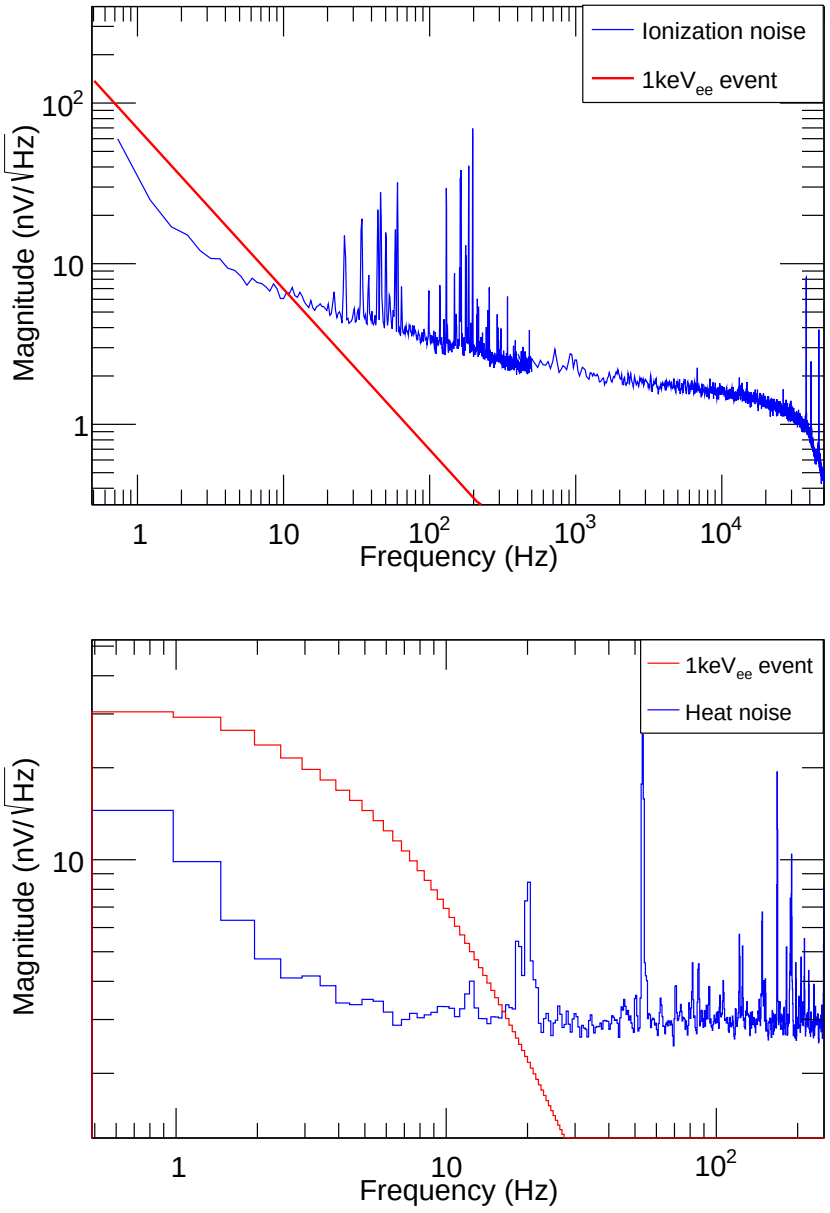

Figure 8. Typical average Fourier noise spectra of an ionization channel (top) and a heat channel (bottom) for an FID detector. In both figures, the red histogram corresponds to the spectrum of a 1 keV$_{ee}$ (electron equivalent) signal.

ORCA software (see section 6.3) to reduce maximally possible 256 kSamples per channel to ±2048 points around the rising part of a pulse [37].

5.4 Upgrade for the Neganov-Luke amplification

As described in refs. [21, 22], charges drifting under an electrical field produce additional heat in a detector by Joule effect. The measurement of such voltage-assisted heat opens access to very low

ionizing events of just several 10's eV_{ee}, therefore providing good prospect for low-mass WIMP searches, as shown in [38, 39]. Within the EDELWEISS-III R&D program, ten bolometer boxes were modified to allow biasing of ionization channels up to ±70 V instead of standard ±10 V, which corresponds to a maximum boost factor of about 48 compared to the non-amplified case (0 V) for electron recoils. This is done by means of operational amplifiers (LTC6090) inserted in each bias line and operated as a "non-inverting amplifier". The amplifier output is connected to the detector via a 20 GΩ resistor to limit the maximum current per detector in case of leakage. The input of the amplifiers is the standard bolometer voltage of ±10 V. The supply voltage of ±70 V is provided by the external power supply EA PS-2843 (max. output 84 V, 3 A).[7] The output of the external power supply is filtered with three stages of low pass filters and currently fanned out to ten bolometer boxes [37]. The implemented scheme does not require any changes to the pre-amplification electronics and needs only minimum adaptation of the acquisition software SAMBA (see section 6.2).

6 Data acquisition system

The EDELWEISS data acquisition system (DAQ) commands the bolometer boxes (see section 5), and therefore controls the biases of the detector sensors. It also manages the digitized data flow that they produce. It provides displays of that data for monitoring purpose, and performs triggering to select and store data on disk. The main user interface program, called SAMBA, runs on a Mac computer (right side of figure 9). It receives data and sends commands via Ethernet to the DAQ crate, consisting of a server computer connected to a VME-based acquisition crate. This system communicates with the bolometer boxes via optical fibers. The transition from analog to digital data is performed in the bolometer boxes, directly attached to the cryostat. Therefore any potential ground loops are avoided, with the ground potential of the cryostat being the same as that of the bolometer boxes.

The use of Ethernet for the input to/output from the DAQ crate enables it to communicate with more than one computer. This flexibility is used to spread the data flow and commands over multiple Mac computers, each controlling up to twelve detectors. It is also connected to an additional PC for additional monitoring and handling the fast ionization channel data flow. The possibility to spread the data flow over a number of parallel computers provides a significant operational flexibility when operating a segmented detector array such as EDELWEISS. The separate data sets recorded by each computer and the muon veto system are synchronized using the unique 10 μs time stamp distributed by the DAQ system.

6.1 The DAQ crate

The DAQ crate receives the digitized data from the optical fibers coming from the 72 bolometer boxes controlling the 36 detectors.[8] It formats the data into Ethernet packets to be sent to the DAQ computers and transmits through optical fibers the commands sent by the DAQ computers to the

[7] EA-Elektro-Automatik, PS 2000 B Triple Handbook, tech. rep. (2013), http://www.farnell.com/datasheets/1634399.pdf.

[8] For each detector, one box controls the four ionization channels and one heat channel, while the other box controls the second heat channel and the relays.

2017 JINST 12 P08010

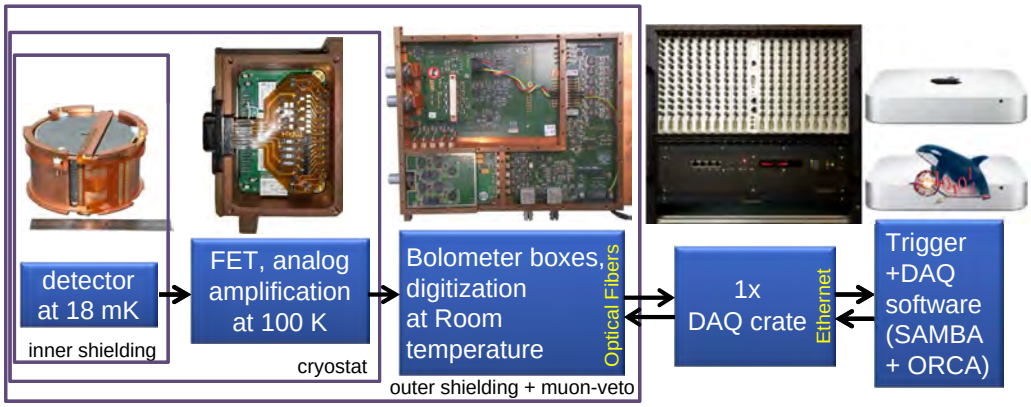

Figure 9. Full EDELWEISS-III data path. 36 detectors are read out via an analog amplification inside the 100-K zone by 72 digitizer bolometer boxes at room temperature. Each bolometer box sends 12 Mbit/s on fiber optics to the DAQ crate. This connects via a server PC and a network to the user interface Macs. Figure adapted from [37].

bolometer boxes, as well as a common clock to all boxes and the muon veto system. It also includes a minimal subset of the muon veto data into the bolometer data.

The system has been designed as an integrated system scalable for ≥ 40 detectors, able to deliver a reliable time synchronization. It features data-reduction capabilities to optimize the network traffic by adding or removing channels depending on their use. The DAQ crate has been developed and manufactured in-house at KIT [40]. It consists of a 6U+2U high 19-inch crate, housing a custom backplane allowing to connect 20 input-output cards (IO-cards) and one central master card. This type of DAQ crate is also used in other astroparticle physics experiments such as the Pierre Auger observatory [41] and KATRIN [42]. For the EDELWEISS experiment the DAQ series have been adapted to the optical fiber input/output to the bolometer boxes. Each IO-card has 6 optical fiber input-output pairs to manage up to 6 bolometer boxes, or 3 detectors. The IO-cards receive the digitized data streams from the bolometer boxes, concentrate it, and remove unused channels. One IO-card receives from the muon veto system a six-bit pattern corresponding to an event in one of its six faces, as well as time stamp information to check the synchronization of the system. In addition, the IO-cards can be programmed to perform event-based readout, a feature used to read out the fast ionization channel in parallel to the 100-kHz data stream. The data stream from the IO-cards is forwarded to a master card in the VME crate (see figure 10). In addition to providing the 48-bit 100-kHz clock used to synchronize the flow of data and commands, the master card sends the data stream via a PCI-Express interface to a Linux-based server computer. The server then produces UDP (User Datagram Protocol) packets that are transmitted to the acquisition computers via a Gigabit Ethernet network.

With 6 channels per detector (4 ionization and 2 heat channels) sampled at 100 kHz with 16-bit resolution, each detector produces a 1.2 MB/s stream of physical data. The total throughput of 43 MB/s for 36 detectors is well below the values of up to 90 MB/s that the DAQ crate has been proven to handle [40].

The three Mac computers each handling the 100-kHz data flow from up to 12 detectors are running a program that can also send the commands needed to configure the bolometer boxes

2017 JINST 12 P08010

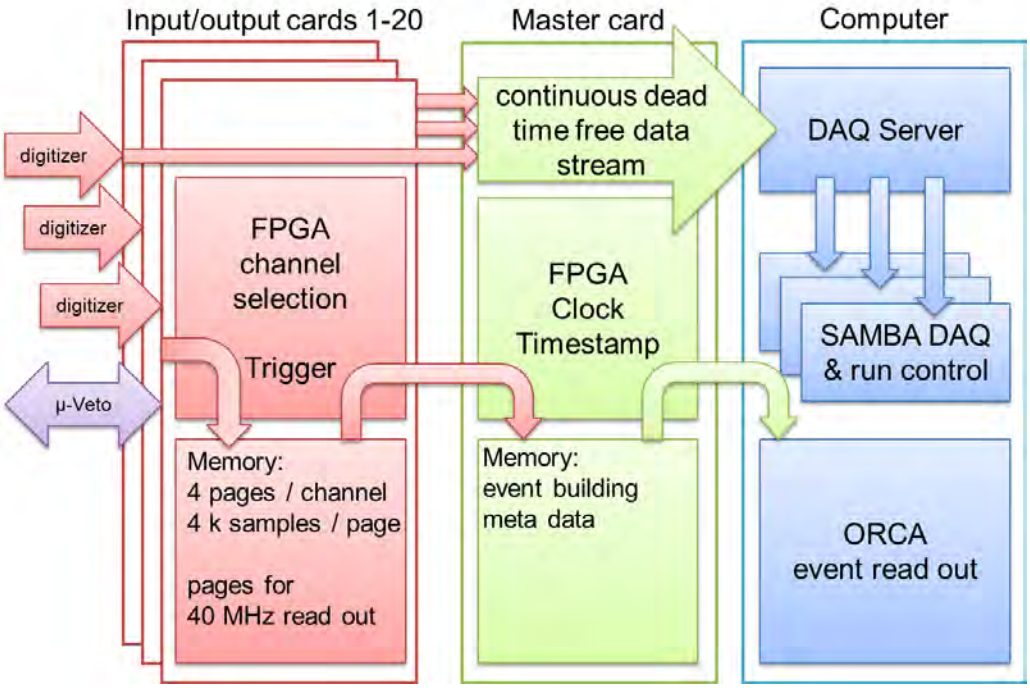

Figure 10. Schematic and simplified view of the data flow in the integrated DAQ system. The system combines an event based readout branch (ORCA, section 6.3) with an independent trigger logic and the dead time free data stream to the EDELWEISS computers (SAMBA, section 6.2). Figure extracted from [37].

(see section 6.2). The commands sent to the bolometer boxes follow the reverse path: from the acquisition computer to the server via UDP packets, through the VME cards via the PCI-Express interface and then back to the bolometer boxes via different optical fibers. A separate Mac computer provides the user interface to handle the data acquisition of the fast 40-MHz ionization data (see section 6.3).

The 100-kHz clock and the corresponding time stamp generated by the master card is not only used to synchronize the sampling of the ADC on all channels, but also provides the frequency and phase of the NTD excitation (section 5.1) and the 64-second cycle for the gate correction of the ionization readout (section 5.2). The time stamp information is used to remove the transient associated with these patterns and, in the case of the gate correction, to calculate precisely the corresponding dead time.

6.2 SAMBA

The application used to manage the EDELWEISS DAQ hardware configuration and the data taking is called SAMBA. The program has been designed for flexibility: for example, the three computers handling up to 12 detectors each can be operated independently, or under the control of a single master computer. The setup is defined in text files that can be modified either directly or via the SAMBA application itself via graphical interfaces. The hardware setup that SAMBA must handle includes, among others, lists of detectors to be read out, their associated bolometer boxes and associated DAQ crate channels, the bias values for the ionization channels, the frequency

2017 JINST 12 P08010

and amplitude of the heat excitations, and the software-controlled gains of the digitizers. Other parameters refer to the processing of the data flow, with software filters, optimized individually for each of the channels, and to the configuration of the trigger that controls the recording of data on disk. Through object-oriented programming, SAMBA can be readily adapted to detector and hardware evolution.

SAMBA receives from the crate server the 100-kHz data from up to 12 detectors. Two levels of digital processing can be performed on each channel. The first corresponds to on-the-fly filters applied to the data before it is stored on disk. A copy of that stream, not saved on disk, can be further processed in order to be used for triggering purpose. The data at either levels of processing can be displayed continuously, either in a time series (in an "oscilloscope" mode), or as power spectra as a function of frequency. The available digital filters are the demodulation of the triangular excitation of the NTD (section 5.1), digital IIR (Infinite Impulse Response) filters, averages, the removal of a repetitive pattern, and the convolution with a user-defined pulse template. Different filters can be applied to each of the channels.

In addition to the "oscilloscope" mode, SAMBA can trigger on a single filtered channel: for instance, during WIMP-search runs the trigger is set on heat detector channels. The second-level filtered data is inspected and, if this channel exceeds a threshold value, a time tag is registered. SAMBA then compares the time tags of all channels to look for coincidences inside a given time window, in which case it determines a common time tag. For each time tag, the first-level data of all channels of the corresponding detectors are saved on disk. The data saved on disk are typically 2.048-seconds wide traces of the heat and ionization signal, sampled at 0.5 or 1 kHz and centered on the time tag, as well as 40.96-ms wide traces of the raw 100-kHz ionization data.[9] The data of neighboring detectors is generally saved in addition, in order to provide ample baseline data for noise and trigger studies. Each event is accompanied by a header indicating the bit pattern of the triggered channels, the level of the trigger threshold for each channel, and the amplitude of each channel in the same units as the threshold value.

SAMBA can be programmed to automatically adjust the trigger level on a given channel in order to maintain a given trigger rate. For instance, in WIMP-search runs, it is typically required that each channel triggers not more than three times per minute and less than thirty times every 10 minutes. If this is not the case, the trigger threshold level is automatically raised, or decreased, respectively, by a fixed amount. This results in a rather constant triggering rate of 50 mHz per channel, irrespective of slow fluctuations in noise levels. As physical event rates in WIMP-search runs are close to 5 mHz per detector, this procedure ensures lowest possible thresholds without being burdened by excessive dead time.

6.3 ORCA

An alternative interface to the DAQ crate is given via an acquisition computer running the ORCA program. This interface, which can configure the DAQ crate, is used in particular when exploiting the 40 MHz time resolved ionization channels. ORCA stands for Object-oriented Real-time Control and Acquisition and is written for the Mac OSX operating system in Objective-C [43]. It was

[9]For the oversampled ionization, each point is the average of hundred or two hundred 100-kHz samples. For the heat, each point is the difference between the average signal during the positive and negative phase of the NTD excitation.

2017 JINST 12 P08010

originally provided with the DAQ crate system, and was adapted to the EDELWEISS data format, the different FPGA register model for hardware access and the bolometer access. In case of 40 MHz time resolved channels, the acquisition computers cannot forward the software triggers of SAMBA fast enough to send a trigger signal to the bolometer boxes and request the 40 MHz ADC traces. Instead, FPGA triggers on the crate IO-cards must be used [36]. Once an event is detected, the ADC trace centered on the event is written to a buffer on the FPGA. Otherwise, the ADC data is discarded. The ORCA readout loop of the DAQ crate computer polls the hardware, reads out events from the buffers and sends the ADC traces to ORCA after adding additional information like time stamps, channel and crate number. ORCA stores the events in a run file, which can be later converted into ROOT [44] format by means of OrcaROOT library. The time-resolved data can be merged with the SAMBA events using the associated time stamp data. As the SAMBA and ORCA acquisition systems are relatively independent, the comparison of the event lists they produce is useful to study potential acquisition dead time [37].

7 Detector performance

The use of the newly designed 800-g FID detectors coupled with upgrades on both electronics and cryogenics systems led to the improvement of the average FWHM of the heat and ionization baseline energy resolutions and better active rejection of background as described in this section.

The double measurement of the heat and ionization energies provides both the recoil energy E_r deposited by a particle interacting in the detector and the recoil type via the estimation of the ionization yield $Q(E_r)$ as a function of the recoil energy [45]:

$$E_r = E_{heat}\left(1 + \frac{V}{\varepsilon_\gamma}\right) - E_{\text{ion}}\frac{V}{\varepsilon_\gamma} \quad \text{and} \quad Q(E_r) = \frac{E_{\text{ion}}}{E_r} \tag{7.1}$$

where V is the bias voltage and $\varepsilon_\gamma = 3\,\text{eV}$ is the average energy needed for an electron recoil to produce an electron-hole pair of charge carriers in germanium. E_{heat} and E_{ion} stand for the heat and ionization energies, respectively, obtained from signal amplitudes, calibrated using electron recoils. The quenching variable $Q(E_r)$ is equal to 1 for electronic interactions by definition, whereas $Q(E_r) \sim 0.3$ for nuclear recoils [45]. Thus the simultaneous measurement of heat and ionization provides an event-by-event identification of the recoil type and allows rejection of the dominant γ-ray backgrounds as well as the majority of β-backgrounds. Residual γ- and surface β-backgrounds are removed using the active rejection power of the FID detector design, as presented in sections 7.4 and 7.5.

7.1 Energy calibration and detector regeneration procedures

Due to the presence of impurities inside the detector, charge carriers can be trapped by these impurities during their migration towards the electrodes. They then cause the formation of space charges that create an electric field in a direction opposite to that from the bias voltage. To limit this effect, so-called regeneration phases are conducted for one hour per day, where γ-radiation is used to break the formed space charges.

Energy calibration and regeneration procedures make use of radioactive sources and have been carried out for all detectors. To avoid background due to these sources during science data

2017 JINST 12 P08010

taking, they have to remain outside the EDELWEISS-III shielding during standard data acquisition and have to be put as close as possible to the detectors only during calibration and regeneration procedures. For this purpose, an automatic source deployment mechanical system has been designed and implemented. This system incorporates two ^{60}Co and two ^{133}Ba radioactive sources.

7.1.1 Radioactive sources

For the detector regeneration, strong ^{60}Co γ-sources ($\sim$ 200 kBq) are used. Calibration of ionization and heat signals of the detectors is carried out using simultaneously two encapsulated sources of ^{133}Ba. The radioactive isotope ^{133}Ba decays by electron capture to ^{133}Cs ($T_{1/2}$ = 10.55 yr), with the emission of γ-rays among which the relevant ones for calibration are 356.0 keV (62.05%) and 383.9 keV (8.94%) [46], which have enough energy to reach the bolometers inside the cryostat.

A low activity (21 $\pm$ 4 neutrons/s) AmBe neutron source is used for neutron calibrations. The source is encapsulated in lead and sealed in a stainless steel container. For the purpose of neutron calibration the source is manually placed at a distance of 8 cm above the top of the cryostat inside the Pb shielding for several hours. Figure 11 shows the ionization yield $Q(E_r)$ versus the recoil energy E_r for AmBe neutron calibration data. The source emits neutrons with energies up to 11 MeV, inducing nuclear recoils with $Q(E_r)$ values gaussian-distributed around a smooth function $Q(E_r) = 0.16E_r^{0.18}$ consistent with the expectations from the Lindhard theory [47] including effects due to multiple scatterings [48].

The AmBe source also emits high energy γ-rays of 4.4 MeV which lose energy via Compton scattering, leading to the population of events distributed around $< Q(E_r) >= 1$. Events between the electron and nuclear recoil bands arise from the inelastic scattering of a neutron on a germanium nucleus. The events along the purple dashed lines correspond to those involving the first (13.28 keV) or third (68.75 keV) excited state of ^{73}Ge.[10] The prompt γ-emission results in an effective quenching Q_{eff} which is the average of the Q values of the neutron and the γ, weighted by their energies.

7.1.2 Energy calibration procedure

The calibration of ionization channels is performed using the 356 keV peak of the ^{133}Ba spectrum to adjust individual gains and cross-talk coefficients. Data taking dedicated to γ calibrations represents around 10% of the data over a cool-down period.

As explained in [20], energy losses are correlated with the energy deposit depth, with a dependence always stronger for the fiducial electrode B (anode) than for the fiducial electrode D (cathode), since the charge trapping is significantly larger for electrons than for holes. The resolution increases with the energy of the signal, with a linear term which is dominated by charge trapping effects. Thus the degradation of resolution with energy is a consequence of charge carrier trapping in the bulk of the detectors.[11] It follows that despite good fiducial ionization baseline resolutions

[10] The 66.7 keV line from the second excited state (half-life of 0.499 s) should appear in the electron recoil band, but it is invisible since it is rejected during the analysis as being similar to an afterpulse.

[11] As demonstrated in [20], event dispersion in the electron recoil band is correlated with charge trapping. It allows correction of trapping effects and improvement of the energy resolution of both fiducial channels. This charge trapping correction procedure also improves heat energy resolution. Nevertheless, no clear improvement is achieved below E_r = 50 keV. For this reason the energy correction is not applied to WIMP search analysis as we expect measured ionization energies due to a WIMP interaction to be below 50 keV.

2017 JINST 12 P08010

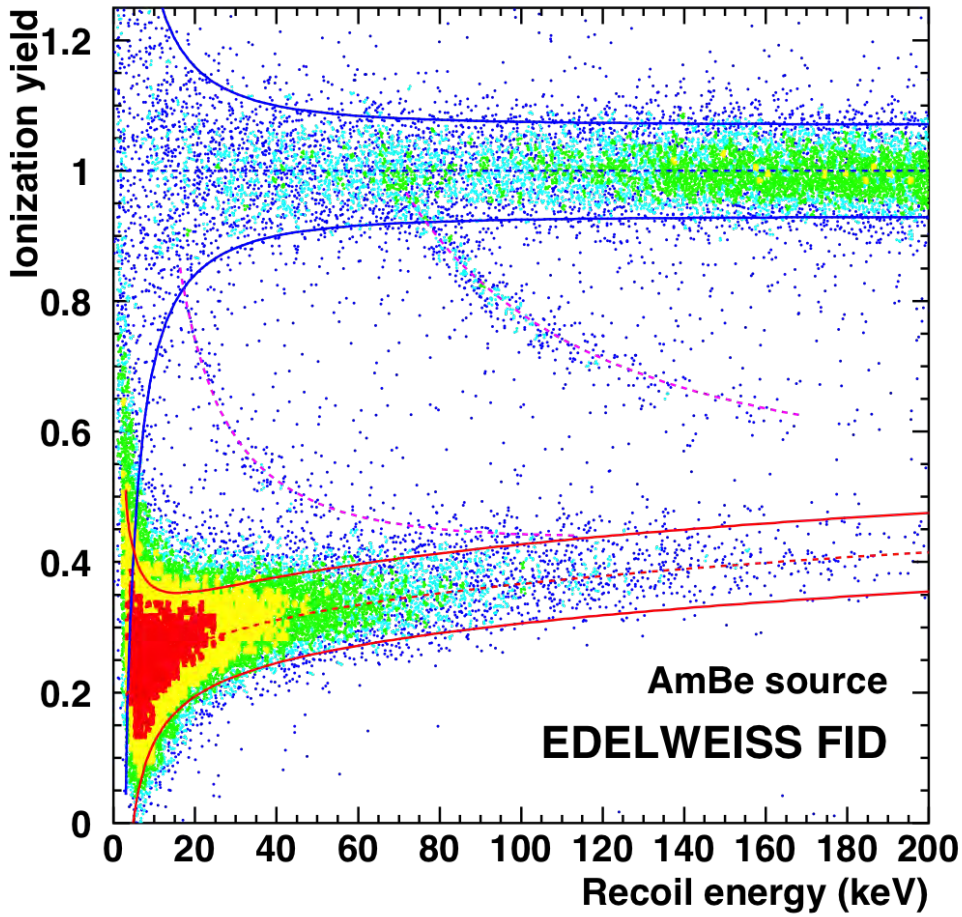

Figure 11. Ionization yield versus recoil energy for a large statistics ($> 3 \times 10^4$) of events from a neutron calibration using an AmBe source. The two red (blue) solid lines delimit the 90% C.L. nuclear (electron) recoil band. Purple dashed lines correspond to inelastic scattering of neutrons on the first (13.28 keV) or the third (68.75 keV) excited state of ^{73}Ge.

between 450 and 600 eV (FWHM) for most of the 800-g FID detectors, as presented in section 7.2, measured resolutions at 356 keV are as large as $5\% \times E_{\text{ion}}$. Nevertheless, these resolutions are sufficient to determine the absolute energy scale with a satisfactory precision. The procedure is carried out in two steps: the fiducial electrode D is first used to adjust the peak position; then the ratios of the amplitude of the D electrode to all other electrodes are determined. The gains and the cross-talk coefficients are obtained for all the electrodes.

After the calibration procedure, individual ionization energies $E_{\text{ion}-x}$ ($x = a,\ b,\ c,\ d$) are reconstructed for both fiducial electrodes B and D and both veto electrodes A and C of each FID detector. Both electronics cross-talks and gains are observed to be constant throughout an overall cool-down period. Due to the FID detector electrode implementation, cross-talk coefficients associated with adjacent channels are around 20–30%.

The heat gains are stable over periods of months but may vary within a few percent between two short data taking periods (around 24h) or at the beginning of a cool-down. These gains are

2017 JINST 12 P08010

measured using the heat-over-ionization ratio of γ-ray background events during WIMP search and calibration runs. This ratio is also used to measure and correct the non-linearities of the heat channels as a function of energy. After calibration one obtains the linear heat energy E_{heat-1} E_{heat-2}) for NTD1 (NTD2), for which electron recoils with energy E_r in the fiducial volume have $E_r = E_{\rm fid} = E_{heat-x}$, with $x = 1,\ 2$ (see table 1 for definitions of variables).

7.1.3 Definition of energy variables

After the calibration procedures, all energy scales are expressed in keV electron equivalent (keV$_{ee}$). For the purpose of the analysis, individual ionization and heat energies can be combined into other energy variables, as seen in eqs. (7.2) and (7.3):

$$E_{dif} = \frac{(E_{\rm ion-b} - E_{\rm ion-d})}{2} \quad ; \qquad E_{\rm fid} = \frac{(E_{\rm ion-b} + E_{\rm ion-d})}{2} \tag{7.2}$$

$$E_i = \frac{(E_{\rm ion-a} + E_{\rm ion-b} + E_{\rm ion-c} + E_{\rm ion-d})}{2} \quad ; \qquad E_{\rm veto} = E_{\rm ion-a} + E_{\rm ion-c} \tag{7.3}$$

where E_{dif} is the difference between the charge collection measured on the two fiducial electrodes, $E_{\rm fid}$ is the fiducial ionization energy, E_i is the total ionization energy and $E_{\rm veto}$ is the veto energy used to define surface events with respect to bulk events.

In addition, E_c is defined as the combined heat energy, which corresponds to the resolution-weighted average of the measured heat energies E_{heat-1} and E_{heat-2} of the two NTDs. All the variables associated with energies and baseline resolutions are listed in table 1.[12]

Table 1. Energy variables and the associated baseline resolutions.

Variable	Description
$E_{\rm ion-a}$, $E_{\rm ion-c}$	Ionization energy of veto channel A and C
FWHM$_{\rm ion-a}$, FWHM$_{\rm ion-c}$	Associated baseline resolutions (FWHM)
$E_{\rm ion-b}$, $E_{\rm ion-d}$	Ionization energy of fiducial channel B and D
FWHM$_{\rm ion-b}$, FWHM$_{\rm ion-d}$	Associated baseline resolutions (FWHM)
E_{dif}	Difference between charge collections measured on the 2 fiducial electrodes
FWHM$_{dif}$	Associated baseline resolution (FWHM)
$E_{\rm fid}$	Fiducial ionization energy
FWHM$_{\rm fid}$	Associated baseline resolution (FWHM)
E_i	Total ionization energy
FWHM$_i$	Associated baseline resolution (FWHM)
$E_{\rm veto}$	Veto ionization energy
FWHM$_{\rm veto}$	Associated baseline resolution (FWHM)
E_{heat-1}, E_{heat-2}	Heat energy of NTD1 and NTD2
FWHM$_{heat-1}$, FWHM$_{heat-2}$	Associated baseline resolutions (FWHM)
E_c	Combined heat energy
FWHM$_c$	Associated baseline resolution (FWHM)

[12]Resolutions FWHM of channel or channel combination var are defined as FWHM$_{var} = 2.35 \times \sigma(E_{var})$.

2017 JINST 12 P08010

The general form of the recoil energy E_r as introduced in eq. (7.1) can be obtained for any interaction from the combined heat signal E_c, after an appropriate subtraction of the Neganov-Luke effect:

$$E_r = E_c \left(1 + \frac{V}{\varepsilon_\gamma}\right) - \sum_j \left(\frac{V_j}{\varepsilon_\gamma} E_{\text{ion}-j}\right) \tag{7.4}$$

where V_j is the voltage applied on electrode j and $E_{\text{ion}-j}$ the asssociated ionization energy. Note that eq. (7.4) holds for interactions taking place in any part of the detector including multiple scatters.

In terms of variables E_{fid}, E_{veto} and E_c, and considering that charges are collected not only on the fiducial electrodes with a difference of potential $V_{\text{fid}} = |V_{BD}|$, but also in the surface volume between one fiducial and one veto electrode with a difference of potential $V' = |V_{AB}| = |V_{CD}|$, the definition of the recoil energy E_r becomes:[13]

$$E_r = E_c \left(1 + \frac{V}{\varepsilon_\gamma}\right) - \frac{1}{\varepsilon_\gamma}\left(V_{\text{fid}}\left(E_{\text{fid}} - \frac{1}{2}E_{\text{veto}}\right) + V' E_{\text{veto}}\right) \tag{7.5}$$

The associated ionization yield is given by:

$$Q(E_r) = \frac{E_i}{E_r} \tag{7.6}$$

In conclusion it is worth mentioning that despite the well-understood charge trapping mechanism leading to broadening of detector resolutions, both ionization and heat calibrations are well controlled, within 5%, for all FID detectors. As an illustration, figures 12 and 13 show cosmogenic lines (as defined in section 7.3.2) for the 24 detectors used in Run 308 for coincidence studies, measured with fiducial ionization energy E_{fid} and combined heat energy E_c, respectively.[14] In both figures the two red dashed lines correspond to the expected 8.98 and 10.37 keV cosmogenic peak positions.

7.2 800-g FID detector baseline resolutions

The baseline resolutions per detector are determined using events for which the considered detector did not trigger the data acquisition. The resulting signal amplitudes for each channel have gaussian distributions. Each channel resolution is determined as the standard deviation of the gaussian fit to the distribution of baseline amplitudes recorded during a time interval of one hour and leads to associated FWHM values. Average FWHM baseline resolutions and online thresholds for physical events in WIMP runs obtained during the long data taking of Run 308 are listed in table 2 for the 24 detectors used for coincidence studies in EDELWEISS-III analyses.

Dispersions from these average FWHM values can be estimated from figure 14 a), which presents baseline fiducial ionization FWHM resolution versus heat baseline FWHM resolution for the 24 detectors used for coincidence studies. The color encoding shows FWHM resolution combinations occurring a certain number of 1 h periods, stars denote the average values per bolometer as given in table 2. Figure 14 underlines that FWHM_{fid} values are mainly below 0.7 keV_{ee} for fiducial ionization energies whereas FWHM_c values are mainly below 1.5 keV_{ee} for

[13] For bulk events with $E_{\text{veto}} = 0$, recoil energy as expressed in eq. (7.5) is identical as the one given e.g. in ref. [49]. Interestingly eq. (7.5) is also valid when the charge is collected only between A and C veto electrodes with $E_{\text{veto}} = 2E_i$.

[14] During Run 308 only 24 detectors were read out over the 36 installed in the cryostat.

2017 JINST 12 P08010

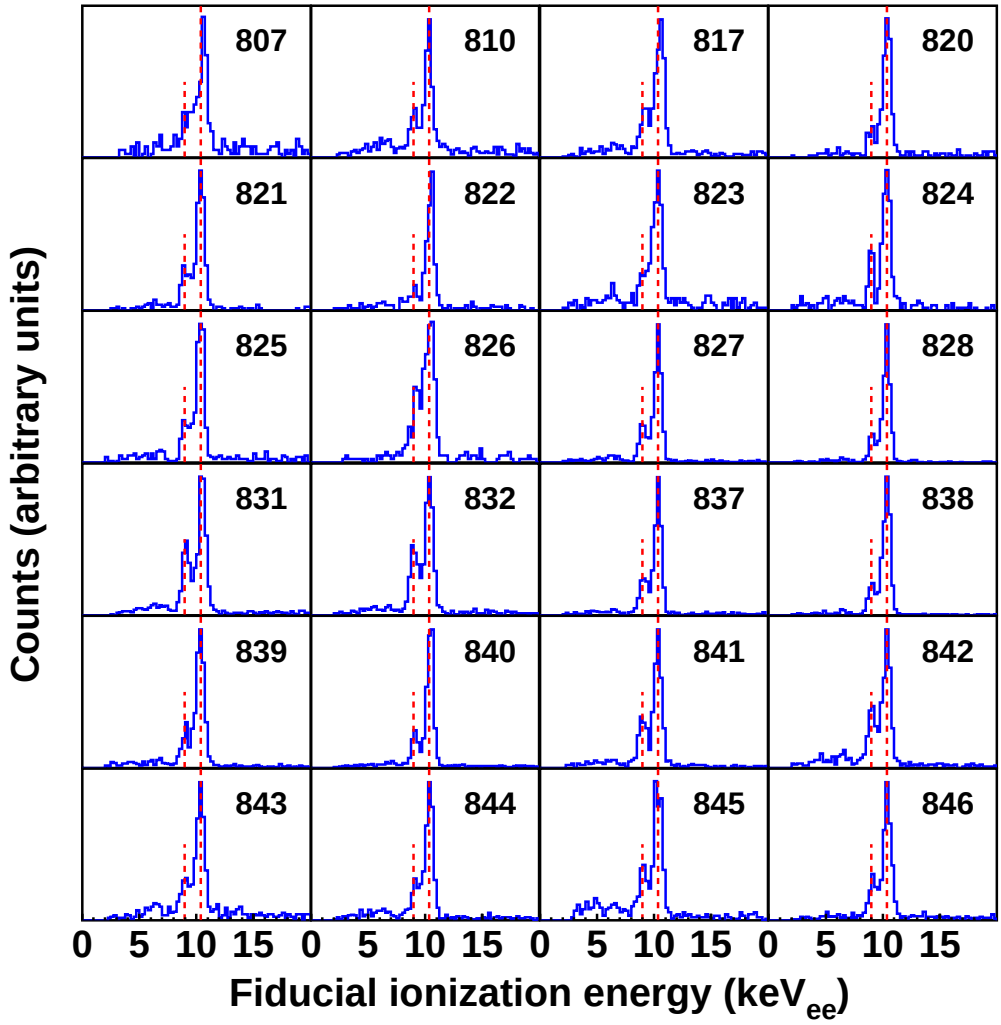

Figure 12. Calibration of ionization energy scales: cosmogenic peaks (as described in section 7.3.2) for the 24 detectors used for coincidence studies, measured with fiducial ionization energy $E_{\rm fid}$. The 8.98 keV and 10.37 keV peaks are found at expected positions, as demonstrated with the two red dashed lines. Calibrations are well under control with non linearities lower than 5%.

heat energies. Such baseline resolutions are good enough for standard mass WIMP search using the 800-g FID detectors, while for low mass studies [50] a subset of 8 bolometers with clearly better resolutions has been used. In the latter analysis time-periods with online threshold less than 1.5 keV$_{ee}$ are selected, and a small fraction of time when the combined heat baseline FWHM$_c$ is larger than 1 keV$_{ee}$ or the fiducial ionization FWHM$_{\rm fid}$ is larger than 0.7 keV$_{ee}$ is rejected (see figure 14 b) and in [50]). This tighter selection changes the resolutions by less than 10%.

7.3 Fiducial volume of the 800-g FID detectors

7.3.1 Definition of fiducial cuts

Following an energy deposit in the bulk, electrons and holes created drift towards the fiducial electrodes B and D whereas for surface events charge collection is shared between one fiducial

2017 JINST 12 P08010

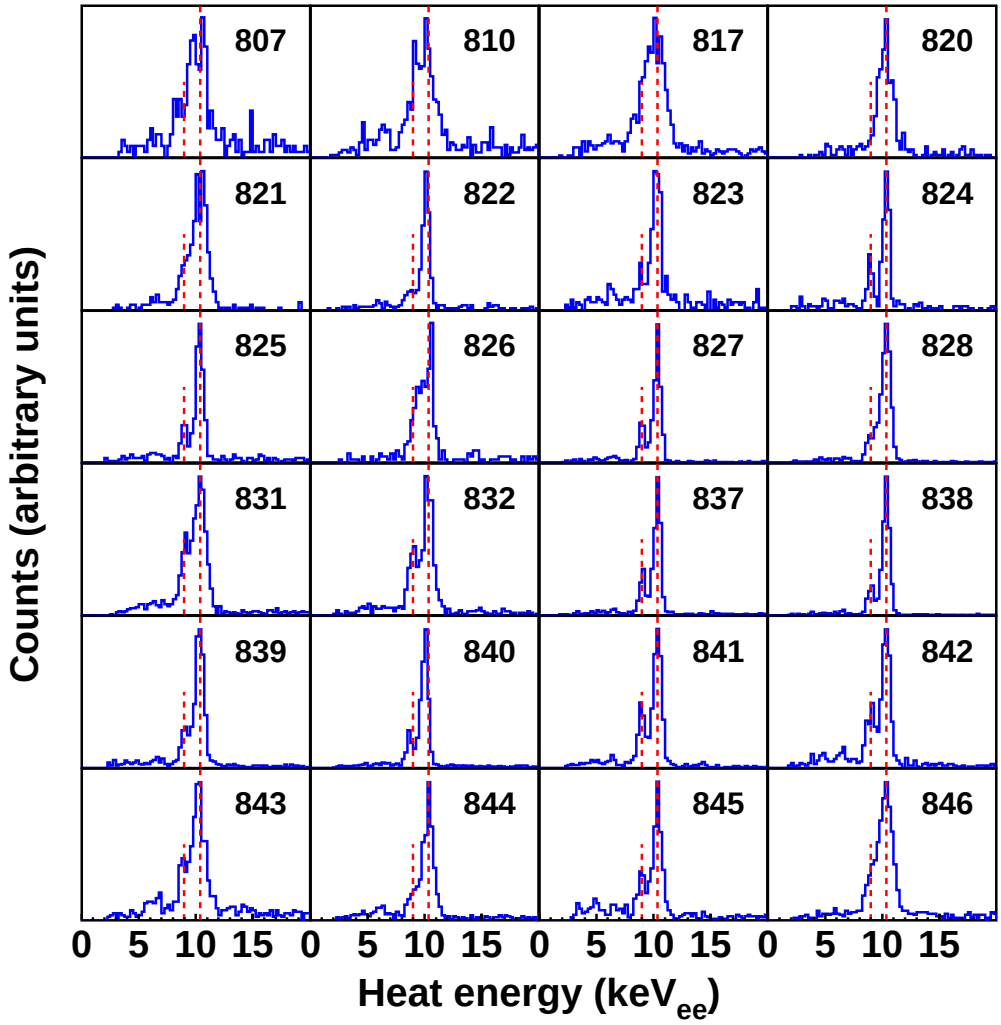

Figure 13. Same as figure 12 for heat energy channels, using combined heat energy E_c.

electrode and one veto electrode (either $B\&A$ or $D\&C$). Fiducial cuts are used to reject surface events (^{206}Pb recoils or surface β and γ events), which could be otherwise misidentified as nuclear recoils due to an incomplete charge collection. The fiducial selection is performed requiring an equal charge of opposite sign on fiducial electrodes and no charge collected on the veto electrodes A and C.

Three cuts are performed to optimize the surface event rejection while keeping an efficiency of fiducial event selection of at least 99% for each cut: two of them concern the ionization energy measured by each of the veto electrodes ($E_{\text{ion}-a}$ and $E_{\text{ion}-c}$); the third cut is performed on charge collection difference E_{dif}. An example of the cuts is given in figure 15 (left), which shows the different event categories in the plane (E_{fid}, $E_{\text{ion}-a}$) and the associated fiducial cut on veto A.

The distribution of fiducial events is also defined by the energy-dependent dispersion, as shown for veto A in figure 15 (right) for events with energies between 320 and 380 keV$_{ee}$ (main γ-line at 356 keV for ^{133}Ba decay, see figure 15 (left)). This dispersion has a nearly gaussian distribution, thus using a cut at $\pm 2.576\sigma$ from the distribution's center provides a fiducial event selection efficiency

2017 JINST 12 P08010

Table 2. Average FWHM resolutions and thresholds for physical events in WIMP runs obtained during EDELWEISS-III data taking (Run 308). $\mathrm{FWHM_{fid}}$, FWHM_i and FWHM_c are associated respectively with E_{fid}, E_i and E_c as listed in table 1. The online threshold is the lowest of the two heat channels and FWHM_c corresponds to the combined heat baseline FWHM resolution.

Detector	FID Bias V_{fid} (V)	Baseline resolutions (keV_{ee}) (FWHM)			Online threshold (keV_{ee})
		$\mathrm{FWHM_{fid}}$	FWHM_i	FWHM_c	
FID807	6.4	0.84	1.19	1.62	3.41
FID810	8	0.51	0.78	1.85	2.93
FID817	6.4	0.56	0.85	1.44	3.41
FID820	8	0.57	0.90	1.03	2.29
FID821	8	0.55	0.89	1.08	2.39
FID822	8	0.53	0.64	0.59	1.32
FID823	8	0.46	0.73	0.78	1.76
FID824	8	0.55	0.75	0.32	0.62
FID825	8	0.45	0.69	0.49	0.94
FID826	16	0.61	0.90	0.28	0.47
FID827	8	0.51	0.80	0.42	0.81
FID828	8	0.59	0.83	0.84	1.59
FID831	8	0.53	0.92	1.15	3.31
FID832	8	0.60	0.89	0.78	1.65
FID837	8	0.54	0.92	0.43	0.98
FID838	8	0.53	0.78	0.44	0.93
FID839	8	0.55	0.92	0.62	1.20
FID840	8	0.53	1.17	0.57	1.44
FID841	8	0.48	0.80	0.53	0.99
FID842	8	0.62	0.93	0.60	1.25
FID843	8	0.56	0.83	1.37	2.59
FID844	8	0.51	0.71	0.94	1.67
FID845	8	0.61	1.27	0.76	1.64
FID846	8	0.67	0.96	1.22	2.82

of 99%. Due to the dispersion enlargement with E_{fid}, the selection has to be reproduced for different fiducial ionization energy intervals.

Fiducial cuts corresponding to baseline resolution conditions of each channel are obtained in a similar way, as shown in figure 16 for veto A (left) and charge collection difference (right) of one detector. Green (red) lines correspond to fiducial cuts during a period of one hour with having the best (the worst) resolution. Orange lines correspond to fiducial cuts for average resolutions. Surface event rejection at low energy is obtained applying quality cuts on $\mathrm{FWHM_{ion-}}_a$, $\mathrm{FWHM_{ion-}}_c$ and FWHM_{dif} baseline resolutions (as defined in table 1). A semi-automatic procedure is carried out using 3 conditions on E_{fid} combined with $E_{\mathrm{ion-}a}$, $E_{\mathrm{ion-}c}$ and E_{dif}, as well as on their baseline resolutions [51]. It allows to ensure a fiducial selection efficiency of 99% independent of the experimental conditions.

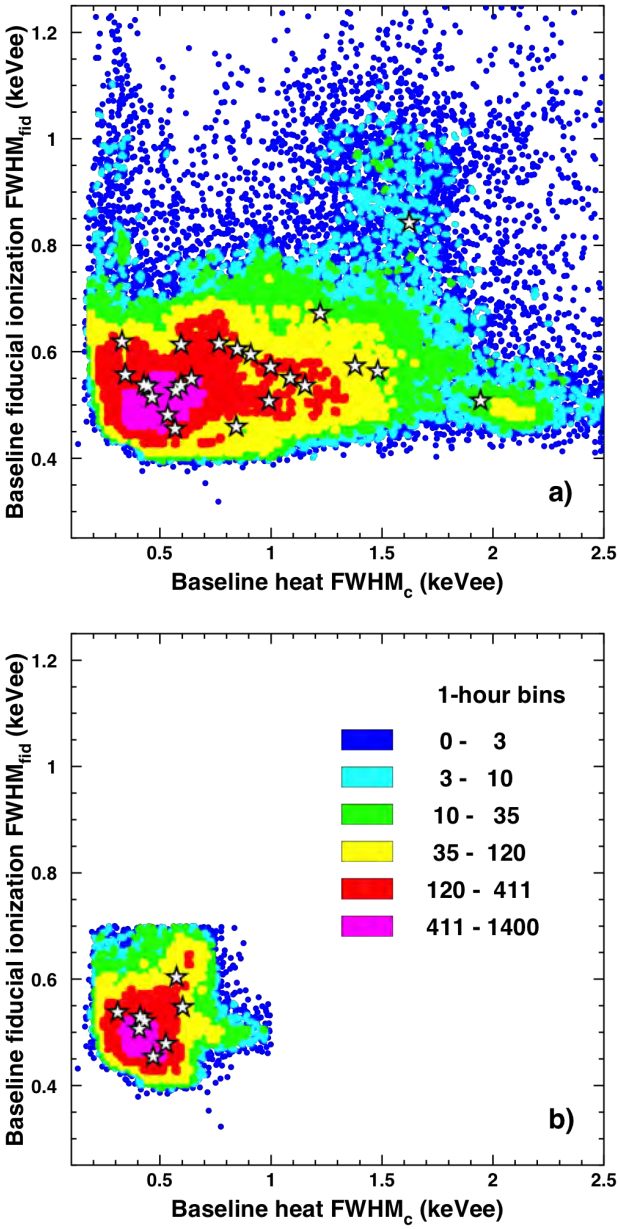

Figure 14. Baseline fiducial ionization FWHM resolution ($FWHM_{fid}$) versus the baseline combined heat FWHM resolution ($FWHM_c$), in keV_{ee} (color code denotes number of 1 h periods, stars represent average bolometer values as given in table 2): a) for the 24 detectors used for coincidence studies; b) after time period selection for the 8 bolometers used for low-mass WIMP studies [50], with online threshold less than 1.5 keV_{ee}, and rejecting a small fraction of time when $FWHM_c$ is larger than 1 keV_{ee} or $FWHM_{fid}$ is larger than 0.7 keV_{ee}.

7.3.2 Determination of the fiducial volume

EDELWEISS-III crystals have been moved to the underground location, they have been exposed to cosmic rays at the surface. This resulted in a production of ^{68}Ge ($T_{1/2}$ = 270.8 d) and ^{65}Zn ($T_{1/2}$ =

2017 JINST 12 P08010

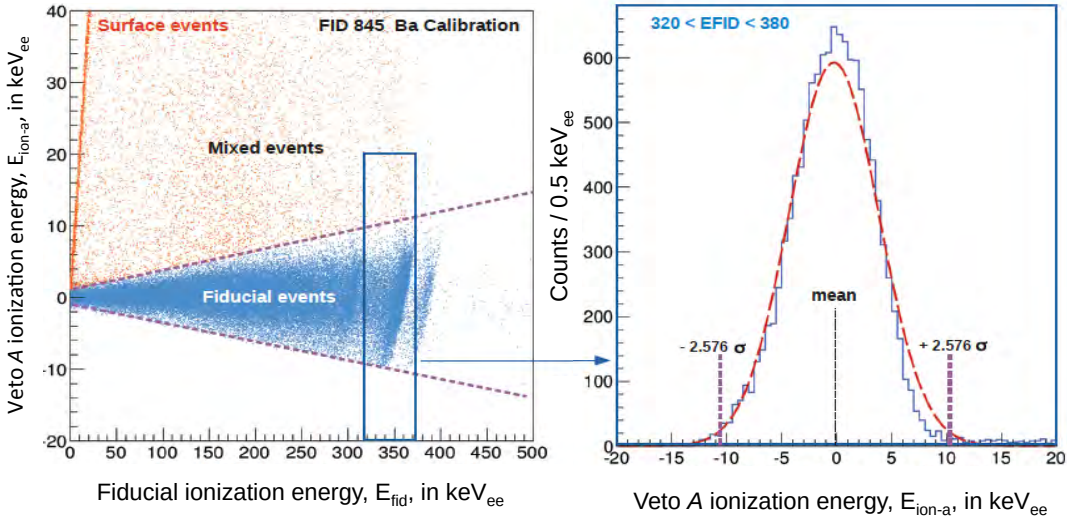

Figure 15. Example of fiducial event selection. Left: distribution of events in the plane (E_{fid}, $E_{\text{ion}-a}$). Selected events after fiducial cut (dashed purple lines) are represented in blue. Overdensity of orange dots corresponds to pure surface events, other orange dots are intermediate events between the two categories. Right: energy distribution for veto electrode A, corresponding to events with fiducial energy E_{fid} between 320 and 380 keV_{ee}, fitted with a gaussian distribution of standard deviation σ. Dashed purple lines correspond to values of $E_{\text{ion}-a}$ at $\pm 2.576\sigma$ from the adjusted distribution center. These values are used to determine the fiducial cut with 99% efficiency for bulk events. Figure extracted from [51].

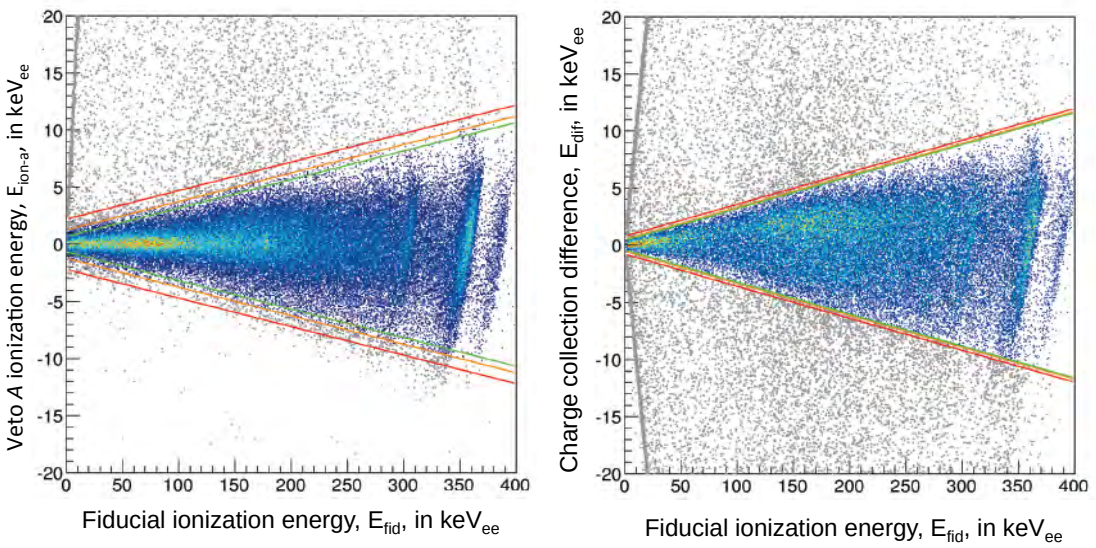

Figure 16. Example of fiducial cut (orange solid lines) after optimized data selection on an hourly basis. Fiducial events are represented as color dots whereas non fiducial events are shown as gray dots. Green and red lines correspond to the fiducial cut for having the best and the worst resolution respectively. Left: cut on $E_{\text{ion}-a}$ for veto A electrode. Right: cut on charge collection difference E_{dif}. Figure extracted from [51].

2017 JINST 12 P08010

244.3 d) isotopes by cosmogenic activation predominantly due to neutron flux. These cosmogenic isotopes decay by electron capture to ^{68}Ga ($T_{1/2}$ = 67.7 min, E_K = 10.37 keV) and ^{65}Cu (stable, E_K = 8.98 keV), accompanied by an X-ray cascade measured as a single-site event inside the detectors, with energy depending on the considered element.[15] ^{68}Ga further decays to ^{68}Zn by electron capture (stable, E_K = 9.66 keV). In addition thermal neutrons absorbed during AmBe calibration by ^{70}Ge isotopes in the germanium crystals produce ^{71}Ge ($T_{1/2}$ = 11.4 d), which also decays by electron capture towards ^{71}Ga (stable, E_K = 10.37 keV). More details on cosmogenic activation in EDELWEISS germanium detectors can be found in refs. [50, 53].

To determine the fiducial volume, one uses these single-site events uniformly distributed in the whole detector volume and obtained during WIMP search data taking. The fiducial volume is calculated from the ratio of the events in the triplet at 8.98, 9.66 and 10.37 keV surviving the fiducial cuts to the total of these events.

Cosmogenic peaks at 8.98 and 10.37 keV are clearly visible for most of the detectors, as seen in figures 12 and 13, respectively, for fiducial ionization energy and combined heat energy. Using the three peaks at 8.98 keV, 9.66 keV and 10.37 keV, the first step of the fiducial volume determination consists of a fit of these lines to gaussian distributions in order to determine the relative fraction of events in each peak of the triplet. A cut on the ionization yield value (see eq. (7.6)), $0.55 < Q(E_r) < 2.5$, rejects ^{206}Pb recoils and most of β events, while keeping more than 96% of γ-ray events in the first 2 mm under the electrodes. Furthermore, a cut on total ionization of $E_i > 5\sigma_{E_i}$ around baseline is applied to reject heat-only events characterized by no ionization signal [54].

The 10 keV triplet can be observed in energy spectra both in ionization energy and recoil energy, for events accepted or rejected by fiducial cuts as shown in figure 17. To better control systematic effects due to background subtraction, two methods are used in order to evaluate the number of events in the peaks in the spectra with and without fiducial selection. The first method consists of counting the number of fiducial events (non-fiducial events) in the energy interval E_i between 7 and 13 keV$_{ee}$ after subtraction of the average background estimated between 3 and 30 keV$_{ee}$ (figure 17 (a) and (b)). The second method consists of fitting the E_r recoil energy spectrum with three gaussian functions with the same width and at relative positions and heights constrained by the values obtained in the fit of the fiducial data described above. The background is a constant multiplied by an error function (Erf) to take into account the efficiency loss due to the 5σ cut on E_i (figure 17 (c) and (d)). In both methods, the fiducial volume fraction is the ratio of the number of fiducial events divided by the sum of fiducial and non-fiducial events. Results are presented in table 3 for 22 detectors.[16] The quoted values are the average obtained using both methods, the difference being used as a systematic uncertainty.

One can see from table 3 that 19 of the 22 bolometers have their fiducial volume fraction compatible within errors with a weighted average value of (74.6 ± 0.4)%, with a reduced χ^2 of 1.04. Three bolometers have lower fiducial volume fractions. Detector FID824 has a spacing between electrodes of 4 mm instead of 2 mm. The FID average thickness of the surface region for a spacing

[15] E_K are binding energies of K-shell electrons. Values of E_K energies are taken from [52].

[16] FID822 (889 g) and FID840 (878 g) detectors are not included, since their fiducial volume measurements are not relevant (fiducial *B* electrode of FID822 had a malfunctioning; *A* and *C* veto electrodes of FID840 had a readout problem leading to a planar configuration for this detector).

2017 JINST 12 P08010

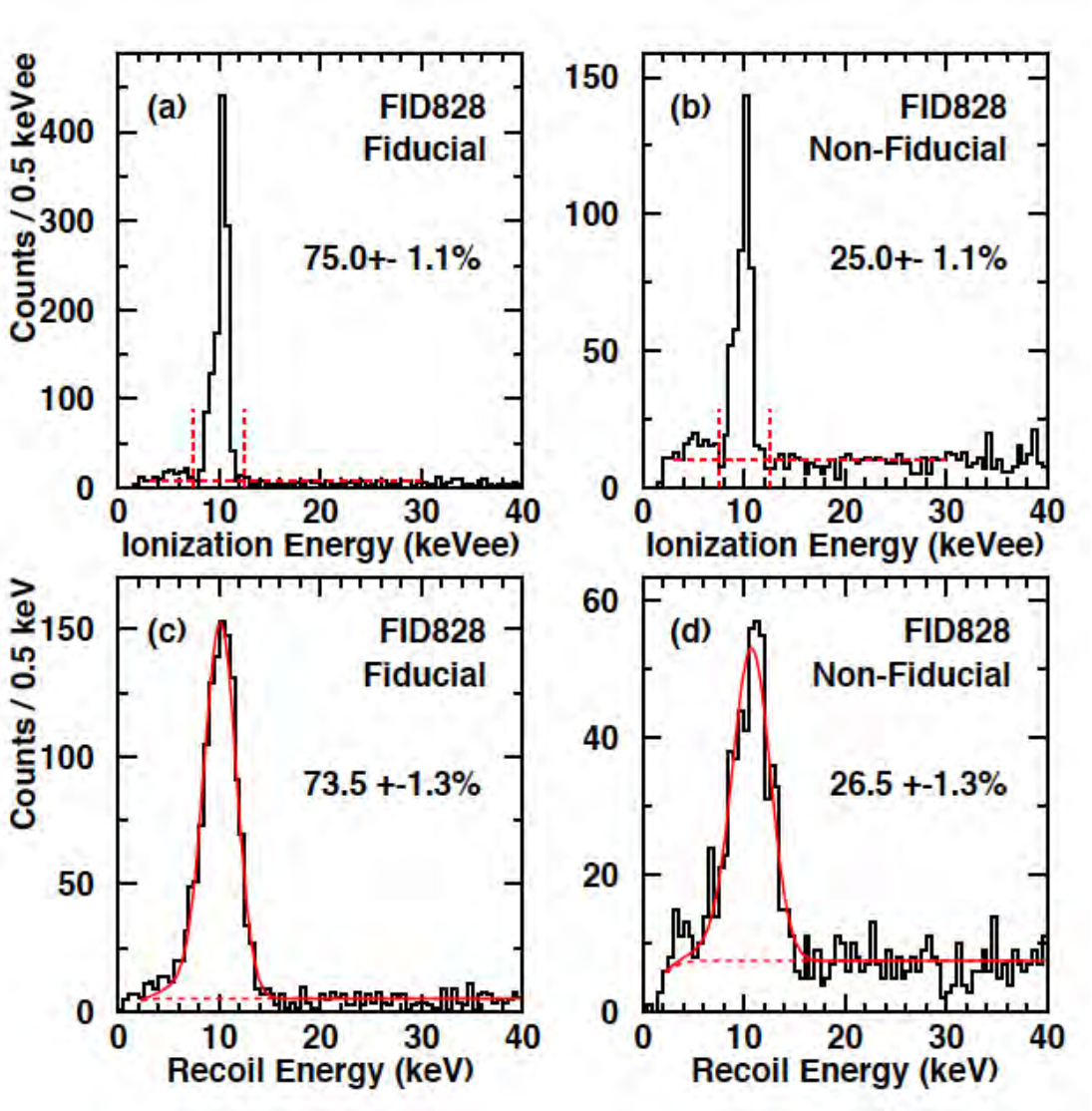

Figure 17. Example of fiducial volume determination for the FID828 detector. Figures (a) and (c) (resp. (b) and (d)) show total ionization energy and recoil energy spectra for the fiducial events (resp. non-fiducial events), obtained after applying $0.55 < Q(E_r) < 2.5$ and $E_i > 5\sigma_{E_i}$ cuts. Associated fiducial volume (in %) as obtained by the two methods described in the text are indicated in (a) and (c) plots.

of 2 mm between electrodes (red region on figure 3) is $\sim$ 2.5 mm. It can be expected to double as the spacing doubles, nearly corresponding to the observed increase of non-fiducial volume in FID824. For the other two detectors (FID807 and FID826) the reduction of the volume fraction appears to be associated with wiring issues on the electrodes, which prevent them to be used for precision measurements. In these detectors some fiducial γ-ray events have ionization yield $Q(E_r) = 0.1$ probably due to a disconnected ring in a fiducial electrode. The analyses of refs. [50, 53, 54] use the fiducial volume fractions of table 3 in order to account for the value of FID824, and the possible $\pm 5\%$ detector-to-detector variation observed in that table.

2017 JINST 12 P08010

Table 3. Fiducial volume fraction and associated total uncertainty, in %, for 22 FID detectors. The quoted errors are the quadratic sum of systematic and statistic errors.

Detector	Mass (g)	Fiducial fraction (%)
FID807	820	55.6 ± 5.9
FID810	820	73.2 ± 3.4
FID817	878	78.3 ± 1.6
FID820	877	72.2 ± 3.3
FID821	878	75.0 ± 3.4
FID823	882	72.7 ± 5.6
FID824	877	62.5 ± 2.3
FID825	878	74.3 ± 2.3
FID826	874	49.2 ± 7.2
FID827	873	74.9 ± 1.1
FID828	871	74.4 ± 1.8
FID831	878	73.2 ± 2.7
FID832	875	70.4 ± 5.2
FID837	875	72.7 ± 1.4
FID838	869	73.8 ± 1.1
FID839	869	76.1 ± 1.1
FID841	878	74.3 ± 1.3
FID842	878	71.3 ± 7.5
FID843	880	70.0 ± 2.3
FID844	875	79.6 ± 3.4
FID845	886	71.7 ± 9.0
FID846	868	76.0 ± 1.8

7.4 γ-ray rejection factor

Using γ calibrations of previous generation ID detectors performed in the context of EDELWEISS-II with a ^{133}Ba source, 6 events out of a total of 3.45×10^5 were found with a reduced charge signal above a 20 keV threshold, which could mimic a nuclear recoil. A likely explanation for these events is the large region of low guard field of the ID detector design: misidentified γ-rays could originate from nonrejected multiple scatterings of γ in the bulk (full charge collection) and in the planar electrode on the side of the detector (incomplete charge collection). The associated probability of γ-misidentification was calculated to be $R_{\gamma-\mathrm{mis-ID}} = (3 \pm 1) \times 10^{-5}$, leading to an expected background from γ-ray leakage of 0.9 events for the 384 kg $\cdot$ d effective exposure of EDELWEISS-II [14].

In the new FID detector design, where all planar electrodes are replaced by interleaved electrodes, this background of misidentified γ is reduced by two effects: firstly the relative probability of Compton scattering in the non-fiducial volume is reduced by the reduction of this volume, and secondly, charge collection in this volume is improved as the electric fields in the non-fiducial region are systematically higher than in the bulk. Preliminary results on an improvement in γ rejection

2017 JINST 12 P08010

had been reported in [55]. We present here an updated measurement, combining this result with additional γ calibration data recorded with ^{133}Ba sources, using the array of 24 FID detectors, more than doubling the total available statistics. The efficiency for detecting nuclear recoils in the combined analysis is shown in figure 18, following the procedure described in [50]. It is 38% at 10 keV and 89% at 20 keV. The irregular rise of the function reflects the varying analysis thresholds of the different detectors and data acquisition periods. Out of the 9.38×10^5 γ-ray events in the

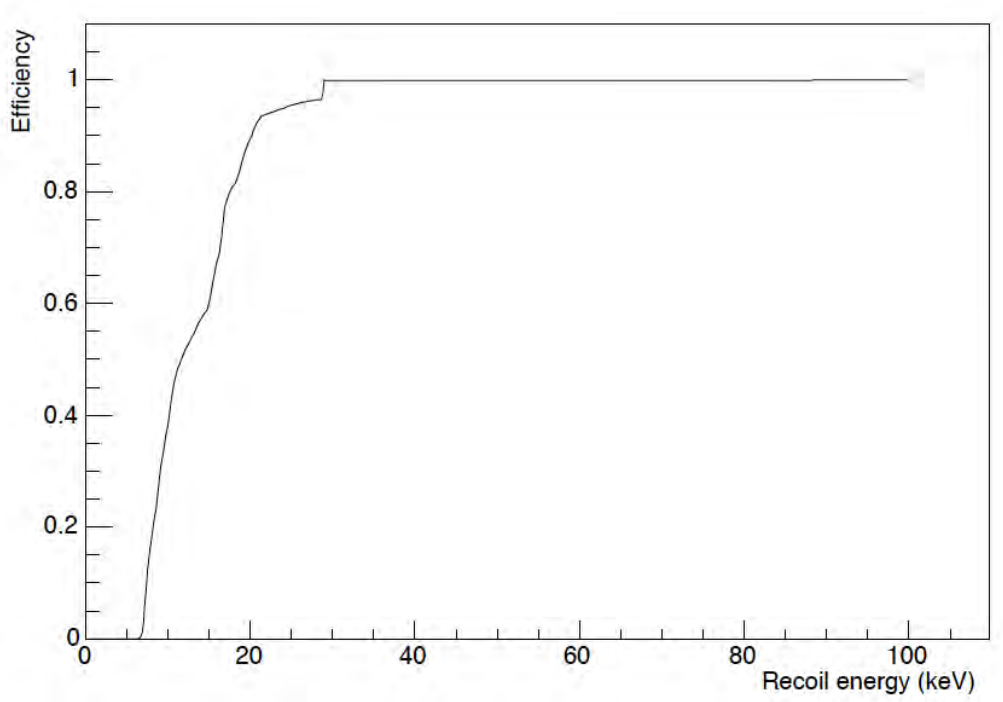

Figure 18. Efficiency curve associated with data presented in figure 19 and resulting from the combination of two different sets of data with FID detectors in the EDELWEISS setup.

sample, shown in figure 19, six events are found below $Q(E_r) = 0.6$ but none are observed in the 90% C.L. nuclear recoil band. Information about the six events are reported in table 4: the first three events were recorded during the 2010 calibration campaign by two of the first FID detectors, whereas the three last events are from Run 308 (see table 2).[17] No systematic effects are seen, with events occurring in five different detectors and six different days.

The 90% C.L. limit on the leakage of γ-ray events above threshold into the nuclear recoil band is $R_{\gamma-\text{mis}-\text{FID}} < 2.5 \times 10^{-6}$, at least a factor 12 better than the leaking fraction measured with ID detectors.

7.5 Surface rejection factor

Events occurring at the detector surface suffer from incomplete charge collection, which leads to an underestimation of the ionization yield $Q(E_r)$. The main surface background source is radon

[17]The first three events have been recorded with FID803 and FID804 detectors. At the time of the measurement, their fiducial ionization resolutions were between 1.5 and 1.7 keV FWHM, and their heat resolutions were between 0.8 and 1.0 keV FWHM.

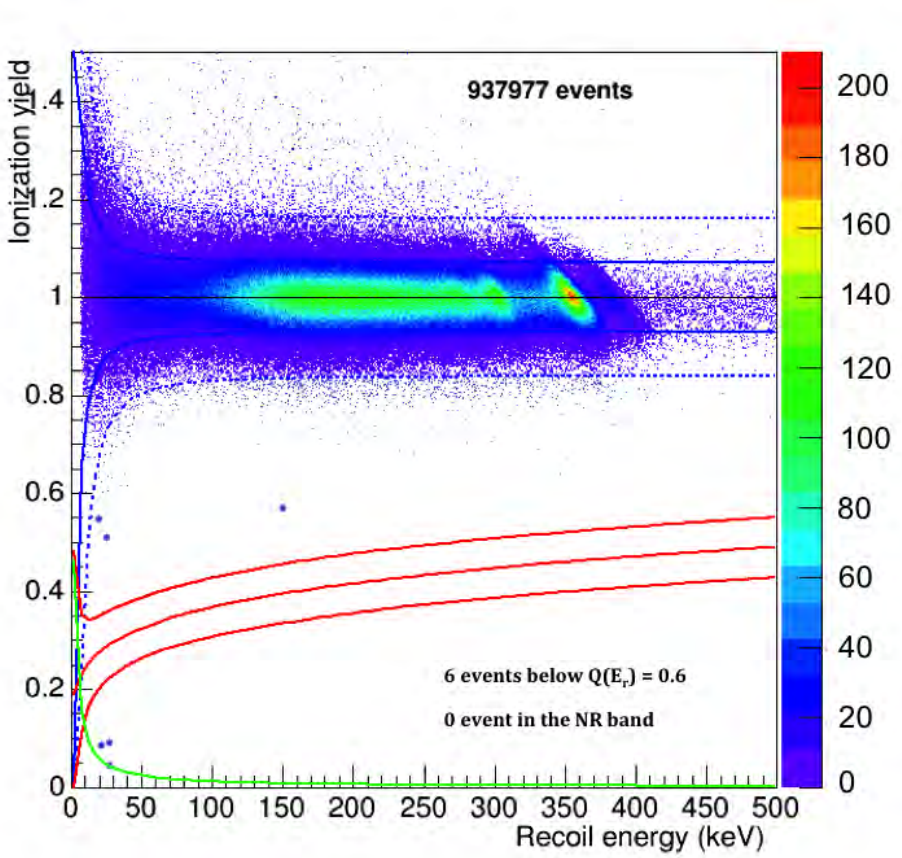

Figure 19. Ionization yield $Q(E_r)$ versus recoil energy E_r for events from γ calibrations with ^{133}Ba sources with FID detectors. Dashed and continuous blue lines correspond to 99.98% C.L. and 90% C.L. electronic recoil bands, whereas continuous red lines correspond to the 90% C.L. nuclear recoil band. The green line corresponds to the fiducial ionization threshold. Although there are 6 single events below $Q(E_r) = 0.6$, none of the 937977 recorded events leaked into the nuclear recoil band.

Table 4. List of events with $Q(E_r) < 0.6$ in figure 19. There is no obvious systematic effect since the six events are associated with different detectors or different dates.

Event number	E_r (keV)	$Q(E_r)$	FID Detector	Event date
1	19.33	0.549	804	Sep. 11th 2010
2	150.26	0.573	804	Oct. 7th 2010
3	25.84	0.512	803	Nov. 20th 2010
4	27.51	0.044	824	Sep. 15th 2014
5	27.69	0.091	821	Nov. 25th 2014
6	21.08	0.089	838	Nov. 26th 2014

daughters deposited on the detector surface and the copper housing. Radon (^{222}Rn, $T_{1/2}$ = 3.84 d) quickly decays (via a series of decays) into the long-lived isotope of ^{210}Pb ($T_{1/2}$ = 22.24 years). As shown in figure 20 (left), the decay of ^{210}Pb leads to the stable ^{206}Pb isotope via the cascade:

$$^{210}\mathrm{Pb} \xrightarrow[Q\,=\,63.5\ \mathrm{keV}]{\beta^-} {}^{210}\mathrm{Bi} \xrightarrow[Q\,=\,1162.7\ \mathrm{keV}]{\beta^-} {}^{210}\mathrm{Po} \xrightarrow[Q\,=\,5407.5\ \mathrm{keV}]{\alpha} {}^{206}\mathrm{Pb} \qquad (7.7)$$

This cascade results in the emission of both low- and high-energy β-particles, an α-particle of 5.3 MeV and a 103 keV recoiling ^{206}Pb nucleus. These emissions are nearly in equilibrium if the contaminated material is significantly older than the $T_{1/2}$ = 138 d of ^{210}Po. The surface rejection factor of ID detectors was measured in the context of EDELWEISS-II using dedicated ^{210}Pb calibrations and was found to be $R_{\text{surf-ID}} = 6 \times 10^{-5}$ events per α at 90% C.L. for a 20 keV threshold [14].

In order to study the 800-g FID bolometer response to α- and β-backgrounds, a dedicated calibration has been carried out in 2012 with two of the first detectors.[18] For a specific data taking period, they have been equipped with a ^{210}Pb source, fabricated by exposing copper adhesive tape to a radon source. This tape was then attached to the inner surface of the copper case of the Ge detector in such a way that it faced all detector surfaces. As previously, the rejection power of the FID detectors against surface events coming from ^{206}Pb recoils, β or α backgrounds is measured from the number of events that are observed before and after surface rejection.

Depending on the particle type and energy, the particles associated with the ^{210}Pb decay penetrate the detector volume to various depths (see figure 20, left), with either complete or incomplete charge collection. Most of these events should be rejected by applying fiducial cuts (section 7.3.1). By counting the number of remaining events after applying these cuts, the number of misidentified surface events is determined: one event has been found at 15 keV in the 90% C.L. nuclear recoil band for an exposure of 9.7×10^4 α-particles, as shown in figure 20 (right), where the remaining events with an ionization yield of ~ 1 are mostly due to the γ-ray background in the experimental site and to cosmogenic activation of the germanium crystal (section 7.3.2). From this observation, a 90% C.L. limit on the surface event leaking factor $R_{\text{surf-FID}} < 4 \times 10^{-5}$ is derived for a recoil energy threshold of 15 keV [56]. This limit is a factor 1.5 better with respect to the ID design and is measured at lower threshold.

The 46 keV γ-rays emitted in the β-decay of ^{210}Pb with a branching ratio of 4.25% and a penetration depth of 0.4 mm in germanium appear with $Q(E_r) = 1$ on figure 20 (top right). These γ-rays are essentially removed by the fiducial cut (figure 20 (bottom right)), consistent with the expectation that most of them are contained within a depth of 2 mm under the surfaces (section 7.3.2).

The cleaning procedure, as described in section 2, allows to reduce surface α contamination due to radon daughters. However it is possible to measure the total rate of α-particles per day for each of the 24 detectors used for coincidence studies (FID detector masses are given in table 3). They appear as a peak of events with E_r = 5.3 MeV accompanied by a tail of α-particles with degraded energies at $Q(E_r) \sim 0.25$ that can be observed on the top right panel of figure 20. The rates vary from 2.00 ± 0.11 to 10.15 ± 0.26 α/d. With the detector mass as given in 3 this leads to an average total rate of 5.45 α/kg/d, with a standard deviation of $\sigma = 2.9$. Thus less than one surface event per fiducial exposure of 3 400 kg · d is expected in the NR band, considering a fiducial volume fraction of 74.6% (section 7.3.2).

8 Performance of the EDELWEISS-III detector array

Despite active and passive shieldings, there remains a small residual neutron background which can mimic WIMPs in the nuclear recoil band. It originates from high energy neutrons produced by

[18] The detectors are FID803 and FID808. At the time of the measurement, their fiducial ionization resolutions were between 0.7 and 1 keV FWHM, and their heat resolutions were between 1 and 1.4 keV FWHM.

2017 JINST 12 P08010

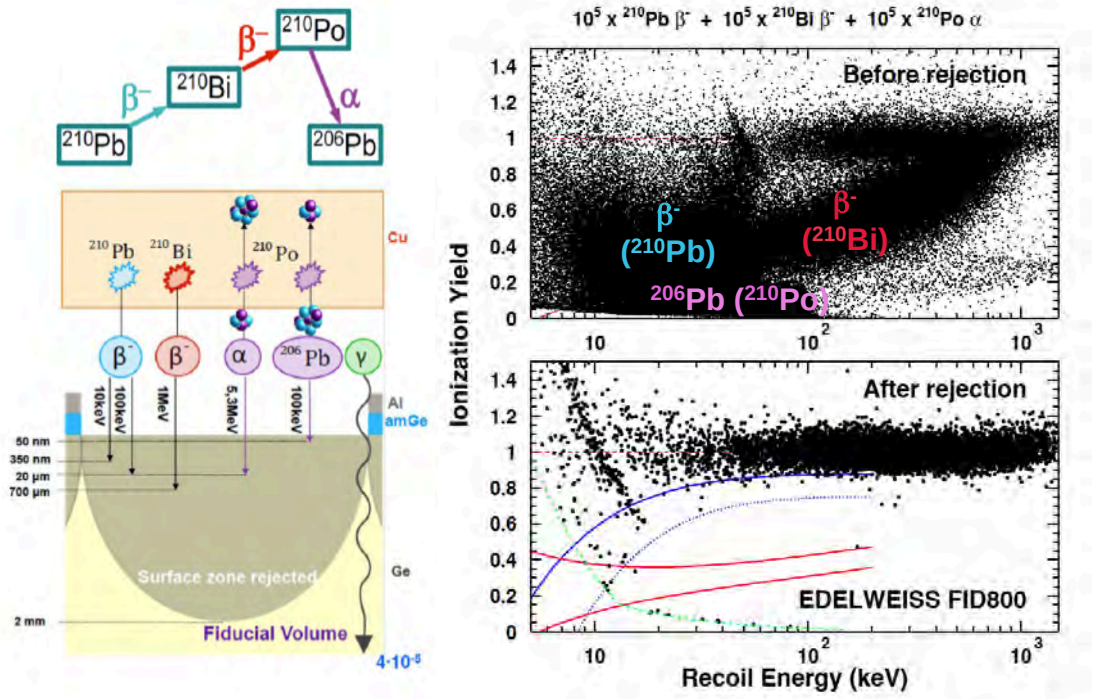

Figure 20. Left: schematic of the surface calibration with a ^{210}Pb source which decays, emitting β- and α-particles of various energies. Right: distribution of ionization yield as a function of recoil energy observed in two 800-g FID detectors, for an exposure to 10^5 ^{210}Pb decays from a source where this isotope is close to equilibrium with its ^{210}Bi and ^{210}Po daughters before (top) and after (bottom) fiducial cuts. The band where 90% of all nuclear recoil events are expected at an ionization yield close to 0.3 is shown in red. The full and dashed blue lines indicate the 90% and 99.98% C.L. regions for γ-rays, respectively. The green dashed hyperbola shows the 2 keV ionization threshold cut. The various populations are indicated accordingly to the color code used in the left schematic. Only one event at 15 keV is remaining inside the nuclear recoil band after fiducial cut [56].

muons that are not tagged by the veto system and from radiogenic neutrons from ^{238}U and ^{232}Th (α, n) reactions and spontaneous fission in the materials surrounding the detectors.

The contamination activity measurements and upper limits associated to the radiopurity budget of the experiment are reported in table 5. The quoted activities of ^{238}U, ^{232}Th and ^{210}Pb assume that all daughters in their chains are in equilibrium. Activities for the ^{232}Th chain are measured using γ-rays from ^{228}Ac, ^{212}Pb, ^{212}Bi or ^{208}Tl, whereas for the ^{238}U chain, γ-rays from ^{214}Pb, ^{214}Bi or ^{234m}Pa are used. The large difference between activity values obtained for ^{238}U and ^{210}Pb can be due to contamination of surfaces with ^{210}Pb.

A special attention was devoted to the activities of the Mill-Max connectors which are the closest to the germanium detectors. Each connector is made of three different components: a pin and a socket, in brass, associated with a copper-beryllium press-fit contact. The activities of these components are listed in the first three lines of table 5. The two brass pieces revealed a specific ^{210}Pb contamination corresponding to a total activity of $\sim$ 0.3 Bq. Also the press-fit contact, even representing less than 10% of the Mill-Max connector mass, is the most important source of ^{238}U close to the detectors, with a total activity of $\sim$ 20 mBq. The precise measurement of U/Th activities

2017 JINST 12 P08010

for the three connector pieces were performed in 2015 using ICP-MS. At that time there was no available alternative to replace these connectors while still providing a highly reliable contact at 18 mK.

8.1 Shielding performance against μ-induced neutron backgrounds

Muon-induced events in germanium bolometers are rejected using the precise synchronisation with the μ-veto system. In a dedicated analysis studying coincidences between the μ-veto system and the bolometers, it was shown that the μ-induced bolometer events can be distinguished from other backgrounds on the basis of their bolometer multiplicity and their total energy deposit in the bolometer. Selecting these events using the hits in the Ge bolometers only, a lower limit of the μ-veto tagging efficiency of $\varepsilon_{\mu-\text{veto}} > 93\%$ (90% C.L.) was derived being limited by the scarce statistics. Geant4-based simulations of muons entering the modified geometry of the experiment were performed in order to derive the rate of all events in the bolometer array induced by muons before applying a veto cut. This rate has been shown to be in good agreement with the measured one extracted from the data [60].

Selecting single fiducial events in the 90% C.L. nuclear recoil band with E_r = [10–100] keV, no coincidence with the μ-veto was identified, leading to an upper limit of the measured rate of μ-induced WIMP-like events in EDELWEISS-III of $\Gamma^{\text{WIMP-like}}_{\mu-\text{ind,meas}} < (1.7 \times 10^{-2})$ events/d (90% C.L.). This rate was found to be $\Gamma^{\text{WIMP-like}}_{\mu-\text{ind,simu}} = (0.76 \pm 0.01(stat)^{+0.26}_{-0.17}(syst)) \times 10^{-2}$ events/d in the corresponding simulation, being compatible with the above upper limit.

For an accumulated exposure of 600 kg · d in the actual geometry of the bolometer array, the pre-veto-cut rate leads to an expected μ-induced background of $N^{\text{WIMP-like}}_{\mu-\text{ind,simu}} = 0.36 \pm 0.02(stat)^{+0.12}_{-0.07}(syst)$ events in the WIMP mass range [10–1000] GeV. After applying the μ-veto cut, an upper limit of $N^{\text{WIMP-like}}_{\mu-\text{ind}} < 0.06$ events (90% C.L.) was derived. These results demonstrate that μ-induced background is negligible for the WIMP search analyses performed with the data of the EDELWEISS-III experiment. More details on the μ-veto, on an equivalent analysis for a low-mass WIMP search in the range [3–30] GeV, and on the measured μ flux can be found in [25, 60].

8.2 Shielding performance against radiogenic neutrons and γ-rays

Preliminary γ and radiogenic neutron background studies have been carried out [29] in order to show that the performance of the EDELWEISS-III environment and shieldings are adequate for dark matter searches.

Radiogenic neutron background, as described in section 4.2, has been studied by Monte Carlo (MC) simulations where several sources of neutrons were considered. In a first step neutron production rates in the materials of the internal parts of the detector and spectra from (α, n) reactions, spontaneous fission and delayed emission due to the decay of radionuclei have been determined using the SOURCES4A code [61] which has been modified to extend the energies of α-particles up to 10 MeV, and to improve and extend the (α,n) cross-section library [62]. Then Geant4.9.6 [63] has been used to propagate neutrons through the experimental setup, assuming secular equilibrium for uranium and thorium decay chains. The number of nuclear recoils observed in an extended region of interest for WIMP search ([10–200] keV) in the fiducial volume and considering one year

2017 JINST 12 P08010

Table 5. The source of background radiation and its mass in the EDELWEISS-III setup as used in the simulations. Decay rates, in mBq/kg, for each radioactive isotope considered are listed in the other columns. The quoted activities of ^{238}U and ^{232}Th assume that all daughters in their chains are in equilibrium. All upper limits are given at 90% C.L.. If not mentioned, the measurements have been performed using Gentiane HPGe detector. Other measurements are: [(1)] U/Th activities measured with ICP-MS in 2015 at ENS-Lyon; [(2)] (GeMPI4) and [(3)] (GeMPI2) by M. Laubenstein (2014) [57]. Abbreviations are used when needed: "conn." for connectors, "cont." for contacts. Also, [(a)] CuC2 copper from Carlier [58]; [(b)] cables for connecting 100 K and 1 K volumes; [(c)] the cryostat structure is made of stainless steel; [(d)] cables for connecting 300 K and 100 K volumes.

Element	Mass (kg)	^{238}U chain		^{232}Th chain	^{40}K	^{60}Co	^{137}Cs
		^{210}Pb	^{238}U	^{232}Th			
Mill-Max conn.[(1)]							
Brass pins	7.39 g	$(1.1 \pm 0.1) \times 10^4$	< 62	< 20	675 ± 221	< 36	< 47
Brass sockets	9.41 g	$(2.6 \pm 0.4) \times 10^4$	< 62	< 20	< 2645	< 129	< 132
CuBe press-fit cont.	1.63 g		$(1.2 \pm 0.2) \times 10^4$	980 ± 196			
PTFE Delrin	0.040	< 26	< 16	1.5 ± 1	< 43	< 2.3	< 2.0
Kapton connectors	0.094	< 187	14 ± 7	67 ± 31	150 ± 98		
PTFE contacts	0.061		10 ± 5	20 ± 7			
Brass FID casings	0.40	524 ± 102	< 16	< 15	< 75	5 ± 3	3 ± 2
Cu Kapton cables	0.51	549 ± 111	8 ± 6	15 ± 10	66 ± 26	3 ± 2	< 4.0
Brass screws	2.0	620 ± 254		3.5 ± 0.9	< 19	< 3.0	2.6 ± 1.5
Cu (NOSV)[(2)]	295		< 0.39	$< 32.10^{-3}$	< 0.15	$(35 \pm 9) \times 10^{-3}$	$< 6.4 \times 10^{-3}$
Cu (CuC2)[(3)] [(a)]	328		$< 40 \times 10^{-3}$	$(24 \pm 12) \times 10^{-3}$	< 0.50	$(42 \pm 16) \times 10^{-3}$	$< 35 \times 10^{-3}$
PE internal	151	< 3.0	0.65 ± 0.08	0.30 ± 0.07	< 1.0	< 0.06	< 0.06
Axon cables[(b)]	3.5	138 ± 53	4 ± 3	5 ± 2	177 ± 22	< 5.0	< 2.0
Other connectors[(b)]	0.43	$(6.0 \pm 0.5) \times 10^3$	$(2.6 \pm 0.4) \times 10^3$	450 ± 44	< 571	< 36	< 39
Cryostat stucture[(c)]	1236		< 1.0	< 1.0			
PCB FET boxes	0.55	$(1.4 \pm 0.3) \times 10^4$	$(7.5 \pm 0.2) \times 10^3$	$(10.1 \pm 0.1) \times 10^3$	$(11.5 \pm 0.6) \times 10^3$		
PCB FID boxes	10.4		< 1660	< 1215			
Al FID boxes	27.8	88 ± 36	4 ± 3	< 2.0	65 ± 34	5 ± 3	2.0 ± 1.3
Axon cables[(d)]	6.32		182 ± 70	13.0 ± 2.5			
Mild steel structure	8 600		< 1.0	< 1.0			
Polyethylene	40 000		< 12	< 0.4	16 ± 2	< 3.0	
Lead	39 000		< 1.0	< 1.0			
Rock [59]			$(10 \pm 3) \times 10^3$	$(10.0 \pm 0.8) \times 10^3$	$(230 \pm 30) \times 10^3$		
Concrete [59]			$(23 \pm 3) \times 10^3$	$(5.7 \pm 0.8) \times 10^3$	$(77 \pm 13) \times 10^3$		

of data acquisition has been derived. Using an array of twenty-four FID detectors with a mean fiducial mass of 620 g each (see table 3), the number of single (multiple) nuclear recoils in the 90% NR band has been found to be 1.4 (3.4) for an exposure of 5 435 kg · d. The simulations in the restricted [10–100] keV range also show a ratio of single over multiple scattering neutron events of 0.45, with a systematic uncertainty of 30% depending on the origin of the neutrons. The spectral shape of the neutron-induced nuclear recoil distribution is relatively independent of the nature and location of the neutron background source.

More importantly the real neutron flux can be checked inside the EDELWEISS-III detector array, independently from the actual WIMP search data, by using events where more than one detector have triggered simultaneously. Figure 21 shows multiple hit events in the NR region registered during the WIMP search data taking periods of Run 308, using all 24 available FID detectors (see table 2). Out of the 18 nuclear recoils in coincidence with another detector observed in the [10–200] keV range for an exposure of 1 309 kg · d, nine have been found in coincidence with the muon veto. The other nine recoils cannot be due to μ-induced neutrons as demonstrated in section 8.1. They are multiple hits with ionization yields consistent with nuclear recoils in all detectors. This number exceeds the expectation for this exposure of 0.8 nuclear recoils associated to multiple hits deduced from the Monte Carlo simulation for this exposure. This excess could be due to defects in the PE shielding, currently under investigation. The observed number of multiple hits has been used to re-scale the radiogenic neutron flux used in the Monte Carlo predictions, as described in [50].

Despite the lead shielding described in section 4, most of the event rate in the FID detectors is due to γ-ray interactions. An analysis of data from EDELWEISS-III in the energy range from 100 keV to 4 MeV (outside the ROI for dark matter searches) has been carried out leading to an average integrated γ counting rate in individual detectors of 370 ± 4 γ/kg/d based on the exposure of about 554 kg · d for the total detection volume. In the fiducial volume, the γ rate in individual detectors in the same energy range is 235 ± 5 γ/kg/d, corresponding to a fiducial exposure of about 380 kg · d. MC simulations with Geant4.9.6 [63] have been carried out to understand the experimental γ-background spectrum. All materials surrounding the detectors in the 10 mK and 1 K volumes along with the shielding have been considered as sources of γ-background with contaminations from uranium and thorium chains, as well as ^{40}K, ^{60}Co and ^{137}Cs isotopes. They have been identified either by γ-spectroscopy in dedicated HPGe screening measurements or by ICP-MS analyses (see section 4 and table 5 in this section).

These contaminations are taken as inputs for simulations. A preliminary comparison of data and simulations has been carried out and a relatively good agreement is observed for the ionization spectrum in both the total volume and the fiducial volume, as described in [29]. The measured γ-background in the fiducial volume is 70 γ/kg/d in the range [20–200] keV, compared to a predicted value of 78 γ/kg/d. The dominant source of this background are the Mill-Max connectors with their press-fit contacts in CuBe glued on the FID detector casings, as already explained at the beginning of section 8.[19] More detailed investigations on neutron and γ backgrounds, both with latest versions of neutron and γ MC simulations, are ongoing [64].

[19]See information on the Mill-Max connectors in https://www.mill-max.com/engineering_notebooks/detail/83.

2017 JINST 12 P08010

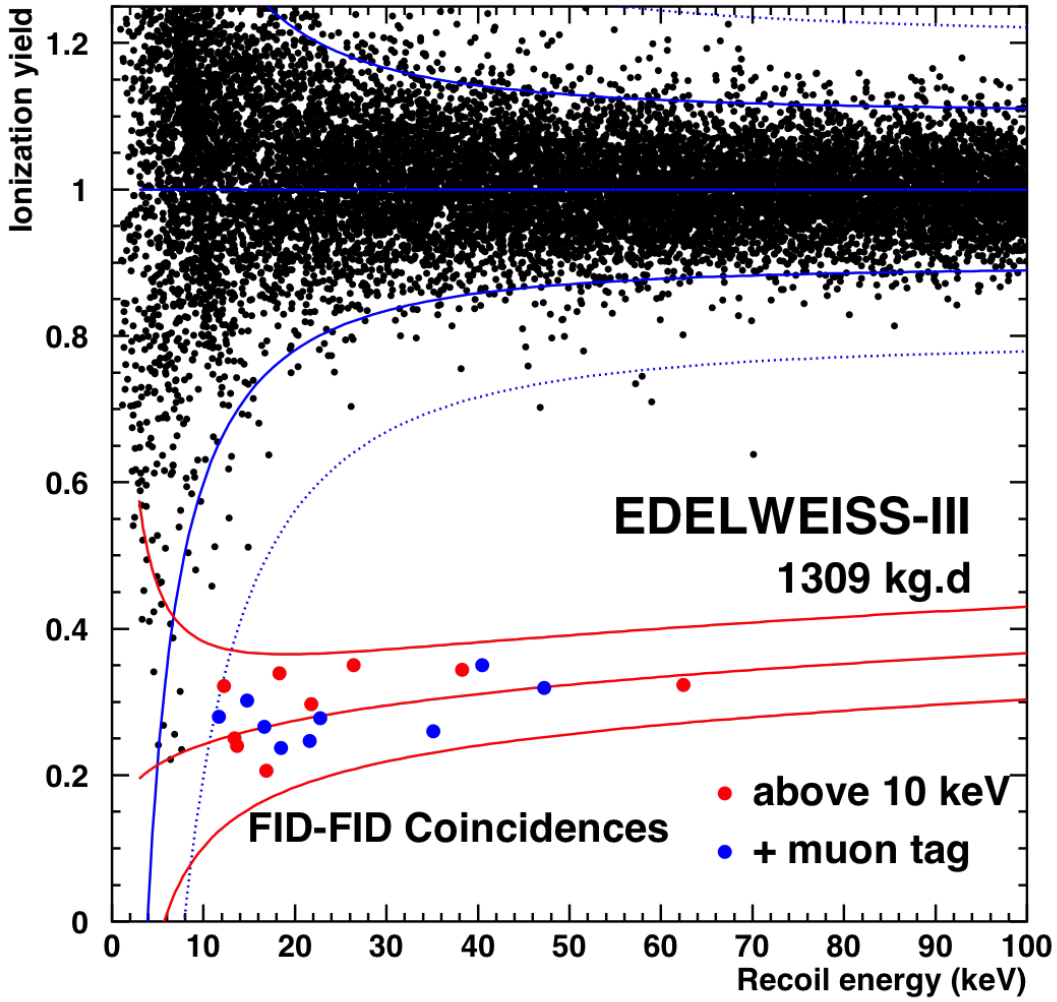

Figure 21. Ionization yield versus recoil energy in the fiducial volume of individual detectors for the 1 309 kg · d effective exposure of Run 308, for hits in coincidence with a signal in at least one other FID detector. The multiplicity associated to each fiducial recoil is evaluated using the entire volume of all detectors. There are 18 such multiple hits in the nuclear recoil band in the [10–200] keV range (colored circles), where nine of them are also in coincidence with the muon veto (in blue) and the nine others are not (in red). The middle red curve shows the mean ionisation yield for the NR band whereas the red curves on both sides show the area where 90% C.L. of nuclear recoil events are expected to lie. Similarly, the middle blue curve shows the average ionisation yield for electron recoils (taken as 1 by definition) whereas the two solid (dotted) curves on both sides show the 90% (99.98%) C.L. areas for electron recoil events.

9 Summary and prospects

In this paper, we reported the design and performance of the EDELWEISS-III dark matter direct detection search experiment operating in the Modane Underground Laboratory using an array of 24 FID cryogenic germanium bolometers. This third phase of the experiment involves upgrades on both the electronics (readout and DAQ) and the cryogenic systems, with new shieldings having been installed. These measures, coupled with the use of the newly designed FID detectors, allowed

2017 JINST 12 P08010

to improve energy resolutions and thus lower the thresholds. The characterization of the detectors and their environment was performed on data sets separated from blinded data for the WIMP search analysis, notably multiple hit events, events outside the fiducial volume and fiducial events with an ionization yield larger than 0.5 with respect to the mean ionization yield from electron recoils. It was based mainly on data obtained during the 10-months Run 308, but also on data from shorter data-taking periods and special calibration data.

During Run 308, the fiducial ionization energy resolutions were typically below 0.7 keV_{ee} FHWM whereas the resolution values were typically below 1.5 keV_{ee} FWHM for heat energies for the whole set of 24 FID detectors used for coincidence studies. A subset of eight FID bolometers with clearly better baseline resolutions less than 0.7 keV_{ee} and 1 keV_{ee} for the fiducial ionization $\mathrm{FWHM}_{\mathrm{fid}}$ and the combined heat baseline FWHM_{c} respectively, has been identified. A low-enough online threshold of less than 1.5 keV_{ee} has been achieved to perform low WIMP mass studies. Also the fiducial volume fraction of the FID detectors has been measured using the activation of the ^{65}Zn and ^{68,71}Ge isotopes, with a weighted average value of $(74.6 \pm 0.4)\%$.

The capability of the FID germanium detectors of clearly separating the electron recoils induced by β and γ radiation from nuclear recoils using a double-readout event-by-event discrimination has been quantified. The rejection of bulk γ-ray events has been measured with γ-calibration data and the limit has been found to be $R_{\gamma-\mathrm{mis}-\mathrm{FID}} < 2.5 \times 10^{-6}$ at 90% C.L., at least a factor 12 better than the leaking fraction measured with the previous generation of detectors. Also the FID detectors allow an efficient rejection of surface β- and α-decays. A value of $R_{\mathrm{surf}-\mathrm{FID}} < 4 \times 10^{-5}$ (90% C.L.) for α-events has been measured using data from a ^{210}Pb source, which demonstrates that less than one surface event per fiducial exposure of 3 400 kg · d is expected leaking in the NR band for a recoil energy threshold of 15 keV.

The efficiency of the μ-veto, which acts as an active shielding against cosmogenic μ-induced neutrons, has been studied. An upper limit of $N_{\mu-\mathrm{ind}}^{\mathrm{WIMP}-\mathrm{like}} < 0.06$ events (90% C.L.) was derived for an exposure of 600 kg · d. It demonstrated that the number of μ-induced background events in the nuclear recoil band is negligible for the EDELWEISS-III WIMP search analyses. Performance of the passive shieldings against neutrons and γ-rays were also discussed together with the current levels of natural radioactivity measured in the experiment. The measured γ-background in the fiducial volume is 70 γ/kg/d in the range [20–200] keV. An unexpected excess of neutron-induced nuclear recoil events (multiple hits) has been observed and is currently under investigation.

These results demonstrate that all elements of the EDELWEISS-III setup have been tested and have exhibited a performance sufficient for low-mass WIMP searches. Extension of the search to higher WIMP mass is only limited by the neutron background inside the cryostat, as the achieved resolutions, rejection capabilities and thresholds of the upgraded EDELWEISS-III detectors are excellent.

Having presented first results on WIMP search [50, 54], EDELWEISS is now focusing on the optimization of the experiment to enhance its sensitivity for low-mass WIMPs through four R&D tasks [65]. The first one is to benefit from the so-called Neganov-Luke boosting effect to lower the energy thresholds. For this purpose upgrades on readout electronics to allow a high ionization biasing up to ±70 V have already been made. Detector surface treatments have been done to ensure small leakage currents at high voltages. Meanwhile, R&D is being carried out on detectors with three other tasks: two of them in order to improve baseline energy resolutions, both in heat and

2017 JINST 12 P08010

fiducial ionization, and the third one in order to understand the origin of heat-only events to reduce their rate significantly.

Acknowledgments

The help of the technical staff of the Laboratoire Souterrain de Modane and the participant laboratories is gratefully acknowledged. The EDELWEISS project is supported in part by the German ministry of science and education (BMBF Verbundforschung ATP Proj.-Nr. 05A14VKA), by the Helmholtz Alliance for Astroparticle Physics (HAP), by the French Agence Nationale pour la Recherche (ANR) and the LabEx Lyon Institute of Origins (ANR-10-LABX-0066) of the Université de Lyon within the program "Investissements d'Avenir" (ANR-11-IDEX-00007), by the P2IO LabEx (ANR-10-LABX-0038) in the framework "Investissements d'Avenir" (ANR-11-IDEX-0003-01) managed by the ANR (France), by Science and Technology Facilities Council (U.K.), and the Russian Foundation for Basic Research (grant No. 07-02-00355-a).

References

[1] L. Bergström, *Nonbaryonic dark matter: observational evidence and detection methods*, *Rept. Prog. Phys.* **63** (2000) 793 [hep-ph/0002126].

[2] G. Bertone, D. Hooper and J. Silk, *Particle dark matter: evidence, candidates and constraints*, *Phys. Rept.* **405** (2005) 279 [hep-ph/0404175].

[3] J.L. Feng, *Dark matter candidates from particle physics and methods of detection*, *Ann. Rev. Astron. Astrophys.* **48** (2010) 495 [arXiv:1003.0904].

[4] J.L. Feng, *Supersymmetry and cosmology*, *eConf* **C 0307282** (2003) L11 [hep-ph/0405215].

[5] D.G. Cerdeno and A.M. Green, *Direct detection of WIMPs*, in *Particle dark matter: observations, models and searches*, G. Bertone ed., Cambridge University Press, Cambridge U.K. (2010), arXiv:1002.1912.

[6] XENON collaboration, E. Aprile et al., *Design and performance of the XENON10 dark matter experiment*, *Astropart. Phys.* **34** (2011) 679 [arXiv:1001.2834].

[7] XENON100 collaboration, E. Aprile et al., *First dark matter results from the XENON100 experiment*, *Phys. Rev. Lett.* **105** (2010) 131302 [arXiv:1005.0380].

[8] LUX collaboration, D.S. Akerib et al., *The Large Underground Xenon (LUX) experiment*, *Nucl. Instrum. Meth.* **A 704** (2013) 111 [arXiv:1211.3788].

[9] PandaX collaboration, X. Cao et al., *PandaX: a liquid Xenon dark matter experiment at CJPL*, *Sci. China Phys. Mech. Astron.* **57** (2014) 1476 [arXiv:1405.2882].

[10] DarkSide collaboration, P. Agnes et al., *First results from the DarkSide-50 dark matter experiment at Laboratori Nazionali del Gran Sasso*, *Phys. Lett.* **B 743** (2015) 456 [arXiv:1410.0653].

[11] G. Angloher et al., *Commissioning run of the CRESST-II dark matter search*, *Astropart. Phys.* **31** (2009) 270 [arXiv:0809.1829].

[12] SuperCDMS collaboration, R. Agnese et al., *Improved WIMP-search reach of the CDMS II germanium data*, *Phys. Rev.* **D 92** (2015) 072003 [arXiv:1504.05871].

2017 JINST 12 P08010

[13] R. Bernabei et al., *Performances of the new high quantum efficiency PMTs in DAMA/LIBRA*, 2012 *JINST* **7** P03009.

[14] EDELWEISS collaboration, E. Armengaud et al., *Final results of the EDELWEISS-II WIMP search using a 4-kg array of cryogenic germanium detectors with interleaved electrodes*, *Phys. Lett.* **B 702** (2011) 329 [arXiv:1103.4070].

[15] EDELWEISS collaboration, E. Armengaud et al., *Background studies for the EDELWEISS dark matter experiment*, *Astropart. Phys.* **47** (2013) 1 [arXiv:1305.3628].

[16] E.E. Haller et al., *Neutron transmutation doped natural and isotopically engineered germanium thermistors*, *SPIE 2198, Instrum. Astron. VIII* (1994) 630.

[17] A. Broniatowski et al., *A new high-background-rejection dark matter Ge cryogenic detector*, *Phys. Lett.* **B 681** (2009) 305 [arXiv:0905.0753].

[18] E. Armengaud et al., *First results of the EDELWEISS-II WIMP search using Ge cryogenic detectors with interleaved electrodes*, *Phys. Lett.* **B 687** (2010) 294 [arXiv:0912.0805].

[19] S. Marnieros et al., *Controlling the leakage-current of low temperature germanium detectors using XeF_2 dry etching*, *J. Low Temp. Phys.* **176** (2014) 176.

[20] EDELWEISS collaboration, Q. Arnaud et al., *Signals induced by charge-trapping in EDELWEISS FID detectors: analytical modeling and applications*, 2016 *JINST* **11** P10008 [arXiv:1606.08097].

[21] B. Neganov and V. Trofimov, *Calorimetric method measuring ionizing radiation* (in Russian), *Otkrytia i Izobreteniya* **146** (1985) 215.

[22] P.N. Luke, *Voltage-assisted calorimetric ionization detector*, *J. Appl. Phys.* **64** (1988) 6858.

[23] National Instruments Corporation, http://www.ni.com/en-gb.html.

[24] Laboratoire Souterrain de Modane, Modane Underground Laboratory, http://www-lsm.in2p3.fr/.

[25] EDELWEISS collaboration, B. Schmidt et al., *Muon-induced background in the EDELWEISS dark matter search*, *Astropart. Phys.* **44** (2013) 28 [arXiv:1302.7112].

[26] S. Rozov et al., *Monitoring of the thermal neutron flux in the LSM underground laboratory*, arXiv:1001.4383.

[27] EDELWEISS collaboration, R. Lemrani and G. Gerbier, *Update of neutron studies in EDELWEISS*, *J. Phys. Conf. Ser.* **39** (2006) 145.

[28] NEMO-3 collaboration, R. Arnold et al., *Results of the search for neutrinoless double-β decay in ^{100}Mo with the NEMO-3 experiment*, *Phys. Rev.* **D 92** (2015) 072011 [arXiv:1506.05825].

[29] EDELWEISS collaboration, S. Scorza, *Background investigation in EDELWEISS-III*, *AIP Conf. Proc.* **1672** (2015) 100002.

[30] Aurubis, https://www.aurubis.com/en.

[31] X. Zhang,*A novel phonon-scintillation cryogenic detector and cabling solution for dark matter direct detection*, Ph.D. Thesis, University of Oxford, Oxford, U.K. (2015).

[32] J. Billard, M. De Jesus, A. Juillard and E. Queguiner, *Characterization and optimization of EDELWEISS-III FID800 heat signals*, *J. Low Temp. Phys.* **184** (2016) 299.

[33] S. Gaertner et al., *A new readout system for bolometers with improved low frequency stability*, *Astron. Astrophys. Suppl. Ser.* **126** (1997) 151.

[34] G.F. Knoll, *Radiation detection and measurement*, 4$^{\text{th}}$ Edition, John Wiley and Sons, New York, U.S.A. (2010).

2017 JINST 12 P08010

[35] EDELWEISS collaboration, B. Censier, *EDELWEISS read-out electronics and future prospects*, *J. Low Temp. Phys.* **167** (2012) 645.

[36] EDELWEISS collaboration, T. Bergmann et al., *A scalable DAQ system with high-rate channels and FPGA- and GPU-trigger for the dark matter search experiment EDELWEISS-III*, *IEEE Nucl. Sci. Symp. Med. Imag. Conf. (NSS/MIC)* (2015) 1.

[37] B. Siebenborn, *Discrimination of surface events with time resolved ionization channels in the EDELWEISS dark matter search*, Ph.D. Thesis, Karlsruhe Institute of Technology, Germany (2016).

[38] SuperCDMS collaboration, R. Agnese et al., *Search for low-mass weakly interacting massive particles using voltage-assisted calorimetric ionization detection in the SuperCDMS experiment*, *Phys. Rev. Lett.* **112** (2014) 041302 [arXiv:1309.3259].

[39] SuperCDMS collaboration, R. Agnese et al., *New results from the search for low-mass weakly interacting massive particles with the CDMS low ionization threshold experiment*, *Phys. Rev. Lett.* **116** (2016) 071301 [arXiv:1509.02448].

[40] EDELWEISS collaboration, T. Bergmann et al., *FPGA-based multi-channel DAQ systems with external PCI express link to GPU compute servers*, *IEEE Real Time Conf.* (2012) 1.

[41] Pierre Auger collaboration, A. Aab et al., *The Pierre Auger cosmic ray observatory*, *Nucl. Instrum. Meth.* **A 798** (2015) 172 [arXiv:1502.01323].

[42] KATRIN collaboration, J. Angrik et al., *KATRIN design report 2004*, Wissenschaftliche Berichte, FZKA-7090 (2005).

[43] M.A. Howe et al., *Sudbury Neutrino Observatory neutral current detector acquisition software overview*, *IEEE Trans. Nucl. Sci.* **51** (2004) 878.

[44] R. Brun and F. Rademakers, *ROOT — An object oriented data analysis framework*, *Nucl. Instrum. Meth.* **A 389** (1997) 81.

[45] EDELWEISS collaboration, A. Benoit et al., *First results of the EDELWEISS WIMP search using a 320-g heat-and-ionization Ge detector*, *Phys. Lett.* **B 513** (2001) 15 [astro-ph/0106094].

[46] Nudat 2.6, *Interactive chart of nuclides*, http://www.nndc.bnl.gov/nudat2/.

[47] J. Lindhard, V. Nielsen and M. Schar, *Approximation method in classical scattering by screen coulomb fields*, *Mat. Fys. Medd. Dan. Vid. Selsk.* **36** (1968) 10.

[48] EDELWEISS collaboration, A. Benoit et al., *Measurement of the response of heat-and-ionization germanium detectors to nuclear recoils*, *Nucl. Instrum. Meth.* **A 577** (2007) 558 [astro-ph/0607502].

[49] EDELWEISS collaboration, V. Sanglard et al., *Final results of the EDELWEISS-I dark matter search with cryogenic heat-and-ionization Ge detectors*, *Phys. Rev.* **D 71** (2005) 122002 [astro-ph/0503265].

[50] EDELWEISS collaboration, E. Armengaud et al., *Constraints on low-mass WIMPs from the EDELWEISS-III dark matter search*, *JCAP* **05** (2016) 019 [arXiv:1603.05120].

[51] Q. Arnaud, *Dark matter direct detection with EDELWEISS experiment: study of signals induced by charge trapping, data analysis and characterization of cryogenic detector sensitivity to low-mass WIMP search*, Ph.D. Thesis, Université Claude Bernard Lyon 1, Lyon, France (2016).

[52] R.B. Firestone and V.S. Shirley, 8th *edition of the table of Isotopes*, John Wiley and Sons, Inc., New York U.S.A. (1996).

2017 JINST 12 P08010

[53] EDELWEISS collaboration, E. Armengaud et al., *Measurement of the cosmogenic activation of germanium detectors in EDELWEISS-III*, *Astropart. Phys.* **91** (2017) 51 [arXiv:1607.04560].

[54] EDELWEISS collaboration, L. Hehn et al., *Improved EDELWEISS-III sensitivity for low-mass WIMPs using a profile likelihood approach*, *Eur. Phys. J.* **C 76** (2016) 548 [arXiv:1607.03367].

[55] EDELWEISS collaboration, A. Juillard, *Status and prospects of the EDELWEISS direct WIMP search experiment*, *J. Low Temp. Phys.* **167** (2012) 1056.

[56] EDELWEISS collaboration, J. Gascon et al., *The EDELWEISS-III project and the rejection performance of its cryogenic germanium detectors*, *J. Low Temp. Phys.* **176** (2014) 870.

[57] M. Laubenstein, private communication (2014).

[58] Carlier Industry, http://www.carlier.cc/indexuk.php.

[59] V. Chazal et al., *Neutron background measurements in the underground laboratory of Modane*, *Astropart. Phys.* **9** (1998) 163.

[60] C. Kéfélian, *Search for dark matter with EDELWEISS-III excluding background from muon-induced neutron*, Ph.D. Thesis, Université Claude Bernard Lyon 1 and Karlsruhe Institute of Technology, (2016).

[61] W.B. Wilson et al., *Technical report LA-UR-02-1839*, Los Alamos, U.S.A. (1999).

[62] V. Tomasello, M. Robinson and V.A. Kudryavtsev, *Radioactive background in a cryogenic dark matter experiment*, *Astropart. Phys.* **34** (2010) 70.

[63] S. Agostinelli et al., *Geant4 — A simulation toolkit*, *Nucl. Instrum. Meth.* **A 506** (2003) 250.

[64] EDELWEISS collaboration, E. Armengaud et al., *Investigation of gamma backgrounds in the EDELWEISS-III environment*, in preparation (2017).

[65] EDELWEISS collaboration, Q. Arnaud et al., *Optimizing EDELWEISS detectors for low-mass WIMP searches*, to be submitted to *Phys. Rev. D* (2017).

2017 JINST 12 P08010